NANOFLUID TO IMPROVE HEAT TRANSFER IN ANNULAR CONCENTERIC HEAT EXCHANGER

SEYEDEH MARYAM HOSSEINI

DISSERTATION SUBMITTED IN FULFILMENT OF THE REQUIREMENTS FOR THE DEGREE OF MASTER OF ENGINEERING SCIENCE

FACULTY OF ENGINEERING
UNIVERSITY OF MALAYA
KUALA LUMPUR

2017

UNIVERSITI MALAYA

ORIGINAL LITERARY WORK DECLARATION

Name of Candidate: **SEYEDEH MARYAM HOSSEINI** I.C/Passport No:

Registration/Matric No: **KGA140086**

Name of Degree: Master of **ENGINEERING**
Title of Project Paper/Research Report/Dissertation/Thesis:

SYNTHESIS OF NANOFLUID TO IMPROVE HEAT TRANSFER IN ANNULAR CONCENTERIC HEAT EXCHANGER

Field of Study: **Heat transfer**

I do solemnly and sincerely declare that:

(1) I am the sole author/writer of this Work;
(2) This Work is original;
(3) Any use of any work in which copyright exists was done by way of fair dealing and for permitted purposes and any excerpt or extract from, or reference to or reproduction of any copyright work has been disclosed expressly and sufficiently and the title of the Work and its authorship have been acknowledged in this Work;
(4) I do not have any actual knowledge nor do I ought reasonably to know that the making of this work constitutes an infringement of any copyright work;
(5) I hereby assign all and every rights in the copyright to this Work to the University of Malaya ("UM"), who henceforth shall be owner of the copyright in this Work and that any reproduction or use in any form or by any means whatsoever is prohibited without the written consent of UM having been first had and obtained;
(6) I am fully aware that if in the course of making this Work I have infringed any copyright whether intentionally or otherwise, I may be subject to legal action or any other action as may be determined by UM.

Candidate's Signature Date

Subscribed and solemnly declared before,

Witness's Signature Date

Name:
Designation:

SYNTHESIS OF NANOFLUID TO IMPROVE HEAT TRANSFER IN ANNULAR CONCENTERIC HEAT EXCHANGER

ABSTRACT

Traditional heat exchanger liquids (e.g., water, ethylene glycol, oil and etc.) possess inherently low heat transfer performance as a consequence of their low thermal conductivities. In recent past, there has been remarkable interest in employing nanofluids (nano-coolants) for increasing thermal performance of these liquids. Nano-coolants taken under investigation in this research were aqueous suspensions of highly conductive nanoparticles in Distilled water (DI water) which provided enhanced thermal properties at even lower nanoparticle concentrations and were employed in different thermal applications such as solar collectors, heat exchangers and electronic cooling systems. The current study highlighted experimental study convective heat transfer as well as friction loss of clove-treated multi-walled carbon nanotubes (C-MWCNTs) and clove-treated graphene nanoplatelets (CGNPs) water based nano-coolants flowing in an annular concentric heat exchanger under turbulent and constant heat flux conditions. The multi-walled carbon nanotubes (MWCNTs) were functionalized covalently in one-pot using free radical reaction in a green and scalable way followed by dispersing the C-MWCNTs in base fluid at various weight concentrations. The functionalized Carbon nanotubes were characterized using, thermogravimetric analysis (TGA), Fourier transform infrared spectroscopy (FTIR), X-ray photoelectron spectroscopy (XPS), Raman spectroscopy, and transmission electron microscopy (TEM). UV-vis spectroscopy was employed to confirm the stability of the nanofluids in DI water. Further, Zeta potential had provided also proof of the presence of hydrophilic groups in the functionalized nanoparticles. The thermo-physical properties of nanofluids have shown a good enhancement compared to that of the base fluid which refers to their application as suitable heat exchanger liquids. The heat transfer and friction loss were studied experimentally in a flow loop with a concentric

annular test section subjected to a constant heat flux of 38346 W/m^2, at the Reynolds number range of 3055 ± 5 to 7944 ± 5.

Numerical simulation was performed as an approximating procedure for prediction of the results in this study. Single-phase mixture model was considered for simulation of the nanofluids flow in three dimensional annular heat exchanger. Primary experiments were performed with the base fluid and the results of the average Nusselt numbers obtained from the experimental were compared with those calculated using empirical equations of Gnielinski and Petukhov, and the results have shown 4 and 9 %, error respectively, within 95% confidence level, which indicates a well reliability and accuracy of the data obtained from the experimental test section. Moreover, convective heat transfer experiments were performed for the nanofluids in annular heat exchanger at the constant heat flux of 38346 W/m^2 at fully developed flow. The data show that addition of low amount of functionalized MWCNTs to the DI base fluid notably elevates its convective heat transfer coefficient compared to that of the DI water. However, there was only small increment in friction factor compared to the data from water alone for all the tested nanofluids. It is worth noting that the significant increment of the performance index and its upward trend compared to that of water represents all the nano-coolants have strong potential for use as effective heat transfer working fluids in various thermal applications.

Keywords: Heat transfer, turbulent, annular heat exchanger, clove, nanofluid.

SYNTHESIS OF NANOFLUID TO IMPROVE HEAT TRANSFER IN ANNULAR CONCENTERIC HEAT EXCHANGER

ABSTRAK

Cecair penukar haba tradisional (sebagai contoh, Air, etilena glikol, minyak dan lain-lain) mempunyai prestasi pemindahan haba yang rendah akibat daripada konduktiviti haba yang rendah. Baru-baru ini, terdapat minat yang tinggi dalam menggunakan cecair penyejuk-nano (nanofluid) untuk meningkatkan prestasi haba cecair-cecair ini. Penyejuk cecair-Nano yang disiasat dalam kajian ini adalah apungan nanopartikel berasaskan air dalam air suling (DI air) yang memberikan sifat termal yang lebih baik walaupun pada kepekatan nano nanopartikel lebih rendah dan digunakan dalam aplikasi terma yang berbeza seperti pengumpul suria, penukar haba dan sistem penyejukan elektronik. Kajian semasa menyerlahkan penyiasatan secara eksperimen pemindahan haba olakan dan kehilangan geseran bagi nanotiub karbon berbilang cengkih terawat dengan dengan cengkih (C-MWCNTs) dan penyejuk cecair nano yang berasaskan graphene nanoplatlet terawat dengan cengkih (CGNPs) yang mengalir di dalam penukar haba sepusat anulus di bawah aliran gelora dan Keadaan fluks haba berterusan. Nanotiub karbon karbon berbilang dinding (MWCNTs) telah diberfungsikan secara kovalen dalam satu bekas menggunakan tindak balas radikal bebas dalam keadaan hijau dan berskala yang diikuti dengan penyebaran C-MWCNTs dalam cecair asas pada pelbagai kepekatan berasaskan berat. Nanotiub karbon yang dicirikan menggunakan analisis termogravimetrik (TGA), transformasi Fourier spectroscopy Inframerah (FTIR), spektroskopi fotoelektron X-ray (XPS), Spektroskopi Raman, dan Mikroskop Elektron Penghantaran (TEM). Spektroskopi UV-vis telah digunakan untuk mengesahkan kestabilan nanofluid dalam air DI. Seterusnya, potensi Zeta juga telah membuktikan kehadiran kumpulan hidrofilik dalam nanopartikel yang difungsikan. Sifat thermo-fizikal nanofluid telah menunjukkan peningkatan yang baik berbanding dengan bendalir asas yang merujuk kepada aplikasi mereka sebagai cecair penukar haba yang sesuai. Pemindahan haba dan kehilangan

geseran telah dikaji secara eksperimen dalam gelung aliran dengan seksyen ujian anulus sepusat tertakluk kepada fluks haba tetap 38346 W/m^2, pada julat nombor Reynolds 3055 ± 5 hingga 7944 ± 5. Simulasi berangka telah dilakukan sebagai prosedur penganggaran untuk ramalan keputusan dalam kajian ini. Model campuran fasa tunggal telah digunakan untuk simulasi aliran bendalirnano dalam penukar haba annulus tiga dimensi. Eksperimen utama dilakukan dengan cecair asas dan hasil purata nombor Nusselt yang diperoleh dari experiment telah dibandingkan dengan nilai yang dikira menggunakan persamaan emperikal Gnielinski dan Petukhov, dan hasilnya menunjukkan 4 dan 9% perselisihan, dengan 95% tahap keyakinan, yang menunjukkan kebolehpercayaan dan ketepatan data yang diperolehi daripada seksyen ujian eksperimen. Tambahan lagi, eksperimen pemindahan haba olakan telah dilakukan untuk bendalir-nano dalam penukar haba anulus pada fluks haba tetap 38346 W/m^2 pada aliran yang terbangun sepenuhnya. Data menunjukkan bahawa penambahan jumlah rendah MWCNT yang difungsikan ke dalam cecair asas DI secara jelas menaikkan pekali pindahan haba olakan berbanding dengan air DI. Walau bagaimanapun, terdapat hanya sedikit kenaikan dalam faktor geseran berbanding dengan data dari air sahaja untuk semua bendalirnano yang diuji. Perlu diingat bahawa kenaikan ketara indeks prestasi dan trend menaik berbanding dengan air menunjukkan semua nano-penyejuk mempunyai potensi yang kukuh untuk digunakan sebagai cecair kerja yang efektif dalam pelbagai aplikasi pemindahan haba.

Keywords: Pemindahan haba, bergolak, penukar haba annulus, cengkih, nanofluid.

ACKNOWLEDGMENTS

In the name of ALLAH, the most Gracious, the most Compassionate.

First, I would like to thank my parents for allowing me to realize my own potential. All the support they have provided me over the years was the greatest gift anyone has ever given me. I would like to specially thank my supervisors, Dr. Chew Bee Tang, Assoc Prof. Kazi Md. Salim Newaz and Dr. Samira Bagheri at UM university for all their invaluable advice and guidance of this research project and thesis. I would like to express my deepest thanks and sincere appreciation to all of my colleagues in university of Malaya, especially Rad Sadri for his encouragement, creative and comprehensive advice, without him, I may never have gotten to where I am today; to Dr. Mohd Nnashrul Mohd Zubir, for his valuable and freely helps and thank you to Mr. Ali Hassan Abdelrazek as well. I am pleased to acknowledge the financial support from University of Malaya Research Grant Scheme (Project no.: RP012B-13AET and GC001D-14AET). Finally, thank you GOD for your blessing through my life and for all the things I have been given.

TABLE OF CONTENTS

ABSTRACT iv

ABSTRAK vi

ACKNOWLEDGMENTS viii

TABLE OF CONTENTS ix

LIST OF FIGURE xiii

LIST OF TABLE xvii

LIST OF SYMBOLS AND ABBREVIATIONS xviii

CHAPTER 1: INTRODUCTION 1

1.1 Problem statement 8

1.2 Scope of study 9

1.3 Objectives 10

CHAPTER 2: LITERATURE REVIEW 11

2.1 Introduction 11

2.2 Suspension of Milli and micro particles 12

2.3 Nanofluids 13

2.3.1 Carbon base materials 14

2.3.1.1 Carbon nanotube(CNT) 14

2.3.1.2 Graphene nanoplatelets(GNP) 16

2.4 Preparation of nanofluids 16

2.4.1 Two-step method 18

2.4.2 One step method 19

2.5 Stability of nanofluids 20

2.5.1 Covalent functionalization 21

2.5.2 Non-covalent functionalization 22

2.5.3 pH control (effect of surface chemical) 23

2.5.4 Ultra-sonication vibration 25

2.6 Thermo physical properties of nanofluids 26

2.6.1 Viscosity 26

2.6.2 Thermal conductivity 28

2.6.3 Density 32

2.6.4 Specific heat capacity 33

2.7 Heat transfer and pressure drop of nanofluid 34

2.8 Simulation study 36

2.9 Summery 39

CHAPTER 3: METHODOLOGY 40

3.1 Materials 41

3.2 Preparation carbon nanocoolants 41

3.2.1 Preparation of clove extract solution 41

3.2.2 Preparation of C-MWCNT-DI water nanofluids 42

3.2.3 Preparation of Clove treated GNPs-DI water nanofluids 44

3.3 Analysis methods 46

3.3.1 FT-IR 46

3.3.2 Raman 47

3.3.3 TGA 48

3.3.4 XPS 48
3.3.5 TEM 49
3.3.6 Zeta potential 50
3.3.7 UV-Vis 51
3.3.8 KD2-PRO 52
3.3.9 Rheometer 52
3.3.10 Density 53
3.3.11 DSC 54
3.4 Experimental procedure 54
3.5 Data analysis 57
3.6 Mathematical formulation and numerical procedure 58
3.6.1 Geometric model and boundary conditions 60
3.6.2 Mesh dependency 62
CHAPTER 4: RESULT AND DISCUSSION 64
4.1 Characterization of clove treated multi walled carbon nanotube 64
4.2 Characterization of clove treated graphene nanoplatelets 72
4.3 Thermophysical properties C-MWCNTs-DI water nanofluids 79
4.4 Thermophysical properties CGNPs-DI water nanofluids 82
4.5 Thermal performance of C-MWCNT-DI water nanofluids 85
4.6 Thermal performance of C-GNPs-DI water nanofluids 95
4.7 Numerical study of heat transfer to Clove treated MWCNT nanofluids 100
4.7.1 Temperature distributions of nanofluids 100

4.7.2 Validation of the present discussion 103

4.7.3 Thermal analysis of C-MWCNT-DI water nanofluid 104

CHAPTER 5: CONCLUSIONS 109

5.1 Suggestion for further works 110

REFERENCES 111

LIST OF PUBLICATIONS AND AWARDS 128

APPENDIX A 129

LIST OF FIGURE

Figure 1.1: Thermal conductivity of some materials (solids and liquids) at 300 °K 2

Figure 1.2: Effects of micro particles and nanoparticles in a cooling system..... 4

Figure 1.3: Length scale and some examples related to nanosized particles. 5

Figure 2.1: Publications in nanofluids ("Web of Science," 2017) 12

Figure 2.2: Carbon nanotube. 15

Figure 2.3: Graphene nanoplatelets..... 16

Figure 2.4: Schematic of nanofluid production system (Eastman et al., 2001) 19

Figure 3.1: Research Process Flowchart 40

Figure 3.2: Procedure used to prepare the clove extract 42

Figure 3.3: Schematic of functionalization procedure of carbon nanotubes..... 43

Figure 3.4: (a) Initiation reaction for free radical grafting, (b) Formation of C-MWCNTs by free radical grafting technique..... 44

Figure 3.5: (a) Initiation reaction for free radical grafting; (b) Formation of CGNPs by free radical grafting technique..... 45

Figure 3.6: FT-IR spectroscopy (Bruker, IFS-66/S, Germany) 46

Figure 3.7: Raman spectra (Renishaw in Via) 47

Figure 3.8: Thermogravimetric analysis (TGA-50, Shimadzu, Japan)..... 48

Figure 3.9: Axis Ultra-DLD system, Kratos Analytical X-ray photoemission spectrometer (XPS)..... 49

Figure 3.10: Hitachi HT7700 transmission electron microscope 50

Figure 3.11: Malvern Instruments Ltd Zeta sizer..... 51

Figure 3.12: Shimadzu UV-1800 spectrophotometer 51

Figure 3.13: Thermal conductivity measurements set up 52

Figure 3.14: Anton Paar rheometer..... 53

Figure 3.15: DE-40 density meter, Mettler Toledo..... 53

Figure 3.16: Schematic diagram and photo of the experimental set-up..... 56

Figure 3.17: Geometric model of the concentric annular heat exchanger 60

Figure 3.18: Computational mesh of the concentric annular heat exchanger: (a) three-dimensional view and (b) front view of the geometric model. Note that the mesh is finer and more clustered near the walls of the concentric annular heat exchanger. 61

Figure 3.19: Schematic flowchart of the trial and error procedure for finding a proper effective simulation data 62

Figure 3.20: Effect of mesh size on the Nusselt number for DI water 63

Figure 4.1: (A) FTIR spectra of MWCNTs and C-MWCNTs, (B) TGA curves of MWCNTs and C-MWCNTs, and (C) photograph of C-MWCNTs dispersed in DI water after three months.....65

Figure 4.2: (a) Raman spectra and (b) wide-scan O1s and C1s XPS spectra for pristine MWCNTs and CMWCNTs.....66

Figure 4.3: C1s XPS spectra for (a) C-MWCNTs and (b) pristine MWCNTs, and O1s XPS spectra for (c) C-MWCNTs and (d) pristine MWCNTs.....68

Figure 4.4: TEM photographs of: (A) pristine MWCNTs, and (B and C) C-MWCNTs 70

Figure 4.5: (a) Colloidal stability of Clove-treated MWCNTs dispersed in DI water and (b) zeta potential values of the C-MWCNT nanofluid as a function of pH . 70

Figure 4.6: FTIR spectra of pristine GNPs and C-GNPs, (B) TGA curves, and (C) Raman spectra of pristine GNPs and CGNPs.....73

Figure 4.7: (a) Wide-scan XPS spectra for the GNPs and CGNPs; High-resolution XPS spectra of the deconvoluted peak components for C1s: (b) GNPs, (c) CGNPs; High-resolution XPS spectra of the deconvoluted peak components for O1s: (d) GNPs, (e) CGNPs 75

Figure 4.8: TEM image of (a) GNPs and (b) CGNPs (c) zeta potential values of the CGNP nanofluid as a function of pH (d) Colloidal stability of Clove-treated GNPs dispersed in DI water.....78

Figure 4.9: Dynamic viscosity of nanofluids containing C-MWCNTs and DI water at a shear rate of 150 s^{-1} (mPa·s).....80

Figure 4.10: Thermal conductivity of C-MWCNT-DI water nanofluids and DI water..82

Figure 4.11: Variation of (a) thermal conductivity, (b) dynamic viscosity and (c) specific heat capacity of CGNP-water nanofluids as a function of temperature and particle concentration 84

Figure 4.12: Comparison between the measured Nusselt numbers of DI water with those calculated from empirical correlations 88

Figure 4.13: Variation of the average heat transfer coefficient for C-MWCNT/ DI water nanofluids versus Reynolds number 89

Figure 4.14: Variation of the Nusselt number for C-MWCNT-DI water nanofluids as the function of Reynolds number 90

Figure 4.15: Plot of the friction factor as a function of Reynolds number for DI water obtained from experiments and empirical correlations 91

Figure 4.16: Plot of (A) pressure drop and (B) friction factor versus the Reynolds number for C-MWCNT-DI water nanofluids in the annular test section 92

Figure 4.17: Plot of performance index versus Reynolds number for the C-MWCNT-DI water nanofluids 93

Figure 4.18: Relative pumping power of the clove treated MWCNTs-water nanofluids and distilled water 94

Figure 4.19: Variation of the average heat transfer coefficient for CGNP/ DI water nanofluids versus Reynolds number 96

Figure 4.20: Variation of the Nusselt number for CGNP-DI water nanofluids as a function of Reynolds number 97

Figure 4.21: Plot of (A) pressure drop and (B) friction factor versus the Reynolds number for CGNP-DI water nanofluids in the annular test section 98

Figure 4.22: Plot of performance index versus Reynolds number for the CGNP-DI water nanofluids 99

Figure 4.23: Relative pumping power of the CGNP-water nanofluids and distilled water 100

Figure 4.24: Inner wall temperature distribution of the concentric annular heat exchanger with (a) DI water and (b) C-MWCNT/DI water nanofluid containing 0.175 wt.% of C-MWCNTs 101

Figure 4.25: Velocity contours of the concentric annular heat exchanger with (a) C-MWCNT/DI water nanofluid containing 0.175 wt.% of C-MWCNTs and (b) DI water 102

Figure 4.26: Comparison of the (a) Nusselt number and (b) pressure drop for DI water obtained from numerical simulations with those from experiments and empirical correlations 104

Figure 4.27: Variation of the local convective heat transfer coefficient obtained numerically for C-MWCNT/DI water nanofluids with different C-MWCNT concentrations for three Reynolds numbers: (a) Re = 3055, (b) Re = 5499 and (c) Re = 7944 106

Figure 4.28: Variation of the average heat transfer coefficient with respect to the Reynolds number for C-MWCNT/DI water nanofluids in the concentric annular heat exchanger 107

Figure 4.29: Variation of (a) pressure drop and (b) friction factor of the C-MWCNT/DI water nanofluids with respect to the Reynolds number 108

LIST OF TABLE

Table 3. 1: The simulation parameters 62

Table 4. 1: Raman spectra analysis results for pristine and clove-treated MWCNTs 67

Table 4. 2: XPS analysis results for pristine and clove-treated MWCNTs 69

Table 4. 3: Raman spectra analysis results for pristine and clove-treated GNPs 74

Table 4. 4: XPS analysis results for GNPs and CGNPs 77

Table 4. 5: Density of C-MWCNT-DI water nanofluids and DI water as a function of temperature 81

Table 4. 6: Density of CGNP-water nanofluids and DI water as the function of temperature and particle concentration 85

Table A. 1: Rang of uncertainty for instrument used in the present investigation 129

Table A. 2: Uncertainty ranges 130

LIST OF SYMBOLS AND ABBREVIATIONS

P	:	Power, Watts
Pr	:	Prandtl number
Q	:	Heat flow, Watts
$\dot{q}$	:	Heat flux, W/m^2
Nu	:	Nusselt number
h	:	heat transfer coefficient
Re	:	Reynolds number
Pr	:	Prandtl number
T	:	Temperature, °C
u	:	Velocity, m/s
x	:	Axial distance
GNP	:	Graphene nanoplate late
MWCNT	:	Multi-walled carbon nanotube
C-MWCNT	:	Clove-treated multi-walled carbon nanotube
CGNP	:	Clove-treated graphene nanoplate late
wt%	:	weight persentage
W	:	Watt
TEM	:	transmission electron microscopy
XPS	:	X-ray photoelectron spectroscopy
FTIR	:	Fourier transform infrared spectroscopy
TGA	:	thermogravimetric analysis
Uv-vis	:	ultraviolet-visible spectroscopy
SDBS	:	Sodium dodecyl benzene sulfonate
SDS	:	Sodium dodecyl sulfonate

Greek symbols :

Δp	:	Pressure drop
ε	:	Performance Index
λ	:	Wall thermal conductivity
μ	:	Dynamic viscosity, $kg/m^2.s$
ρ	:	Density, kg/m^3
τ	:	Shear stress, Pa
ω	:	Fiber coarseness, kg/m
K	:	Thermal conductivity, W/m.K
φ	:	Mass fraction

Subscripts :

b	:	bulk
i	:	inlet
m	:	mass
o	:	outlet
t	:	Thermocouple
w	:	wall
bf	:	base fluid
nf	:	nanofluid
avg	:	average

CHAPTER 1: INTRODUCTION

Rapid growth of power consumption simultaneously with the development of different sectors, such as industrial, infrastructure, transportation, defence, space, etc, the call for saving energy is a daily campaign; in addition, managing of high thermal loads has become critical. For these reasons, energy efficiency should be enhanced in heating and cooling systems for all the sectors mentioned above. The fluid used for cooling or heating a system, or to transfer heat from one part to another part is called heat transfer fluid. For energy efficient operation, the conventional technique of heat transfer practiced by means of flowing fluids including water, mineral oils and ethylene glycol have to be replaced by the enhanced thermal conductive fluids. In spite of the low heat transfer properties of such fluids which obstruct the performance of the heat transfer equipment there had always been the desire and would always remain in demand, because of their simple characteristics. The systems working with the conventional heat transfer fluids, in applications same as power generation, refining and petrochemical, are very large and includes considerable amount of heat transfer working fluids, however in specific usages like electronics, cooling in laptops and microprocessors, cooling in space applications and many other areas, the small heat exchangers are needed, and these usages have a significant relationship between the mechanical system size, and the cost related to operation and manufacturing. If developments may be done in the existing systems of heat transfer such as increasing the heat transfer fluid performance, smaller heat exchanger and hence, a lesser space would be required to handle a specified amount of cooling load, the situation would lead to smaller heat transfer systems with lower capital costs and higher energy efficiency. Micro-channel heat exchanger could be developed in HVAC and automotive industries with the space saving and lighter weight features. These advantages could also come out as an attractive approach to companies in saving more

material. Low heat transfer performance reduced the efficiency of lower thermal conductivity of the base liquids (i.e. water, ethylene glycol and oil). In this pursuit, numerous researchers have been investigating better methods to enhance the effective thermal conductivity of heat transfer liquids. For the first time, long ago the basic concept of dispersing solid particles in fluid (millimeter or micrometer sized) to enhance the thermal conductivity was introduced by James clerk Maxwell (W Yu & Choi, 2003). Over the years the incorporation into base liquid the high thermal conductive particulate solid such as metals and metal oxide had been used for enhancement of thermal conductivity (Ahuja, 1975a, 1975b; Hetsroni & Rozenblit, 1994; S. Lee, Choi, Li, & Eastman, 1999; Sohn & Chen, 1981; Xuan & Li, 2000) Metallic solid particles have higher thermal conductivities compared to the conventional heat transfer base liquids for example at room temperature, copper has 700 and 3000 times greater thermal conductivity than those of water and engine oil respectively as shown in Figure 1.1 (S. Choi, Zhang, & Keblinski, 2004; Komarneni, Parker, & Wollenberger, 1997)

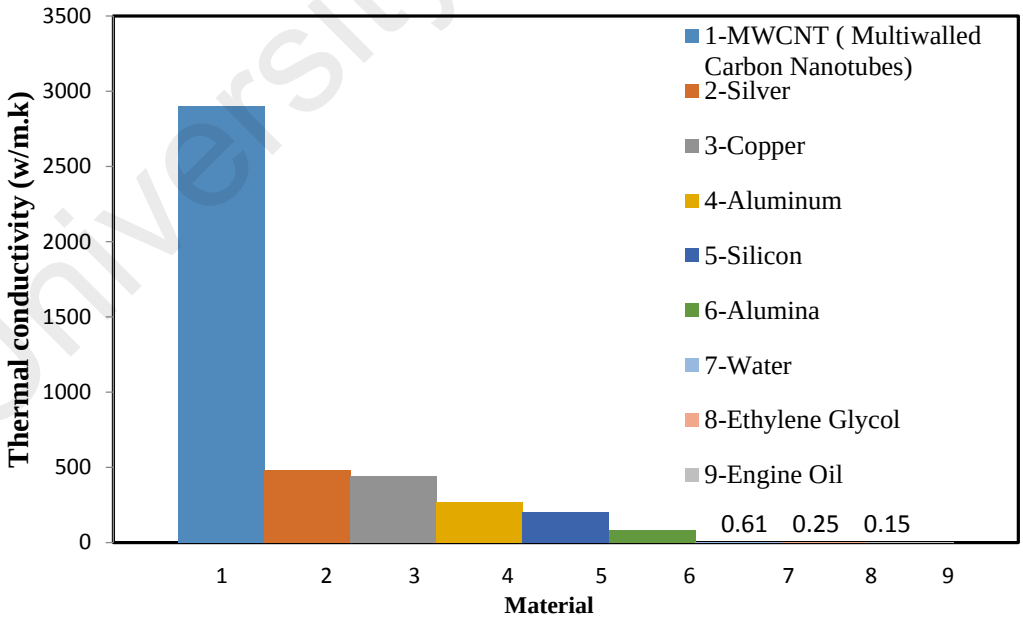

Figure 1. 1: Thermal conductivity of some materials (solids and liquids) at 300 °K

Metallic solid particles have higher thermal conductivity than non-metallic particles except some substances like Carbon Nanotubes (CNT) and diamond (Marquis & Chibante, 2005). Despite the improved thermal conductivity by dispersing solid particles (mm or μm sized) in the based fluids, it could not be used in practical application due to the problems associated with the sedimentation, erosion, fouling and increased pressure drop in the flow channel and also channel clogging which could be caused by poor suspension stability, particularly in the case of mini and micro channels (Ding, Alias, Wen, & Williams, 2006; Trisaksri & Wongwises, 2007; L. Wang & Wei, 2009). Over the last several decades, scientists and engineers have attempted to develop fluids, which offer better cooling or heating performance for a variety of thermal systems compared to conventional heat transfer fluids. Until for the first time choi et al. (S. U. Choi & Eastman, 1995) at the Argonne National Laboratory employed the particles of nanometer dimension (nanoparticle) suspended in solution as nanofluid and showed considerable increase in the nanofluid thermal conductivity. This new class of heat transfer fluids (nanofluids) is engineered by dispersing nanometer sized (one billionth of a meter) solid particles, rods or tubes (nanotube) in traditional heat transfer fluids. The higher solubility and dispersibility of nanoparticles in base fluid will hinder quick sedimentation and decrease clogging in the heat exchanger's walls. The superior thermal conductivity of nanoparticle suspensions (nanofluids) leads to greater performance, energy efficiency, and finally lower operating costs. They can deduct energy consumption for pumping working fluids. Miniaturized systems require smaller inventories of fluids where nanofluids can be used. Heat transfer systems can be lighter and smaller. In vehicles, smaller components cause better fuel savings, gasoline mileage, lower emissions, and finally a cleaner environment. Actually, it is the target of Nanofluid suspensions to achieve the highest thermal properties with lower concentration and good stability. Thermal conductivity enhancement of nanofluids offers plenty of benefits and

applications like higher heat transfer, decreased pumping power, lighter and smaller cooling systems, reduced inventory of heat transfer working fluids, reduced friction coefficients and improved wear resistance. So those kinds of benefits, are notable in the prepared nanofluids for various applications such as coolants, lubricants, hydraulic fluids and metal cutting fluids (Saidur, Leong, & Mohammad, 2011). Compared with millimeter or micrometer sized particle suspensions, Nanofluids have higher stability due to the ultra-small particle size, and can have dramatically higher thermal conductivities (Byl, Liu, & Yates, 2005; Ding et al., 2006; Saidur et al., 2011). Nanofluids does not carry too big a momentum as in case of micro fluids, which reduced erosion and wear in tube and channel, Figure 1.2 compares the effect of micro particles and nanoparticles at the same volume concentration in a cooling system.

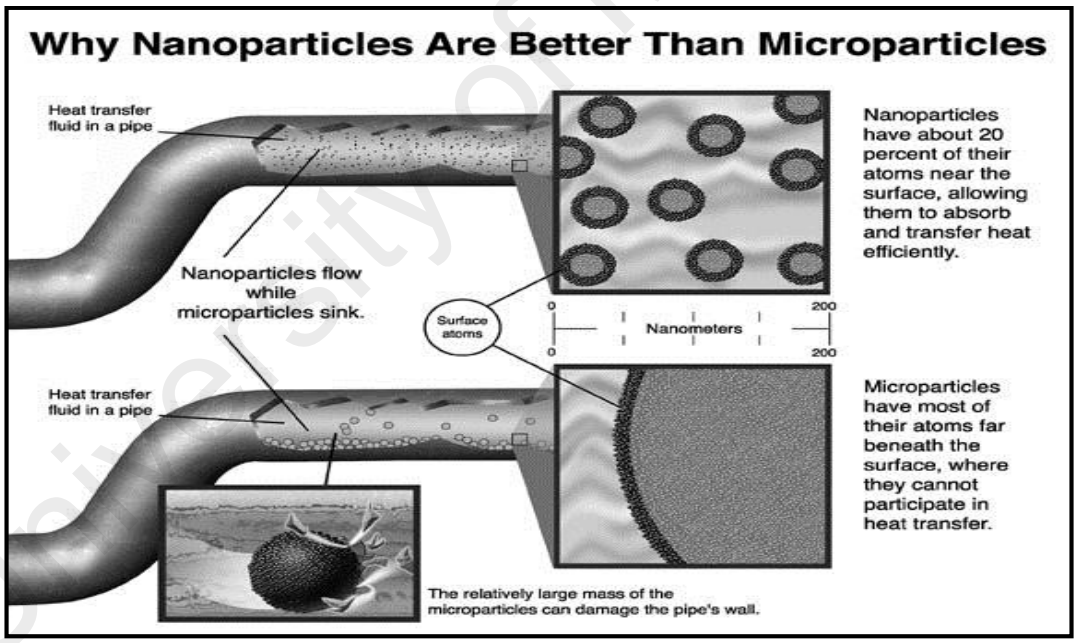

Figure 1. 2: Effects of micro particles and nanoparticles in a cooling system

As nanofluids, these liquid suspensions containing particles significantly smaller than 100 nm at least in one dimension (Ding et al., 2006). Serrano et al.(Serrano, Rus, & Garcia-Martinez, 2009) provided an excellent example of nanometer in comparison with millimeter and micrometer to understand clearly as presented in Figure 1.3, where

nanosized particles could be either spherical or cylindrical. The metal and metal oxide nanoparticles are generally synthesized in spherical form; however, carbon nanoparticles could be synthesized both in spherical and cylindrical form. Of the two forms of carbon nanoparticles, the cylindrical form is more common and is called as (CNT) carbon nanotubes. A kind of these nanotubes is called multi-walled carbon nanotubes (MWCNT) which are more popular in heat transfer based applications.

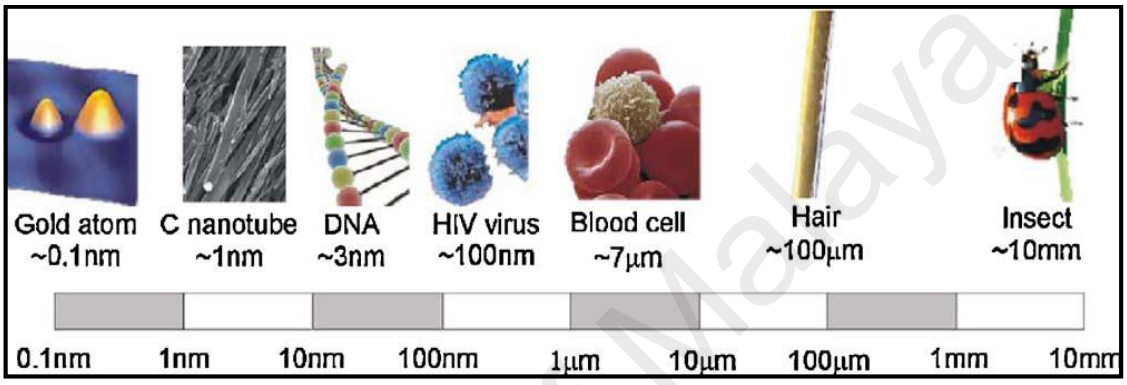

Figure 1. 3: Length scale and some examples related to nanosized particles

From the investigations in the past decade, nanofluids were found to exhibit significantly higher thermal properties, in particular, thermal conductivity and convective heat transfer than those of base fluids, Liu et al.(Liu, Lin, Huang, & Wang, 2006), Eastman et al.(Eastman, Choi, Li, Thompson, & Lee, 1997), Yu et al.(Wei Yu, Xie, Chen, & Li, 2009), and Mintsa et al.(Mintsa, Roy, Nguyen, & Doucet, 2009), Hwang et al. (Y Hwang, Park, Lee, & Jung, 2006), Eastman et al.(Eastman, Choi, Li, Yu, & Thompson, 2001), Xuan, Y. and Q. Li (Xuan & Li, 2000), Putra Nandi(Putra, Thiesen, & Roetzel, 2003), P. Garg et al.(Garg et al., 2009), Murshed (Murshed, Leong, & Yang, 2005), Hong et al.(T.-K. Hong, Yang, & Choi, 2005) and, li and Peterson (Ding et al., 2006), observed great enhancement of nanofluids' thermal conductivity. Dispersion of copper nanoparticles and alternatively carbon nanotubes provided the most promising result so far with observed thermal conductivity enhancement of 40% and 160% respectively in

comparison to the base fluid (Assael, Chen, Metaxa, & Wakeham, 2004; S. Choi, Zhang, Yu, Lockwood, & Grulke, 2001; Eastman et al., 2001).

Choi *et al.* (S. U. Choi & Eastman, 2001) found that the effective thermal conductivity of the CNTs aqueous suspensions is greater compared to that for water. They experimentally measured the effective thermal conductivity of a nanofluid containing 1.0 vol.% of multi-walled carbon nanotubes suspended in synthetic poly (α-olefin) oil and announced an enhancement of 160% in thermal conductivity (S. Choi et al., 2001). The researchers also studied the effect of sonication time on the dynamic viscosity, thermal conductivity and dispersion of MWCNT aqueous nanofluids. The results represented that the effective thermal conductivity of the nanofluid suspension increases and the viscosity decreases by elevating sonication time and temperature. The maximum increment of thermal conductivity was found to be 22.31% (ratio of 1.22), respectively, at the temperature and sonication time of 45°C and 40 min. (Sadri et al., 2014b). Philip et al. (Philip, Shima, & Raj, 2007) investigated the effective thermal conductivity enhancement of kerosene-based Fe_3O_4 colloidal suspensions under the influence of a magnetic field and the data showed that the thermal conductivity enhanced 300% ($k_{nanofluid}/k_{base\text{-fluid}} = 4.0$) at the concentration of 6.3 vol.% and particle size of 6.7 nm.

Enhancement of convective heat transfer of nanofluids was reported by Zeinali Heris et al.(Zeinali Heris, Nasr Esfahany, & Etemad, 2007), , Jung et al.(Jung, Oh, & Kwak, 2009), Kim et al.(D. Kim et al., 2009) and Sharma et al.(Sharma, Sundar, & Sarma, 2009). Pak and Cho (Pak & Cho, 1998) investigated the heat transfer performance of γ-Al_2O_3 and TiO_2 nanoparticles dispersed in water and flowing in a horizontal circular tube at turbulent flow and constant heat flux conditions. The results represented that the Nusselt number of the nanoparticles aqueous suspensions increases by increasing the Reynolds number and nanoparticles concentrations. Moreover, they discovered that the convective heat transfer coefficient of the nanofluids is lower than that for water by 12% for a given

condition when the particle loading is 3 vol.%. They proposed a new heat transfer correlation to predict the convective heat transfer coefficient of nanofluids in turbulent flow regime. Annular heat exchangers are commonly used in industrial applications, particularly in heat transfer equipment. These heat exchangers have gained much attention from scientists and researchers and they have been used in various thermal systems such as air-conditioning, electronic devices, heating and ventilation systems, turbomachinery, gas turbines and nuclear reactors. Hence, investigating the heat transfer characteristics of annular heat exchangers and devising a novel technique to improve their performance play a key role in promoting energy savings (E Abu-Nada, Masoud, & Hijazi, 2008; Eiyad Abu-Nada & Oztop, 2009). Weerapun Duangthongsuk et al. (Duangthongsuk & Wongwises, 2009) studied the friction factor and convective heat transfer of TiO_2 aqueous suspensions (concentration of 0.2 vol.%) in a horizontal double-tube counter flow heat exchanger under turbulent conditions. They discovered that the convective heat transfer coefficient of nanofluids is slightly greater than that of the base fluid by about 6-11% and increases by decreasing the fluid temperature. Moreover, they showed that the temperature of the heating fluid has no significant effect on the heat transfer coefficient of the nanofluid. Izadi et al. (Izadi, Behzadmehr, & Jalali-Vahida, 2009) simulated the forced convection flow of Al_2O_3/water aqueous suspensions through a two-dimensional annular heat exchanger (in which the working fluid was Al_2O_3-water nanofluid) using the single-phase method under turbulent conditions. The results showed that the dimensionless axial velocity profile does not remarkably vary with the nanoparticle volume fraction. However, the temperature profiles are affected by the nanoparticle concentrations. They found that the convective heat transfer coefficient increases by increasing the nanoparticle concentration. CNT nanofluids have garnered much interest among scientists and researchers because of their remarkable physical and chemical properties (Gan & Qiao, 2012; Pramanik & Singha, 2015). Indeed, it has been

proven in previous studies that CNT nanofluids have high thermal and electrical conductivities (Harris; Otsubo, Fujiwara, Kouno, & Edamura, 2007) as well as excellent mechanical properties (M.-F. Yu, Files, Arepalli, & Ruoff, 2000). However, the main disadvantage of CNTs is their poor solubility and processability since they easily become entangled and moreover, they tend to aggregate in polar fluids. It has been shown that non-covalent functionalization of CNTs based on the π-π interactions of aromatic organic molecules such as sodium dodecyl sulfate (SDS) and cetyltrimethyl ammonium bromide (CTAB) improves the solubility of CNTs in polar solvents (Sadri et al., 2014b). Various techniques have been employed for covalent modification of carbon nanotubes such as treatment with ozone, oxidation, fluorination and free radical addition, 1,3-dipolar cycloaddition, nucleophilic addition, alkylation, plasma modification. Among these techniques, free radical grafting is a desirable technique for large-scale synthesis of CNTs with versatile functional groups due to its facile treatment and high reactivity (Yang, Qiu, Xie, Wang, & Li, 2010). In this technique, peroxides, aryl diazonium salts, substituted anilines or benzophenone are used as the starting materials (Peng & Wong, 2009; Yang, Qiu, Xie, et al., 2010). However, all of the aforementioned techniques typically require very harsh and drastic reaction conditions.

1.1 Problem statement

Fluids flow in the annular heat exchangers and their convective heat transfer are significant factor in the engineering systems due to their technological usages for instance thermal storage systems, cooling core of nuclear reactors, solar energy systems, electrical gas-insulated transmission lines, cooling systems, thermal insulation, gas-cooled electrical cables, compact heat exchangers, cooling of electronic devices, boilers and aircraft fuselage insulation to underground electrical transmission cables (Eiyad Abu-Nada & Oztop, 2009; Duka, Ferrario, Passerini, & Piva, 2007; Mohammed, 2008;

Passerini, Ferrario, & Thäter, 2008). Therefore, studies on the convective heat transfer in annular pipe heat exchangers are essential (Kashani, Jalali-vahid, & Hossainpour, 2013).

Most of covalent modification techniques of carbon materials involves many reaction steps, and the reagents and chemicals employed in these techniques are greatly prone to oxidation. These techniques can also damage the sp^2 hybridized carbon atoms of nanotubes, which in turn, have an influence on the electrical, thermal and optical properties of the carbon materials (Yang, Qiu, Xie, et al., 2010). These techniques also lead to other problems such as health hazards, equipment corrosion and environmental pollution. Hence, there was a critical need to develop a functionalization method that is environmentally friendly (Yang, Qiu, He, et al., 2010) in order to tackle the above-mentioned issues.

1.2 Scope of study

This study highlighted the development of an environmentally friendly, cost-effective and industrially scalable method for synthesizing MWCNTs and GNPs covalently functionalized with cloves, and to determine the effectiveness of this technique in improving convective heat transfer coefficient in an annular heat exchanger relative to that for water. In order to verify the success of the functionalization method, the clove-treated MWCNTs are characterized using FTIR, TGA, Raman, XPS, TEM, UV-vis spectroscopy and Zeta potential. Following this, the clove-treated MWCNTs and GNPs are dispersed into distilled water at three different nanoparticle concentrations of 0.075, 0.150 and 0.225 wt.% and, 0.025, 0.075 and 0.1wt% respectively. The rheological and thermo-physical properties as well as the Nusselt number, heat transfer coefficient, loop efficiency and performance index are evaluated for the C-MWCNT-DI water and CGNP-DI water nanofluids flowing through an annular heat exchanger in turbulent flow conditions.

1.3 Objectives

The principal objectives of the present research are summarized below:

1. To produce an environmental friendly, scalable, facile, covalent functionalization technique for synthesizing new types of nanofluids containing carbon nanotubes (CNTs) and graphene Nanoplatelets (GNPs)
2. To investigate convective heat transfer and friction loss of the developed nanofluids in annular concentric heat exchanger.
3. To conduct a Simulation study of the heat transfer to nanofluids in annular heat exchanger and compare the simulation data with the experimental data.

CHAPTER 2: LITERATURE REVIEW

2.1 Introduction

Energy management is a major concern for the most industries and technologies such as cooling devices, solar collectors and heat exchangers. However, the poor thermal conductivity of coolant (use water, propylene glycol, ethylene glycol and oil) limits the effectiveness and applications of heat transfer. So, a search for high efficiency heat transfer fluid is a challenging task for today. An innovative way to enhance liquid thermal conductivity is the dispersion of highly conductive solid particles within the base fluid (Ding et al., 2006).

Historical evidence has shown that nanoparticles and nanofluids were initially exploited by the artisans for color and shine effect, apparently no one was aware of their particles size and abnormal properties. Medieval artisans used the gold nanoparticles suspension for coloring the windows glass of cathedral. Also in 15^{th} century, Italian`s potters applied metal nanoparticles in liquid host to make shiny pottery (S. U. Choi, 2009).

Study to develop advanced energy transmission fluids began in 1985 at Argon National Laboratory (ANL). Masuda et al. (Masuda, Ebata, Teramae, & Hishinuma, 1993) firstly, studied thermal conductivity and viscosity influence of ultra-fine alumina, titanium dioxide and silicon dioxide in Japan. Following Masuda, Choi (S. U. Choi & Eastman, 1995) came up with the result of enhanced thermal conductivity of colloidal dispersion with nanoparticles which coined them nanofluids. Indeed, ANL`s research was the first coherent research in nanofluids and thermal conductivity enhancement; although some parts were in common with Masuda`s work but there were several distinctions between them. Dramatic enhancement of thermal conductivity of nanofluids, reported by previous researchers, attracted the present scientists and commercial investigators to launch an expansion effort on exploration of properties and utilization of nanofluids. The

importance and attraction of this area is apparent from compilation report on publication about nanofluids, Figure 2.1.

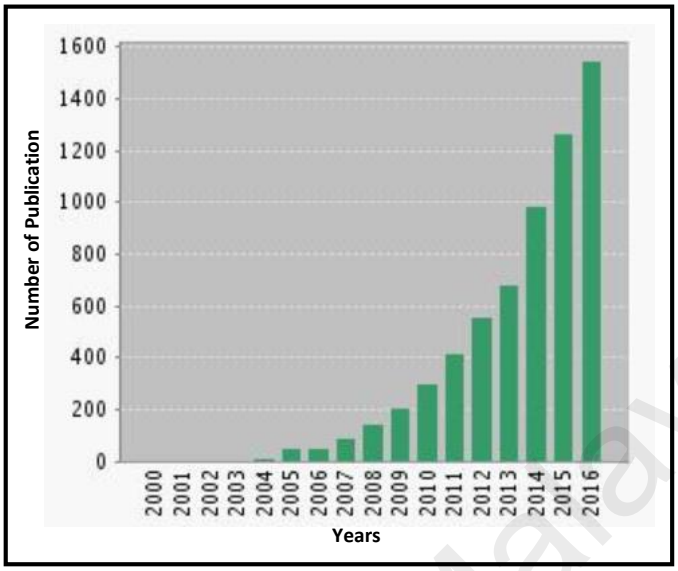

Figure 2. 1: Publications in nanofluids ("Web of Science," 2017)

Many scientists and engineer studied nanoparticle production and preparation of nanofluids for experimental and application. Also, they investigated effective function on thermal conductivity, viscosity and heat transfer of nanofluid suspensions like particle size and volume concentration, temperature, etc. In this chapter, review and discussion on experimental and basic theoretical activity in synthesis, thermophysical and heat transfer are presented.

2.2 Suspension of Milli and micro particles

Introducing of suspended solid particles into fluids is an innovative way of improving the thermal conductivities of fluids. The theoretical aspects of effective conductivity of the suspensions were first presented by Maxwell more than 140 years ago (1873) and the theory was applied for the particle suspensions from millimeter to micrometer size (Chol, 1995; Ghadimi, Saidur, & Metselaar, 2011).

Slurries can be prepared by adding various types of powders such as metallic, non-metallic and polymeric particles. The fluids containing suspended particles have shown higher thermal conductivities than that of common fluids. Generally, metals in solid form at room temperature show higher thermal conductivities than those of liquids. The thermal conductivity of copper could be taken as an example which is at ambient temperature about 700 times and 3000 times higher than those of water and engine oil respectively (Kakac & Pramuanjaroenkij, 2009; kumar Saini & Agarwal). Practically metallic liquids show higher thermal conductivities than that of nonmetallic liquids. Thus suspensions of solid metallic particles are expected to bear significantly higher thermal conductivities compared to the conventional heat transfer fluids (Mirmasoumi & Behzadmehr, 2008a). Despite the improved heat transfer coefficient of the base fluids including solid particle additives their practical application are limited due to the recurring problem of sedimentation of the large particles, clogging of flow channels, erosion of pipelines and introducing of additional pressure drops (Ding et al., 2006).

2.3 Nanofluids

Nanofluids, which are solid–liquid mixture materials containing nanometer sized solid particles, fibers, rods or tubes suspended in different base fluids (Mohamoud et al.), provide a promising technical selection for enhancing heat transfer because of its many advantages besides anomalously high thermal conductivity. Nanofluids represent the improved stability compared with conventional fluids added with micrometer or millimeter-sized solid particles because of size effect as well as Brownian motion of the nanoparticles in liquids (Mohamoud et al.).

With such ultrafine nanoparticles, nanofluids can flow smoothly in a microchannel without clogging and the size of the heat transfer system can be reduced for the use of nanofluids with high heat transfer efficiency. Various nanoparticles, such as carbon base

nanomaterials and metal-oxides (copper oxide (CuO), aluminum oxide (Al_2O_3), ron(III) oxide ($Fe_2O_{3)}$ and silicon dioxide (SiO_2)) have been used to produce nanofluids with enhanced thermal conductivity. Recently, remarkable enhancement in thermo-physical, rheological and heat transfer properties of carbon based nanofluids was reported in the literature (Ding et al., 2006; Singh & Gupta, 2016; Zubir et al., 2015).

2.3.1 Carbon base materials

Carbon nanostructures are carbon allotropes with at least one dimension in the nanometer range. Among different nanoparticles, carbon nanotubes (CNTs) in multi-walled, double or single types as one dimensional carbon nanostructures and graphene nanoplatelets(GNPs) as two dimensional carbon nanostructures have gained special interest caused by unique thermal, mechanical and electrical characteristics which make them suitable candidate for heat transfer issues (Fan, Zhang, & Liu, 2016).

2.3.1.1 Carbon nanotube(CNT)

Carbon nanotubes are allotropes of carbon, structured as long, thin hollow cylinders of carbon (Figure 2.2). A typical nanotube has the diameter of the order of a nanometer and the length of the order of a few micrometers. They can be thought of as a sheet of graphite (a hexagonal lattice of carbon) rolled into a cylinder. They were discovered in 1991 by S. Iijima (Iijima, 1991). He reported the first observation of multi-walled carbon nanotubes (MWCNT) in carbon-soot made by arc-discharge. About two years later, he made the observation of single-walled nanotubes (SWCNT)(Iijima & Ichihashi, 1993). The basic structural difference between MWCNT and SWCNT is that the former has concentrically nested multiple layers of graphene structures whereas the later has only a single layer of graphene structure. These intriguing structures have given a very broad range of electronic, thermal, and mechanical properties which have sparked excitement amongst the researchers in recent years. SWCNTs exhibit certain important electric

properties which are not shared by the MWCNTs and thus are more likely candidates for miniaturizing electronics. One useful application of SWCNTs is in the development of the first intramolecular field effect transistors (FETs)(Martel et al., 2001). On the other hand, MWCNTs have certain distinguished mechanical and thermal transport properties which make them suitable for applications related to structural composites, energy storage and heat transfer. Basic study had been performed over the past decade and indicated that carbon nanotube could possess a thermal conductivity order of magnitude greater than copper, ~3000 W/m-K for MWCNTs (P. Kim, Shi, Majumdar, & McEuen, 2001) and ~6000W/m-K for SWCNTs(Berber, Kwon, & Tomanek, 2000). This suggests that carbon nanotubes possess the potential to enhance thermal conductivity of base fluids like mineral oils, ethylene glycol, water, etc., even when added in small quantities. Though, SWCNTs have more potential to improve thermal conductivity; however, due to cost advantage and comparatively easy agglomeration of MWCNTs, they have been studied more in heat transfer applications. The peculiar property of MWCNTs has made researchers interested all together in an area directed towards heat transfer-based nanotechnology applications.

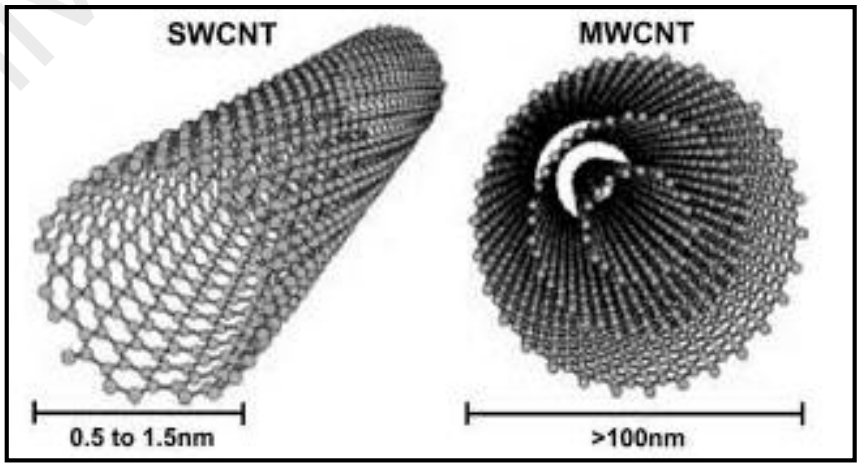

Figure 2. 2: Carbon nanotube

2.3.1.2 Graphene nanoplatelets(GNP)

Graphene nanoplatelets, a two-dimensional atomic sp^2 carbon layer,(Figure 2.3) by representing outstanding properties such as high specific surface area and excellent thermal conductivity which have attracted researchers in the last few years (Loh, Bao, Ang, & Yang, 2010). These unique properties make it a promising additive for many applications such as inkjet printing, conductive thin films, solar cells, polymer composites, aerogels and heat exchangers (Allen, Tung, & Kaner, 2009; Worsley et al., 2010). Nevertheless, the peculiar characteristics of a nanofluid cannot be achieved simply by mixing the pure fluid with nanoparticles. In fact, to high specific surface area, graphene presents tendency to agglomerate by strong π-π stacking interaction, while the dispersibility of graphene in aqueous media is considered as one of the most important factor in heat transfer equipment, films and composites (Sadri et al., 2016; Yang, Qiu, Xie, et al., 2010).

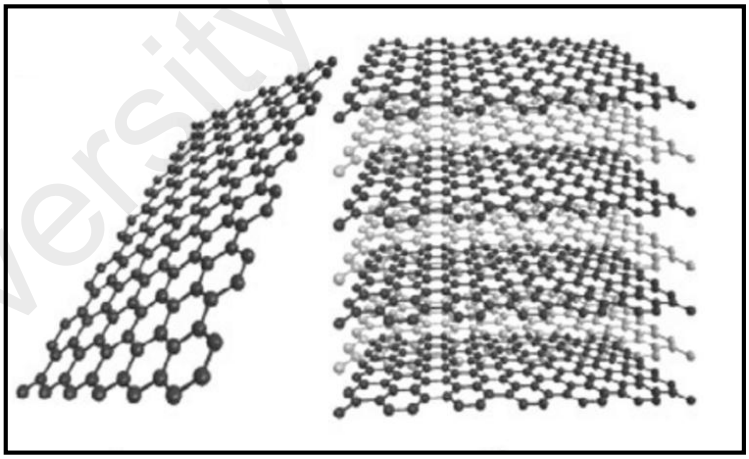

Figure 2. 3: Graphene nanoplatelets

2.4 Preparation of nanofluids

A dominant influence on behavior of nanofluids is governed by the preparation procedure of them. Proper dispersion of nanoparticles in base liquid, stability of suspensions, durability and stable thermal conductivity of nanofluids are playing crucial roles in production of nanofluids. In general nanoparticles are produced in two ways, such

as the physical processes which includes the inert-gas-condensation technique and mechanical grinding method, and the chemical processes that include chemical precipitation, micro-emulsions, chemical vapour deposition, spray pyrolysis, and thermal spraying. In presence of oleic acid dispersant the suspensions of iron nanoparticles could be synthesized by Sonochemical approach (Q. Yu, Kim, & Ma, 2008). Generally, nanofluids are the suspension of nanoparticles such as metals (Cu, Ag, Au), ceramics (Al_2O_3, CuO, TiO_2, SiC) and also carbon components (GNP, MWCNT) in proper liquid like water, ethylene glycol and oil.

The small spherical particles velocity in suspension at the stationery state follow the Stokes law (Hiemenz, 1986).

$$V = \frac{2R^2}{9\mu}(\rho_p - \rho_l).g \tag{2.1}$$

Where, V is the particle's sedimentation velocity; R is the spherical particle's radius; μ is the liquid medium viscosity; ρ_p and ρ_l are the particles and the liquid medium densities respectively and g is the acceleration of gravity.

In this equation a balance of the gravity, buoyancy force, and the viscous drag of the suspended nanoparticles are properly presented. Considering Eq. (2.1), the speed of sedimentation of the nanoparticles could be retarded by executing the following measures: (1) reducing R, the nanoparticles size; (2) increasing μ, the base fluid dynamic viscosity and (3) lessening the difference of density between the base fluid and nanoparticles (ρ_p ρ_l). It can be seen that the reduction of the particle size should significantly reduce the speed of the nanoparticles sedimentation and make better the stability of the nanofluid suspensions, as V is equivalent to the square of R. As per the colloidal chemistry theories, when the particle size reduces to a critical size, Rc, then there will be no sedimentation due to the Brownian motion of the nanoparticles dispersed in base fluid (diffusion). Even though, smaller size particles have the greater surface

energy, which also increases the possibility of aggregation in particles. In fact the preparation of stable nanofluid suspensions are strongly connected with the addition of smaller nanoparticles and prevention of the aggregation process (Wu, Zhu, Wang, & Liu, 2009).

Generally, nanofluids are the suspension of nanoparticles such as metals (Cu, Ag, Au), ceramics (Al_2O_3, CuO, TiO_2, SiC) and also carbon components (Diamond, MWCNT) in proper liquid like water, ethylene glycol and oil, the procedure of mixing nanoparticles with basic liquid are divided in two main techniques: two-step method and one –step method

2.4.1 Two-step method

The first and classic method of preparing the nanofluids was the two-step method, which was also the most common way for nanofluids synthesis in the last decade. In this method the prepared nanoparticle by physical or chemical methods are dispersed in base liquid. The size of nanoparticles is maintained to prepare different nanofluids with different particle size and having different properties. One of the disadvantages of this method is agglomeration and settlement of nanoparticles in host liquid due to van der Waals bonding effect. Ultra sonication or advanced mechanical mixing devices are used for well dispersion of nanoparticles and reduction of agglomeration effect. Sonication and mixing time should be optimized for obtaining suspension of smaller nanoparticle size, higher stability loading to higher thermal conductivity and also lower viscosity of nanofluids (Tavman & Turgut, 2010). This method has shown a fairly good result for oxide nanoparticles (S. U. Choi, 2009).

2.4.2 One step method

Nanofluids containing metal nanoparticles such as copper is preferred to prepare in one step method to prevent nanoparticles from oxidation. In this process the nanoparticles are formed and dispersed in the fluid in a single process. Direct evaporation has occurred in one step method which prevents nanofluid from agglomeration and produce nanoparticles which remain dispersed and stable in the base fluids. With reference to Figure 2.4, the current technique involves condensing of nanophase powders from the vapor phase directly into flowing low-vapor-pressure liquid in a vacuum chamber (Chopkar, Das, & Manna, 2006; Eastman et al., 2001). Well dispersed copper nanoparticles (Cu) in the ethylene glycol enhances the base fluid thermal conductivity up to 40% at the nanoparticle concentration of 0.3 vol%, which is markedly higher than that of the prediction of the effective medium theory (Wenhua Yu, France, Routbort, & Choi, 2008).

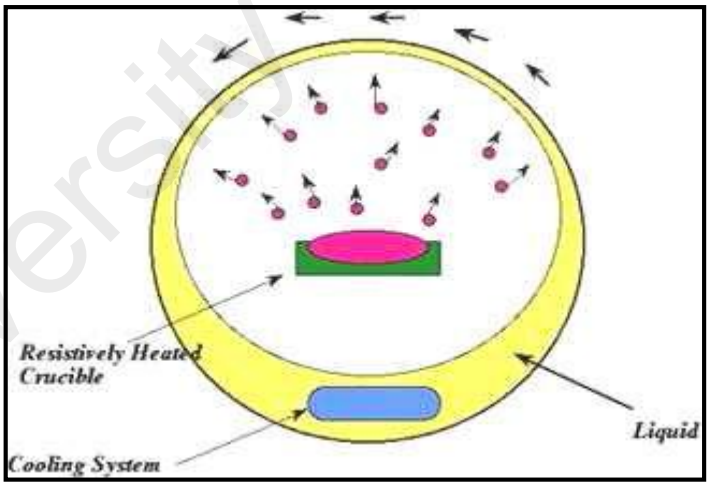

Figure 2. 4: Schematic of nanofluid production system (Eastman et al., 2001)

The production of nanofluid in one step method was small quantity and that was specifically for research purpose. However, it is unlikely to become the backbone of commercial nanofluid production. Mass production by this method would be difficult for two reasons. The processes operated in vacuum is significantly slow in production of

nanoparticles and nanofluids which limits the rate of production. Furthermore, the physical process of one step method is expensive.

These two methods are the most regular ways to produce nanofluids but there is still other way for nanofluids production like shape and size control synthesis of ZnO that has shown a good potential for controlling nanoparticles (Cao, Cai, & Zeng, 2006).Recently W.Yu et al. proposed a phase transfer method for kerosene based Fe_3O_4 nanofluids, which compared to two step technique needs less sonication time. There is no clear relation between particle size and sonication time (W.-Y. Chen & Chen, 2010). In this work, emphasis has given on carbon nanotubes dispersed in deionized (DI) water based on their optimal thermal properties as reported by others.

2.5 Stability of nanofluids

Preparation of a homogeneous nanoparticle suspension is still imposing a handle for the researchers because the strong van der Waals interactions force between particles always is resulted in formation of aggregation. A Stable nanofluid is obtained by the application of some methods including chemical or physical treatment. The methods are included the surface modification of the suspended nanoparticles, addition of surfactant, or usage of strong forces on the clustered nanoparticles. In order to modify hydrophobic behaviour of nanomaterials and enable dispersion in an aqueous media the propagating surface-active agents are loaded to the aqueous suspensions (Evans et al., 2008; Y Hwang et al., 2006; H. Zhu et al., 2007). Without any treatment there will be clogging, aggregation and sedimentation of the particles in the nanofluid suspension which could declining the suspension properties of effective thermal conductivity and dynamic viscosity and increase the specific heat. It is acknowledged by some researchers that the theory of aggregation or clustering is one of the most principal specifications of stability and phenomenal improvement in effective thermal conductivity of nanofluid suspensions

(Evans et al., 2008; Timofeeva et al., 2007), even though this finding may be more particular to the nanoparticles with high aspect ratio, containing single-walled nanotubes (SWCNTs). Philip et al.(Philip et al., 2007) and Evans et al. (Evans et al., 2008) stated that the high aspect ratio structure of the fractal-like clusters or agglomerations is a main reason of quick heat flow over long distances. They said that the thermal conductivity enhancement for the well dispersed composites were less in comparison to the composites with fractal clusters which showed notable increments, even with significant interfacial resistance. Moreover, Researchers (Gharagozloo & Goodson, 2010) evaluated fractal dimensions for the nanoparticle concentrations of 1 vol%, 3 vol% and 5vol% for Al_2O_3 in H_2O and discovered that clustering is a main factor for the enhancement of the measured thermal properties of the colloidal nanofluids. Contrary to this issue, another understanding showed that clustering and agglomeration reduced the enhancement of the thermal conductivity and stability. Hong et al. (K. Hong, Hong, & Yang, 2006; Özerinç, Kakaç, & Yazıcıoğlu, 2010) observed that the Fe nanofluids experienced the enhanced thermal conductivity due to their broken clusters during sonication, although this increment deducted as a function of elapsed time after dispersion. It is inferred that the stable nanofluids does not carry much emphasis as in case of agglomeration and clustering, which reduced erosion and wear in tube and channel.

Hence several methods were employed to improve stability of graphene in aqueous and organic media by chemical and physical methods containing covalent and non-covalent functionalization of graphene pH control and ultra-sonication.

2.5.1 Covalent functionalization

Recently, chemical functionalization is conducted with the assistance of hydrophilic organic groups like carboxyl, esters, alkalis and amine groups on the surface of carbon nanomaterials, which ensures the stability of the nanoparticles in the aqueous media. The

bundles of pipes are broken up into smaller bundles or individual tubes during the functionalization. Oxidizing carbon nanoparticles by the usage of strong acids, the mixture of sulphuric and nitric acids (Yang, Qiu, Xie, et al., 2010), is announced as an effective method of synthesizing water soluble carbon nanomaterials although there are many covalent reactions on carbon base nanomaterials such as, radical addition, alkali metal reduction, , Bingel cyclopropanation, nitrene cycloaddition, 1,3-dipolar cycloaddition, electrophilic addition, nucleophilic addition, carbene addition and Diels-Alder cycloaddition (Sun, Fu, Lin, & Huang, 2002; Tasis, Tagmatarchis, Bianco, & Prato, 2006). The free radical coupling is a promising method of functionalization of carbon nanostructure which has depicted facile way of covalent functionalization. In this method peroxides and aryl diazonium salts, substituted anilines and benzophenone were utilized as starting materials (Peng & Wong, 2009; Sadri, Hosseini, Kazi, Bagheri, Ahmed, et al., 2017; Sadri, Hosseini, Kazi, Bagheri, Zubir, et al., 2017; Sarsam et al., 2017).

2.5.2 Non-covalent functionalization

Sedimentation of nanoparticles in the nanofluids are retarded by the application of non-covalent functionalization method as one of the general methods for ceasing sedimentations. The stability and solubility of nanoparticles in aqueous media could be improved by the addition of surfactants as the hydrophobic surfaces of nanoparticles are altered to hydrophilic surfaces and contrariwise for non-aqueous base fluids. So utmost caution should be considered to employ adequate surfactant since insufficient amount of surfactant cannot make an appropriate coating that will induce electrostatic repulsion and compensate the van der Waals attractions forces (Yujin Hwang et al., 2008). Popular surfactants being noted in the literature can be enlisted as SDBS (Li et al., 2008; X.-j. Wang & Zhu, 2009), sodium dodecyl sulfate (SDS) (Yujin Hwang et al., 2008; Y Hwang et al., 2007), salt and oleic acid (Ding et al., 2007; Yujin Hwang et al., 2008), cetyl tri methyl ammonium bromide (CTAB) (Pantzali, Mouza, & Paras, 2009), dodecyl tri

methyl ammonium bromide (DTAB) and sodium octanoate (SOCT) (Madni, Hwang, Park, Choa, & Kim, 2010), hexadecyl tri methyl ammonium bromide (HCTAB), poly vinyl pyrrolidone (PVP)(Sato et al., 2011) and Gum Arabic (J. H. Lee, 2009). Selection of the proper surfactant is the most important part of the addition of surfactant method for stabilization of nanofluids. It used surfactants are anionic, cationic or non-ionic (H.-t. Zhu, Lin, & Yin, 2004) in nature. Surfactants has the drawbacks such as the elevated temperatures (X.-Q. Wang & Mujumdar, 2008; Wen, Lin, Vafaei, & Zhang, 2009) above 60 ^{O}C (Murshed, Leong, & Yang, 2008) where the bonding between nanoparticles and surfactant could be damaged. Due to the disintegration of the bondage of the nanofluids will lose its dispersibility and finally sedimentation of the particles will be happened (Azizi, Hosseini, Zafarnak, Shanbedi, & Amiri, 2013; Ghadimi et al., 2011).

2.5.3 pH control (effect of surface chemical)

The electro kinetic properties of a nanoparticles aqueous suspension are directly linked to its stability. A well-dispersed stabilized suspension could be obtained by introducing strong repulsive forces through a high surface charge density (Chou & Liao, 2005; X.-j. Wang & Zhu, 2009). Xie et al. (Xie, Lee, Youn, & Choi, 2003) observed a good stability of carbon nanotube in water by simple acid treatment of carbon nanotubes which converted the hydrophobic surface nature to hydrophilic as a result of the formation of hydroxyl groups. Enhancement of the thermal conductivity of the nanofluids is mainly dependent on the state of surface charge (Huang et al., 2009). In some experiments the pH variation was found influencing the shape conversion (Hadjov, 2009). Particles repel or attract each other in a liquid suspension. The distance between particles and the total interface energy E_{tot} that is the sum of the van der Waals attraction E_A and the electrostatic repulsion E_{el} between them are governed by the attraction or repulsion of the particles. The DLVO theory with the surface potentials φ_{d1} and φ_{d2} could be applied to evaluate approximately the E_{el} between two charged particles:

$$E_{el} = \frac{\epsilon_0 \epsilon_1 r_1 r_2}{r_1 + r_2} \left\{ 2\varphi_{d1}\varphi_{d2} \ln\left[\frac{1 + exp(-kx)}{1 - exp(-kx)}\right] + (\varphi_{d1}^2 + \varphi_{d2}^2) \ln[1 - exp(-2kx)] \right\} \quad (2.2)$$

Where, r is the radius of particles and x is an interparticle surface-to-surface distance, where the other symbols are representing their conventional meanings. The higher potential (φ_d or f) remarkably develops a larger potential obstacle for agglomeration. The interparticle (mobility-equivalent spherical particles) distance is about 100 nm for thein CuO nanofluid suspension at concentration of 0.3 vol.% and PZC (point of zero charge) of about 8.5–9.5.

Here, the colloidal suspension stability is needed to quantify with regard to collision efficiency α, which is responsible for colloidal nanoparticle growth. Then the rate constant of aggregation is related with the reciprocal value of the stability coefficient W, $k = \alpha k d_{iff} = k_{diff}/W$. Where, k_{diff} shows the rate constant of the agglomeration or coagulation between uncharged nanoparticles. A general relation of stability coefficient W to the total interaction energy E_{tot} can be derived by equation (2.3).

$$W = 2r \int_0^{\infty} exp\left(\frac{E_{tot}}{k_b T}\right) \frac{d_x}{(2r + x)^2} \quad (2.3)$$

By employing SDBS in Cu–H_2O nanofluid suspension, the surface charge of the nanoparticles increases with the pH of the colloidal suspension goes far from the isoelectric point. The zeta potential and the colloidal particles increase with the occurrence of further frequent attacks to the surface phenyl sulfonic and hydroxyl groups by potential-determining ions (phenyl sulfonic, H+ and OH group). Thus the thermal conductivity of the fluid changes with the enhancement of the suspension stability (Li et al., 2008). Effect of pH on nanofluids of Al_2O_3 was also investigated by Lee and co-

workers (K. Lee et al., 2009). The experimental results illustrated that when the nanofluid suspension had a pH value of 7.66, the agglomeration size was augmented by 51% and when it had a pH value of 1.7, the agglomerated particle size was deducted by 18%. Due to reduction in electric repulsion force the particles aggregated more as in pH value of 7.66. Hydroxyl groups (–OH) responsible for dispersion are produced at the surface of the Al_2O_3 particle when the Al_2O_3 particles are immersed in water. Solution pH basically governs the relevant reaction. With the lower pH level of the solution the hydroxyl groups (–OH) react with H+ from water which is resulted in a positively charged surface. Accordingly, the hydroxyl groups (–OH) react with OH from water and generates a negatively charged surface at the higher pH values of the colloid above the PZC(Peterson & Li, 2006).

2.5.4 Ultra-sonication vibration

The previously addressed techniques were developed to modify the surface characteristics of dispersed nanoparticles and to extinguish the creating of agglomeration of particles for preparing the stable suspensions. Homogenizer, processor and ultrasonic bath are all strong instruments for disintegrating the agglomerations or clusters compared to the others like high shear and magnetic stirrer as experienced by different researchers. However if it is not done in a controlled way, then it may physically damage the nanostructure by decreasing the corresponding aspect ratio (Ghadimi et al., 2011). Rad Sadri et al.(Sadri et al., 2014a) investigated the effects of ultrasonication, temperature and surfactant on the thermo-physical properties of multi-walled carbon nanotube (MWCNT) nanofluids. The results showed that the sonication time influences the thermal conductivity, viscosity and dispersion of nanofluids. It was found that the viscosity of MWCNT nanofluids increases to a maximum value at a sonication time of 7 min and subsequently decreases with a further increase in sonication time.

2.6 Thermo physical properties of nanofluids

In understanding the convective heat transfer behavior of the nanofluids the thermo-physical properties are some of the essential parameters. In this project, different thermo-physical properties are taken under consideration such as density, specific heat capacity, thermal conductivity, and viscosity.

2.6.1 Viscosity

Viscosity, dynamic property of fluids is used for calculation of pumping power in heat transfer system and plays a significant role in application of fluids. In industry, an optimization is needed between dynamic viscosity and heat transfer capability since it has a significant direct on the sizing of the heat transfer devices. As nanofluids are involved, to enhance the efficiency of system by increasing the thermal conductivity and in fact heat transfer of flowing fluid. Effect of any negative parameter on efficiency must be retarded; therefore, viscosity of nanofluids is taken under investigation to assess the efficiency of nanofluids. Experimental results for the dynamic viscosity of aqueous nanofluids are much limited than that of thermal conductivity. Also current studies in viscosity of CNTs Nanofluids (Ding et al., 2006; Garg et al., 2009; Phuoc, Massoudi, & Chen, 2011) are much less than metal oxide nanoparticles nanofluids. The parameters against which viscosity was studied were particle volume concentration, temperature and shear rate. These studies reveal that aqueous carbon nano materials Nanofluids behave as non-Newtonian shear-thinning fluids. Additionally, understanding flow behavior of carbon nanotube (CNT) nanofluids by developing mathematical viscosity models is an important area for taking the research into the next Phase. However, the viscosity of high aspect ratio nanofluids (Ding et al., 2006) are available from the prediction of a few empirical and analytical models. Spherical nanoparticles of metal oxides are mainly focused on the works having their basis from Einstein theory. In case of carbon

nanomaterials nanofluid, those models are incapable to correlate the experimental results properly because the shape of carbon nanomaterials does not satisfy previous assumptions. It is difficult to do particle size characterizations for cs and subsequently incorporate those characterizations in the Einstein viscosity model (Equation 2.4).

$$\mu_e = (1+ 2.5\nu_p)\mu_m \tag{2.4}$$

Where, μ_m, ν_p, and μ_e, are viscosity of the base fluid, particle volume fraction in the dispersion, and effective viscosity of the dispersion respectively. CNT aqueous nanofluids have indicated shear thinning or pseudo-plastic kind of non-Newtonian behaviour (Ding et al., 2006). However, there are a few works which have been done for correlating this behaviour with the theoretical models of non-Newtonian viscosity (Ding et al., 2006). The theoretical models contain the equations to correlate shear stress of a flowing fluid to shear rate. This could help in classifying the flow behaviour of the new nanofluids considering the behavioural parameters so far studied for different nanofluids, and thus it will help in directing future rheological studies. Power Law (Eq 2.5) and Herschel Bulkley equation (Equation 2.6) are the extensively employed models for the non-Newtonian flow.

$$\tau = K.\gamma^{\wedge} n \tag{2.5}$$

$$\tau = \tau' + K.\gamma^{\wedge} n \tag{2.6}$$

Where, γ, K, τ, &, τ' and n are respectively, shear rate, flow consistency index, shear stress, yield shear stress and flow behaviour index. The value of parameters ‘K’ and ‘n’ signify the flow behaviour in quantitative and qualitative terms respectively. A high value of ‘K’ is attributed to high viscous behaviour and a low value of ‘n’ is attributed to high degree of non-Newtonian behaviour of the fluid. Additionally, a few works have been performed on study of the influence of processing or ultra-sonication time and Temperature (Garg et al., 2009) on the dynamic viscosity of MWCNT nanofluids. The

motivation of theoretical model improvment for CNT suspensions could be obtained from the experimental work in this area.

2.6.2 Thermal conductivity

Heat transfer in a process can be increased by altering variety of parameters like temperature difference, heat transfer surface area and heat transfer coefficient of the flowing fluid. Heat transfer coefficient is mainly represented by function of Nusselt number, and thermal conductivity of fluid. Hence thermal conductivity enhancement of nanofluids became significant in heat transfer development of nanofluids. As previously noted, Argon National Labrotory (ANL) was the pioneer in nanofluids arena. Since then, numerous researches have been launched about thermal conductivity enhancement of metal oxide and carbon-based nanofluids. Based on literature, some parameters influence the thermal conductivity of nanofluids, such as Particle size, Material, Morphology, Particle concentration, Base Fluid Material, Temperature, Additives, Acidity (pH) and Particle Motion.

As the sequence of experiments and exploration of various nanofluids in Argon National Lab (ANL) continued, for the first time a dramatic enhancement of thermal conductivity observed by Choi et al. (S. Choi et al., 2001) for multiwalled carbon nanotubes (MWCNT) dispersed in synthetic poly (α-olefin) oil as a base fluid, they propagated a nonlinear of thermal conductivity enhancement up to 160% at only 1vol% concentration of Carbon nanotubes in oil. They have also explained the cause of this anomalous enhancement of strangely higher magnitude than theoretical prediction for nanofluids with particle high thermal conductivity (3000 w/m.k), shape and size of the carbon nanotubes. Xie et al. (Xie et al., 2003) subsequently published data where, enhancements in thermal conductivity were propagated for decene, ethylene glycol and water as base fluids. Data of Assael et al. (Assael et al., 2004; Assael, Metaxa, Arvanitidis,

Christofilos, & Lioutas, 2005) were studied on MWCNT nanoparticles stabilized in base fluid using nanosperse AQ, CTAB and SDS and as surfactant. Even though, both of these published works had much less enhancements in comparison with those reported by Choi et al. (S. Choi et al., 2001). In their analysis Xie et al. (Xie et al., 2003) had experienced the maximum enhancement of thermal conductivity of only 20% for 1% carbon nanotubes in decene by volume, whereas Assael et al.(Assael et al., 2004) observed the enhancement of 38%, for 0.6 vol% MWCNT`s-water nanofluids, using 0.1 wt% SDS (sodium dodecyl sulfate). Other researchers (Wen & Ding, 2004) observed 28% and 23% enhancements, respectively, at 20 ^{O}C and 40 ^{O}C for 0.84 vol% MWCNT aqueous nanofluids using SDBS as the dispersant. Their results were comparable with the data of Xie et al. and Assael et al. (Assael et al., 2004). In the comparison there was variations in the thermal conductivities and interfacial resistances of the used CNTs and those were the main reasons for the observed discrepancies with respect to Choi et al. (S. Choi et al., 2001). Additionally, poly-α olefin was used as the base fluid by Choi et al. (a lower thermal conductivity than water). They had reported the high percentage enhancement though the absolute enhancement was not as high as expected. SDBS was found to fail at elevated temperatures (Wen & Ding, 2004). Ding et al. reported a set of results using Gum Arabic as surfactant (Ding et al., 2006) and found the thermal conductivity enhancement of 79% and 28%, respectively, at 30 ^{o}C and 25 ^{o}C with weight concentration of 1% MWCNT in water. The researchers obtained the thermal conductivity enhancement increasing temperature and CNT concentration. The enhancement of the thermal conductivity was little higher than the values reported by Assael et al. (Assael et al., 2004), Xie et al., (Xie et al., 2003) and Wen and Ding. (Wen & Ding, 2004). They inferred that the prevailing discrepancy could be associated with the thermal properties of CNTs used, liquid-CNT interfacial resistance, and the aspect ratio of the CNTs used. In addition to that the base liquid also has some influence.

Lately L.Chen and H. Xie (L. Chen & Xie, 2010) by using Cationic Gemini as a surfactant reported thermal conductivity enhancements of 34.3% and 5.6% at a volume fraction of 0.6% with temperatures of 65℃ and 5℃ respectively, and shown the temperatures strongly effects on enhancement of thermal conductivity of MWCNT aqueous nanofluids dispersed by using cationic gemini surfactants. The enhancement is a bit lower than that published by Ding et al.(Ding et al., 2006). Moreover A. Indhuja et al (Indhuja, KS, Manikandan, & KS, 2013) reported the thermal conductivity enhancements of 8% and 33% at a concentration of 5 wt% with temperatures of 28 ^{O}C and 60 ^{O}C respectively.

Up to the present, published data in MWCNT based nanofluids mostly are paid attention to the thermal conductivity enhancement with parametric effects of base fluid, nanoparticle volume concentration, and temperature. Though parametric effects of particle size (Length and diameter) (Amrollahi, Hamidi, & Rashidi, 2008; Ruan & Jacobi, 2012), dispersant (surfactant)(Assael et al., 2004; Assael et al., 2005; Wen & Ding, 2004)and acidity (Ding et al., 2006) have been considered, only a few works have been focused in this area. As nanotubes are cylindrical in nature and exist as agglomerates, direct particle size characterization using techniques like Dynamic Light Scattering (DLS) is difficult for nanotubes. The mechanism of thermal conductivity increment in CNTs suspensions is still not quite developed. Many factors are claimed for the cause of enhancement. Studies revealed that the nanotubes are fast diffuser of current and heat (Berber et al., 2000). The ballistic conduction property of nanotubes is assigned to the large phonon mean-free path in the CNTs. As a result, the CNTs in liquids change the phenomena of heat conduction from diffusion in liquids to both fast diffusion and ballistic heat conduction or fast diffusion. Moreover, there is proof that an organized solid-like structure of a fluid at the interface region is a governing factor enhanced conduction heat dissipation from a solid wall to an alongside base fluid (Suzuki, 2000).

Therefore, it has been suggested that this organized liquid/solid interface structure leads to the energy transport across the interface. In addition to the previous works, Jang and Choi (Jang & Choi, 2004) postulated another theory considering the nanoparticles Brownian motion as a potential factor for thermal conductivity enhancement of nanofluids by increasing temperatures. The mechanism revealed that by elevating temperature the dynamic viscosity of the base fluids decreases and accordingly the Brownian motion of the dispersed nanoparticles increases. It has been assumed that convection-like effects are enforced by particles Brownian motion which leads to thermal conductivity increment. Keblinski et al. (Keblinski, Phillpot, Choi, & Eastman, 2002) inferred that the enhancement of thermal conductivity of the nanofluids are not likely governed by the Brownian motion. Several years later Amrollai et al (Amrollahi et al., 2008) studied the effects of ultra-sonication time on sedimentation and thermal conductivity of carbon nanotubes-ethylene glycol suspensions and found strong dependence of the effective thermal conductivity on temperature and volume fraction of CNT nanofluids. In general, the thermal conductivity of the nanofluids suspensions increases by increasing ultra-sonication time. Brownian motion and the inter-particle potential, which influences the particle motion, were proposed to account for the phenomenon. Some researchers (Yang, Grulke, Zhang, & Wu, 2006) studied the impact of sonication energy/time on thermal conductivity of carbon nanotube-oil nanofluids and noted that the effective thermal conductivity reduced by increasing sonication energy/time. In the following works, Garg et al. (Garg et al., 2009) published the effect of ultra-sonication energy on the thermal conductivity and viscosity of Gum Arabic added MWCNT-water nanofluids. An optimum ultra-sonication energy (or sonication time) was found to exist that would be sufficient to achieve nanotubes' dispersion, without causing breakage of nanotubes. At the optimum ultra-sonication time of 40 min (energy of 113

J/g), a thermal conductivity enhancement of 20% was observed for 1 wt% MWCNT-water nanofluids.

Recently Ruan and Jacobi (Ruan & Jacobi, 2012) proved that the thermal conductivity of MWCNT-ethylene glycol suspensions was increased nonlinearly with an increase in sonication time/energy, and they obtained the maximum enhancement of thermal conductivity of 23% at a weight concentration of 0.5 % with the elapsed time of 1355 minutes. In addition, they observed that both the agglomerate sizes and the length of carbon nanotubes were reduced by the processes of sonication. But the reduction the agglomerate size is more important than the reduction of Length. In spite of these researches and experiments it can be found that stabilization by ultra-sonication is a usual way to crash the agglomerations and improve dispersion of nanoparticles into the base fluids. Although, there are limited reported research are available about sonication effects on properties of Carbon nanotubes nanofluids.

Wei YU et al. investigated a thermal conductivity of nanofluids containing graphene sheets in ethylene glycol media and reported up to 86% enhancement for 5.0 vol.% graphene dispersion (Wei Yu, Xie, Wang, & Wang, 2011). Moreover, Tessy Theres Boby and Ramaprabhu synthesized exfoliated graphene nanofluids with water and ethylene glycol as base fluids then investigated their thermal and electrical conductivities. They reported 14% enhancement in thermal conductivity for volume fraction of 0.056% at 25 °C with deionized water as base fluids(Baby & Ramaprabhu, 2010).

2.6.3 Density

Like viscosity, density of any fluid also has direct impact over pressure drop and pumping power and it also effects on Nusselt number, Reynolds number, thermal diffusivity as well as convective heat transfer coefficient of a heat transfer working fluid. Nevertheless, just a limited number of researches have been condcuted on density of

nanofluids. Sommers et al. (Sommers & Yerkes, 2010) found a linear relationship between density and particle concentration for Al_2O_3–propanol nanofluid. Vajjah et al. (Vajjha, Das, & Mahagaonkar, 2009) have also investigated on density of Al_2O_3, ZnO_2 and Sb_2O_4:SnO_2 EG-W based nanofluids.

2.6.4 Specific heat capacity

The specific heat capacity of a pure substance or a mixture is conventionally defined as the heat required to raise the temperature of 1 mole of the substance under specified conditions. The accurate determination of specific heat is very important in evaluating the thermal performance of nanofluids. For example, it is needed in the measurements of the thermal conductivity (S. K. Das, Putra, Thiesen, & Roetzel, 2003) the thermal diffusivity and the spatial temperature inside the flow in natural convection, it is one of the key parameters for describing the nano- fluids and the convective flow status (Zhou & Ni, 2008). As a result of considering the low nanoparticle volume fraction in base fluids, in some studies, the impact of nanoparticles on the specific heat capacity (C_P) of nanofluids seems too little to be taken into account (Yang, Zhang, Grulke, Anderson, & Wu, 2005). However, in most cases the volume fraction of nanoparticles has strong influence on the C_p (Buongiorno, 2006; Maïga, Nguyen, Galanis, & Roy, 2004). In the absence of available experimental data, two models have been extensively applied in the experimental and numerical nanofluid investigations.

Model I. Analogous to the mixing theory for ideal gas mixtures the specific heat of a nanofluid is expressed as

$$C_{p,nf} = \varphi C_{p,n} + (1 - \varphi) C_{p,nf} \tag{2.7}$$

Where, the subscripts n_f, n, and f refer to the nanofluid, base fluid, and nanoparticle, respectively. Due to the simplicity, Eq (2.7) has been used as a known formula in the

assessment of the heat transfer performance of nanofluids in many experimental investigations (S. K. Das et al., 2003) and theoretical simulations (Maïga et al., 2004).

Model II. This model is based on the classical and statistical mechanism (Avsec & Oblak, 2007; Buongiorno, 2006). Assuming that the base fluid and the nanoparticles are in thermal equilibrium, the nanofluid specific heat C_P should be predicted with the expression

$$C_{p.nf} = \frac{\varphi(\rho C_p)_n + (1-\varphi)(\rho C_p)_f}{\varphi\rho_n + (1-\varphi)\rho_f} \quad (2.8)$$

Where, ρ is the density. In this model, the density variations of the nanofluid, nanoparticle and base fluids are involved. Equation (2.8) has also been adopted as a base formula in many nanofluid investigations, such as in the theoretical models of anomalous thermal conductivity, the thermal diffusivity measurement, and the heat transfer in convection (Zhou & Ni, 2008).

2.7 Heat transfer and pressure drop of nanofluid

The primary interest in nanofluids is the possibility of using these fluids for heat transfer purposes. So, the nanofluids are expected to be used under flow condition. To know how these fluids will behave, more studies on its flow and heat transfer feature are needed. Heat transfer between a fluid and a surface due to the microscopic motion of the fluid relative to the surface is defined as convective heat transfer. The effectiveness of heat transfer is described by the heat transfer Coefficient, h, which is a function of a number of thermophysical properties of the heat transfer fluids, among them the most significant ones are the thermal conductivity (k), heat capacity (C_P), viscosity (μ), density(ρ), and surface tension (σ). Although, measurement of the thermal conductivity provides an idea of how effective a nanofluid is as a thermal fluid, it does not show the entire picture. Recently, more tests have been conducted to investigate the performance

of the nanofluids in a convective situation. This is a more telling test because it is much more similar to practical applications, and shows what effects of particle size and viscosity might have on (Williams, Buongiorno, & Hu, 2008) a nanofluid's performance. The majority of these studies have used a pipe flow set up (Anoop, Sundararajan, & Das, 2009). These studies agreed that the nanofluids heat transfer coefficient has significantly improved. Anoop et al.(Anoop et al., 2009) found 25% increase in alumina nanofluids, with even greater increases in the entrance region. However, an increase in thermal conductivity does not necessarily imply an increase in heat transfer coefficient. Wang et al. (X. Wang, Xu, & S. Choi, 1999) estimated the viscosity of Al_2O_3 and CuO nanoparticles dispersed in water, vacuum pump fluid, engine oil and ethylene glycol and found 30% enhancement with Al_2O_3/water nanofluid at 3% volume concentration. Suresh et al. (Suresh, Chandrasekar, Selvakumar, & Page, 2012) experimentally investigated the convective heat transfer and friction factor characteristics in the plain and spiralled rod inserts in a plain tube under laminar flow with constant heat flux with Al_2O_3-water nanofluids. The experimental results of Nusselt number for 0.5% nanofluid with spiralled rod inserts under laminar flow showed a maximum of 24% higher than the plain tube and the isothermal pressure drop of nanofluids with spiraled rod inserts were about 5% to 15% higher than the plain tube. Syam Sundar et al. (Sundar, Singh, & Sousa, 2013) studied and theoretical determined the effective thermal conductivity and viscosity of magnetic Fe_3O_4/water nanofluid. The thermal conductivity and viscosity of the nanofluids were increased with an increase in the particle volume concentration. Viscosity enhancement was greater compared to thermal conductivity enhancement at the same volume concentration and temperature. Heris (Heris, Etemad, & Esfahany, 2006) found that copper based nanofluids had provided an increase in thermal conductivity. However, aluminium based nanofluids showed greater increases in heat transfer coefficient. The authors observed that the larger particle size and larger viscosity of the

copper fluids caused worst performance in convection tests. Although these anomalies have been reported by others, there has been far too little testing done to offer conclusive explanations why some nanofluids provide small improvement in convection than in conduction.

Shear rate is a parameter which can affect the thermal conductivity of nanofluid. Lee and Irvine investigated the effect of shear rate on the thermal conductivity of Non-Newtonian fluids. (D.-L. Lee & Irvine, 1997). They found that increasing the shear rate would increase the thermal conductivity of the fluid. Shin and Lee (Shin & Lee, 2000) measured the thermal conductivity of suspensions containing micro particles (20-300μm) under Couette flow. This study also showed that increasing the shear rate had increased the thermal conductivity of the fluids. Although neither of these studies used nanofluids, they are still relevant. Any practical application of nanofluids would subject them to shear. Understanding how they perform under shear, is therefore critical. A setup of similar to that used by Shin and Lee was used in this study to determine the effects of shear on nanofluids.

2.8 Simulation study

Numerical investigations on nanofluids reported in the literature are classified and accumulated on the basis of single and multiphase models. Variable or Constant effective thermo-physical characteristics with adding the temperature term into the expression are considered in the single phase model. Presently intensive efforts are given on formulating the thermo-physical characteristics of nanofluids suspensions considering the nanoparticle size, morphology, temperature, and other physical impacts. Thus the single phase model is the most appropriate if the nanofluid characteristics are adequately assessed with higher conformity simulation involving less computational time and complexity. On the other hand, in multiphase flow both the solid particles and the liquid

movement are considered at various velocities due to external factors such as turbulent, Brownian and gravitational effects. The relative motion concept provides relative friction leading to other effects such as turbulent damping due to resultant forces acted on the particles.

Other interaction such as diffusion also introduces changes in the transport mechanism of the flow. Thus, the dynamics of the nanoparticles and their interaction with the flow field can be observed and quantitatively determined. Simulation using the single phase model on nanofluids with constant thermophysical properties was successfully done by Maiga et al. (El Bécaye Maïga et al., 2006; Maiga, Palm, Nguyen, Roy, & Galanis, 2005) who investigated nanofluid convection effect on uniformly heated tube as well as systems of parallel, coaxial and heated discs. The studies were performed both for the laminar and turbulent regimes and observed enhancement in heat transfer performance at constant Re which varied with the particle concentration and transport properties. Palm et al. (Palm, Roy, & Nguyen, 2006) first investigated the effect of temperature dependent properties in nanofluid convective performance who established formulas that incorporated temperature variable on dynamic viscosity and thermal conductivity calculations in addition to the particle loading. Afterward the laminar convective heat transfer flow between two coaxial and parallel disks with central axial injection were numerically simulated with the new set of correlations by them. further, they performed comparative investigation with the previous literature work performed by Maiga et al. (Maïga et al., 2004). They highlighted a significant difference between the application of variable and constant properties, illustrating the fact that temperature is a significant factor in propagating actual behaviour of nanofluid in shear flow. Numerical investigations on laminar to turbulent convective heat transfer using variable properties were performed by other researchers and reported different results (V Bianco, Chiacchio, Manca, & Nardini, 2009; Namburu, Das, Tanguturi, & Vajjha, 2009). Bahazamehr et al.

(Behzadmehr, Saffar-Avval, & Galanis, 2007) used the mixture model to simulate convection heat transfer in circular tube under turbulent regime. They indicated that the use of single phase model overestimate the actual Nu obtained through the experiment by Xuan and Li (Xuan & Li, 2003).

However, the utilization of mixture model indicated close agreement in comparison with the experimental data. They said that the accuracy of the proposed model can be further improved by taking into account the thermo-physical characteristics for nanofluid instead of considering volume fraction dependent nanofluid properties. Mirmousmi and Bahazamehr (Mirmasoumi & Behzadmehr, 2008b) and Akbarinia and Behzadmehr (Akbarinia & Behzadmehr, 2007) had also used the mixture model for laminar convection heat transfer investigation. The major difference between these studies is the parametric specification of the model whilst Mirmousmi and Bahazamehr (Mirmasoumi & Behzadmehr, 2008b) utilized a horizontal heated tube while the later worked on curved tube. The influence of nanoparticle size fluctuation ranging upwards from nanometer to micrometre for thermal performance was conducted by Akbarinia (Akbarinia & Behzadmehr, 2007) and they observed degradation of thermal performance. Recently, Bainco et al. (Vincenzo Bianco, Manca, & Nardini, 2011) conducted a numerical investigation on convective heat transfer of Al_2O_3 nanofluid using a mixture model in turbulent regime. In this research, the concentration gradient between laminar sublayer and bulk regions was taken into account by them which constitutes the variation in conductivity and viscosity without considering the effect of temperature contribution on the change of working fluid characteristics. The previous researchers had reported that the change in convective transport phenomena in relation to the increase in Reynolds number and particle loading was confirmed by them. Further, They implied a close agreement between the computational results and those calculated using empirical

correlation by Pak an Cho (Pak & Cho, 1998) and acknowledged the usage of mixture model to provide better evaluation of nanofluids suspensions heat transfer phenomena.

2.9 Summery

There are many theoretical and experimental works have been done on internal flow of nanofluids under different geometries and flow regimes but there are a few available investigations considered annular pipes. Moreover, there is no comprehensive study on green nanofluids flow in annular pipes.

CHAPTER 3: METHODOLOGY

The experiments were carried out in several stages. Firstly, the pristine MWCNTs and GNPs were covalently functionalized with cloves, and the C-MWCNTs-DI water and C-GNPs-DI water nanofluids were characterized using various analytical instruments. Following this, the thermo-physical properties of the synthesized nanofluids and base fluid were determined. Lastly, the convective heat transfers and frictional properties of the clove treated carbon nanofluids flowing through an annular heat exchanger were investigated then the results were compared with the numerical findings.

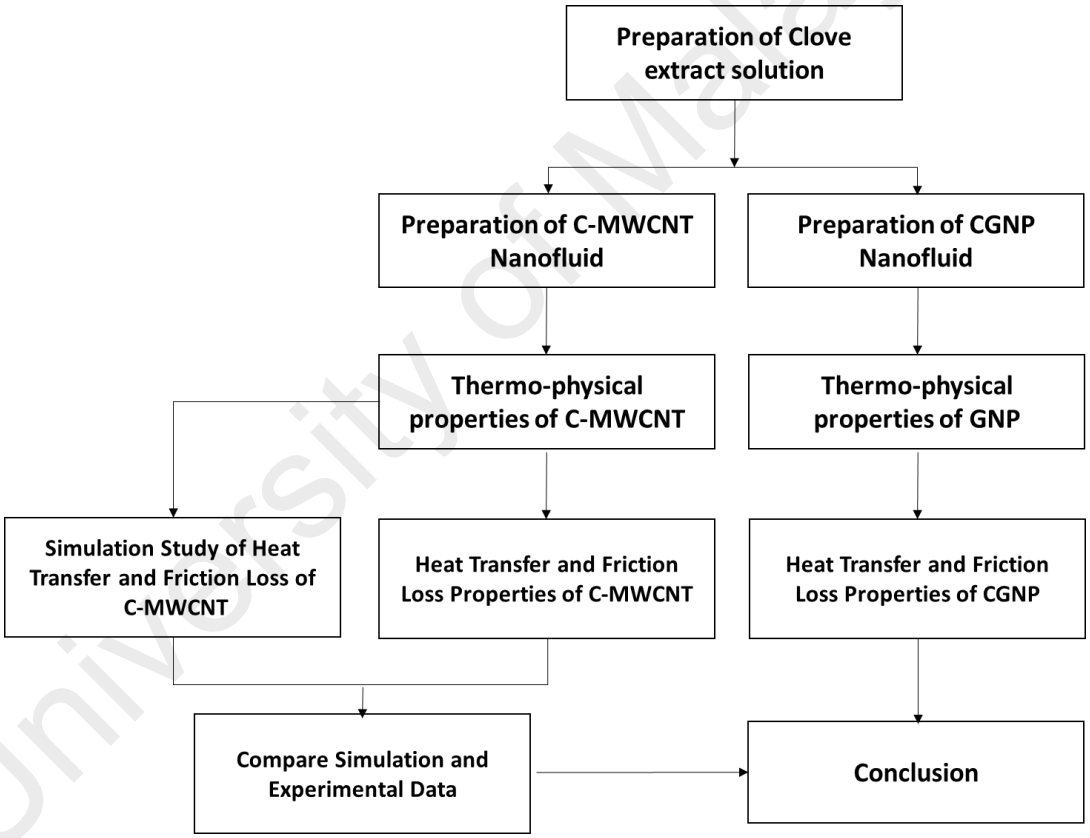

Figure 3. 1: Research Process Flowchart

3.1 Materials

Pristine multi-walled carbon nanotubes (MWCNTs) with a diameter less than 30 nm and purity of more than 95% and pristine graphene nanoplatelets (GNPs) with the thickness, lateral size, specific surface area and purity of 2 nm, 2 μm, 750 m^2/g and 99.5%, respectively were purchased from Nanostructured & Amorphous Materials Inc., (Houston, TX, USA) and XG Sciences, Lansing, MI, USA respectively. Hydrogen peroxide (H_2O_2, 30% concentration) was purchased from Sigma-Aldrich (M) Sdn. Bhd., Selangor, Malaysia. Fresh cloves, the sources of eugenol, vitamin C (ascorbic acid), and eugenyl acetate were purchased from a grocery store in Iran.

3.2 Preparation carbon nanocoolants

A novel, facile and eco-friendly technique for covalent functionalization of carbon nanostructures (MWCNTs and GNPs) with cloves was introduced for the first time in this study in order to prepare highly dispersed carbon nanomaterials in aqueous media. In this technique, eugenol and eugenyl acetate (which are the main component of cloves (Parthasarathy, Chempakam, & Zachariah, 2008)), were grafted onto the MWCNTs and GNPs using hydrogen peroxide and ascorbic acid (also a component of cloves) as the redox initiator (Mohammed, Abdulkadhim, & Noori, 2016). The clove extract solution was prepared using the following procedure.

3.2.1 Preparation of clove extract solution

Firstly, 20 g of ground cloves were added into a beaker containing 1000 ml of distilled water preheated at 80°C. The solution was then homogenized in heating mode at an agitation speed of 1000 rpm for 30 min. Lastly, the clove extract solution was filtered using a 45 μm polytetrafluoroethylene (PTFE) membrane in ambient conditions, using

Vacuum Filtration System (Vilkhu, Mawson, Simons, & Bates, 2008; Zubir et al., 2016) (Figure3.2).

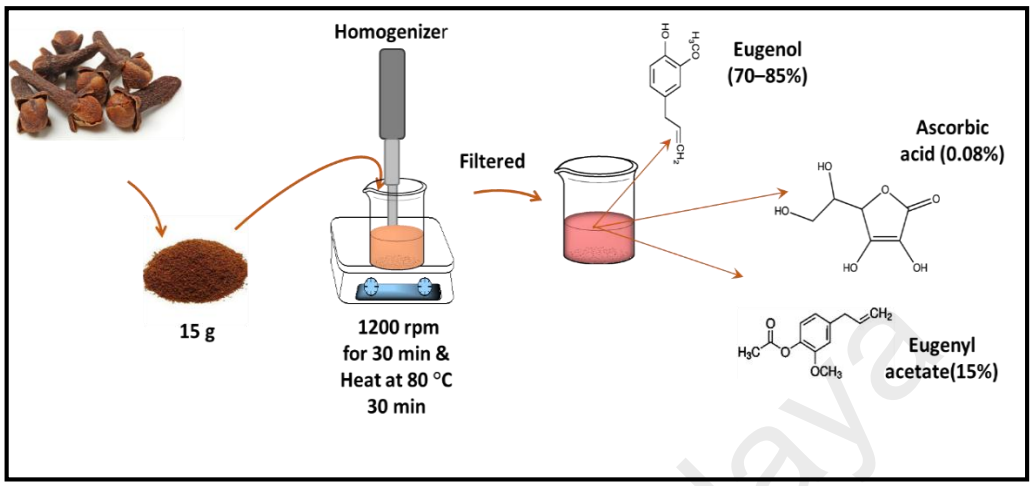

Figure 3. 2: Procedure used to prepare the clove extract

3.2.2 Preparation of C-MWCNT-DI water nanofluids

The clove-treated MWCNTs (C-MWCNTs) were prepared using the following procedure. Firstly, 5 g of pristine MWCNTs were poured into a beaker filled with 1000 ml of clove extract solution, followed by continuous stirring for 15 min to achieve a homogeneous black suspension. Then 35 ml of concentrated (30%) hydrogen peroxide was added gradually into the reaction mixture throughout the sonication time of 10 min. After sonication, the reacting mixture was heated at 80°C under reflux for 14 hours. The resultant suspension was centrifuged repeatedly at 14000 rpm and then washed with large amounts of distilled water until the suspension attained a neutral pH of 6-9. The functionalized sample was dried in a vacuum oven overnight at 60°C. In order to synthesize the C-MWCNT-DI water nanofluid, the C-MWCNTs were ultra-sonicated with distilled (DI) water as the base fluid for 10 min. It was observed that the clove-treated MWCNTs were highly stable in aqueous medium. The nanofluid were prepared for three different concentrations of C-MWCNTs: 0.075, 0.125and 0.175 wt.%. The graphical presentation of the sample preparation procedure is shown in Figure3.3.

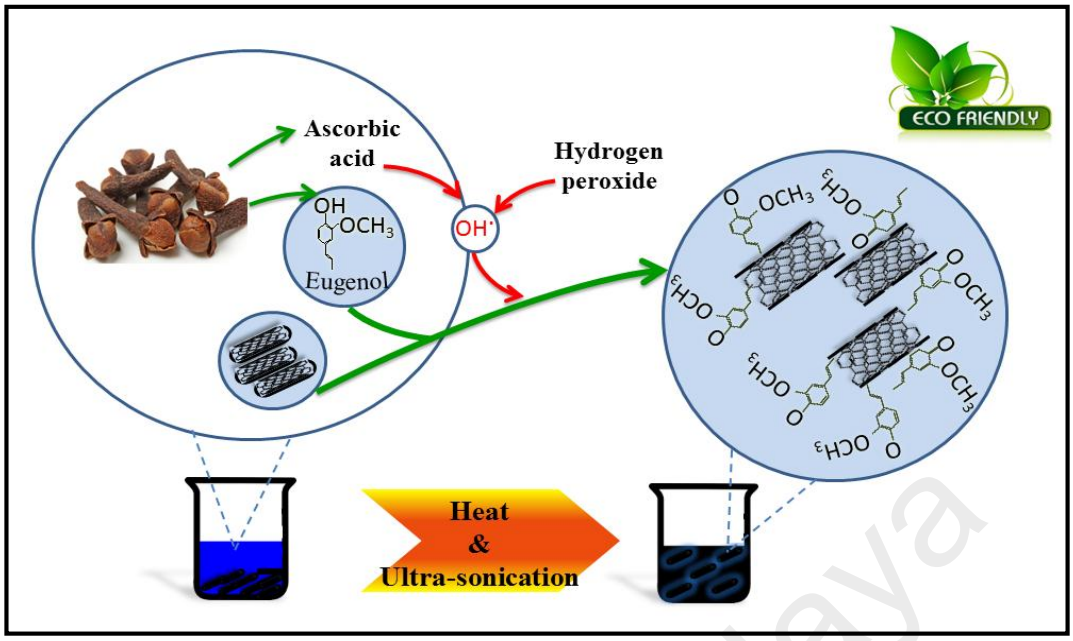

Figure 3. 3: Schematic of functionalization procedure of carbon nanotubes

Figure 3.4 (a) shows the initiation reaction for free radical grafting. In the initiation step, the ascorbic acid (*i.e.* vitamin C) reacts with hydrogen peroxide (a free-radical oxidizer that generates non-toxic by-products and leaves no chemical residue), producing hydroxyl radicals (Kitagawa & Tokiwa, 2006; Weydemeyer, Sawdon, & Peng, 2015). At high temperatures, the hydrogen peroxide becomes unstable and decomposes spontaneously into hydroxyl radicals. These reactions continue to take place at 80 °C in harmless water (Baskaran, Mays, & Bratcher, 2004). Figure 3.4 (b) shows that most of the generated hydroxyl radicals will attack eugenol to produce free radicals on the eugenol structure, which leads to linkage of the activated eugenol onto the surface of MWCNTs. In addition, the hydroxyl radicals can attack the MWCNTs directly, leading to formation of hydroxyl groups on the surface of MWCNTs.

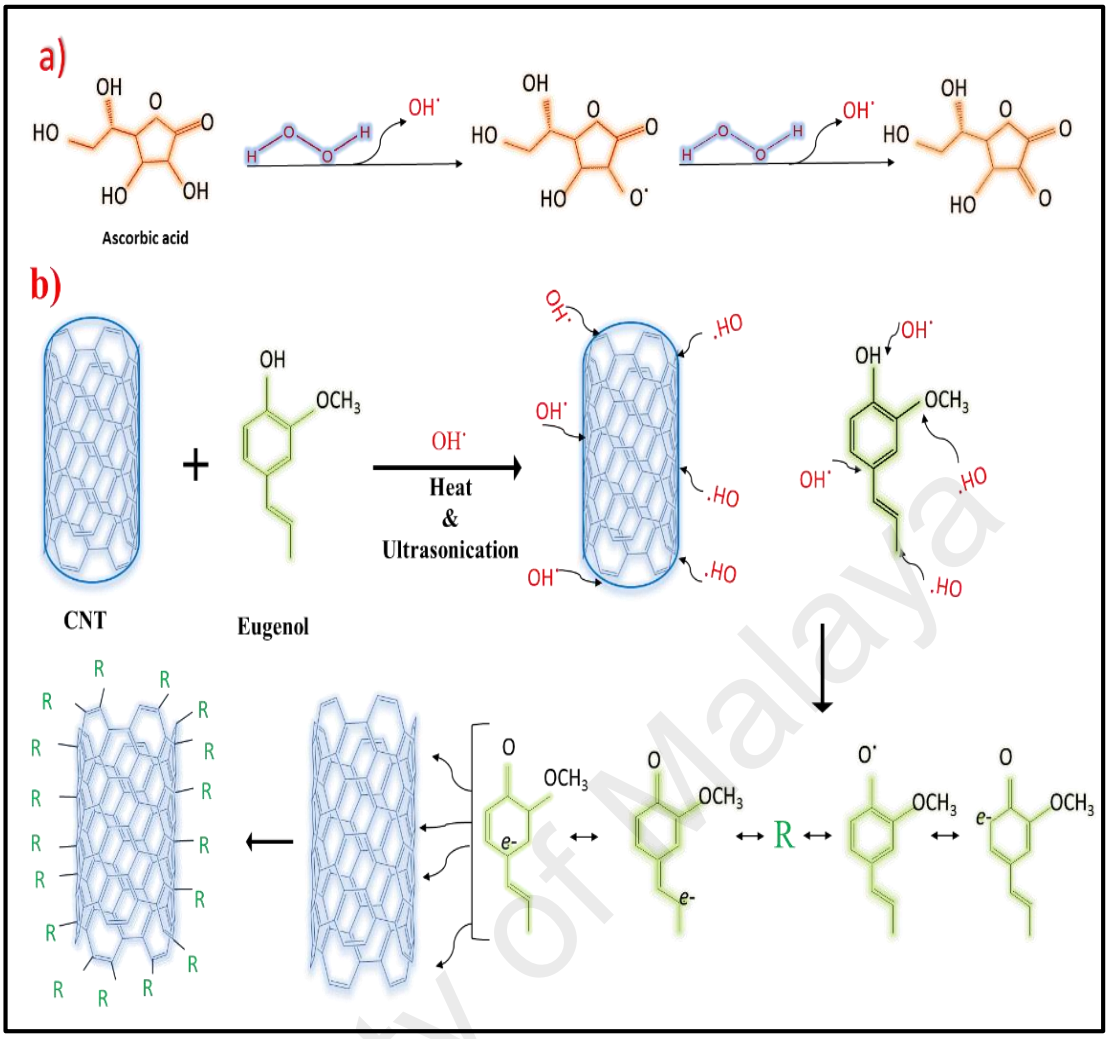

Figure 3. 4: (a) Initiation reaction for free radical grafting, (b) Formation of C-MWCNTs by free radical grafting technique

3.2.3Preparation of Clove treated GNPs-DI water nanofluids

The functionalization procedure was practiced as follows. Firstly, 5 g of pristine GNPs was poured into a beaker filled with 1000 ml of clove extract. This solution was stirred continuously for 15 min in order to achieve a homogeneous black suspension. Following this, 35 ml of hydrogen peroxide was added drop by drop into the reaction mixture throughout the sonication time of 10 min. Then it was heated at 80°C under reflux for 14 hrs. The resultant suspension was centrifuged at 14000 rpm and washed with a significant amount of DI water repeatedly until a neutral (pH of 6-9) was obtained in the suspension. The functionalized sample was then dried in a vacuum oven overnight at 60°C. It was discovered that the clove-treated GNPs (CGNPs) were highly stable in

aqueous medium, as expected. CGNP-water nanofluids were then synthesized as follows. In this study, DI water was taken as the base fluid. The CGNPs were dispersed into DI water by ultra-sonication for 10 min. The particle concentrations of the CGNPs were varied as 0.025, 0.075 and 0.1 wt%. Here, the free radial grafting pathway was adopted for functionalization.

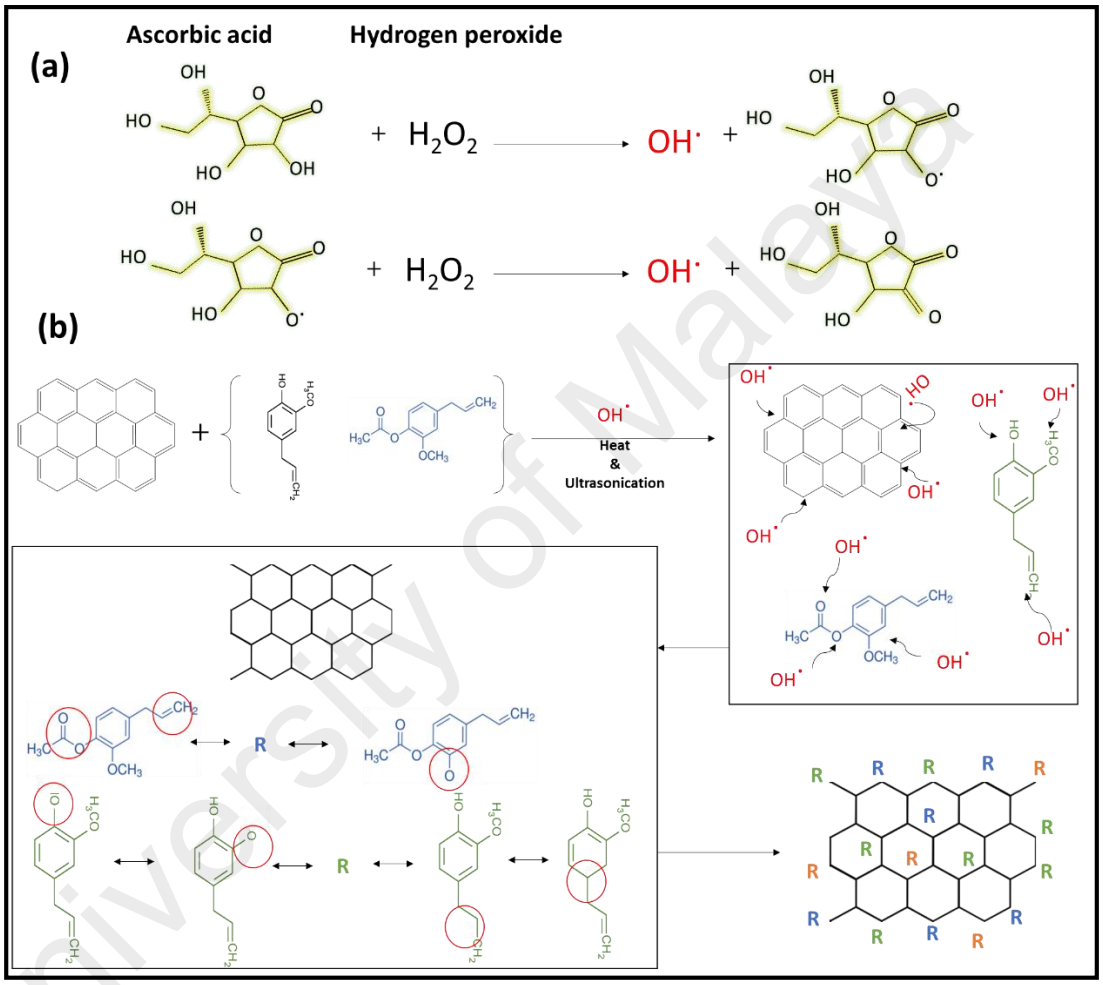

Figure 3. 5: (a) Initiation reaction for free radical grafting; (b) Formation of CGNPs by free radical grafting technique

The initiation reaction is illustrated in Figure 3.5 (a). Here, the vitamin C reacts with hydrogen peroxide, resulting the formation of hydroxyl radicals (Kitagawa & Tokiwa, 2006; Weydemeyer et al., 2015). It was attempted to highlight that the hydrogen peroxide became unstable such that it decomposed spontaneously into hydroxyl radicals at high temperatures (*e.g.* 80°C) (Baskaran et al., 2004). How the eugenol and eugenyl acetate

were grafted onto the surface of the GNPs are predicted in Figure 3.5 (b). Here, the hydroxyl radicals attacked the eugenol and eugenyl acetate, resulted the formation of free radicals on their structures. That led to the linkage of the activated components onto the surface of the GNPs. The hydroxyl radicals also attacked the GNPs directly, leading to the creation of hydroxyl groups (–OH) on the surface of GNPs.

3.3 Analysis methods

3.3.1 FT-IR

Fourier Transformation Infrared Spectrometer (Bruker, IFS-66/S, Germany) at the wave ranges of 4000-400 cm-1 was employed to analyse functional groups on the surface of the carbon nanostructures. Fourier transform infrared spectroscopy (FT-IR) samples were prepared by grinding a very low proportion of dry material with potassium bromide (KBr) to form a very fine powder. This powder was then compressed into a thin pellet for analysis. Figure 3.6 shows Fourier Transformation Infrared Spectrometer (Bruker, IFS-66/S, Germany).

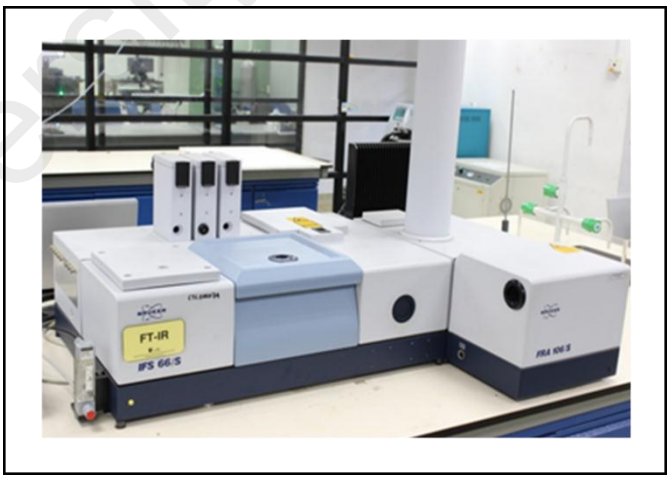

Figure 3. 6: FT-IR spectroscopy (Bruker, IFS-66/S, Germany)

3.3.2 Raman

Raman spectroscopy is becoming a technique of increasing relevance for the characterization of carbon materials. Apart from being non-destructive, it is simple and rather sensitive not only to the crystal structure (the long range order), but also to structural changes occurred at the molecular level (the short range order). Therefore, Raman spectroscopy has the high potential to access the chemical functionalization status.

Raman scattering, of monochromatic light, usually from a laser in the visible, near infrared, or near ultraviolet range. The laser light interacts with molecular vibrations, phonons or other excitations in the system, resulting in the energy of the laser photons being shifted up or down. The shift in energy provides information about the vibrational modes in the system. Raman spectra were collected using a Renishaw in Via Raman spectrometer equipped with laser excitation at 514nm. (Figure 3.7)

Figure 3. 7: Raman spectra (Renishaw in Via)

3.3.3 TGA

TGA is a thermal analysis technique, whereby modifications in the structure of materials are evaluated with varying temperature in a controlled atmosphere. The TGA instrument (TGA-50, Shimadzu, Japan) continuously weighs a sample as it is heated to temperatures of up to 1000 °C for coupling with Mass spectrometry gas analysis. As the temperature increases, various components of the sample are decomposed and the weight percentage of each resulting mass change can be measured. (Figure 3.8)

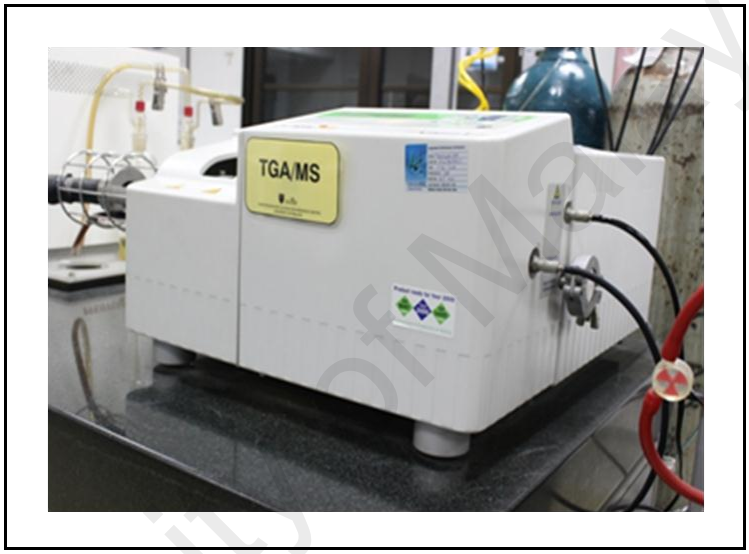

Figure 3. 8: Thermogravimetric analysis (TGA-50, Shimadzu, Japan)

3.3.4 XPS

X-ray photoelectron spectroscopy (XPS) is a surface-sensitive quantitative spectroscopic technique that measures the elemental composition at the parts per thousand range, empirical formula, chemical state and electronic state of the elements that exist within a material. XPS spectra are obtained by irradiating a material with a beam of X-rays while simultaneously measuring the kinetic energy and number of electrons that escape from the top 0 to 10 nm of the material being analyzed. Axis Ultra-DLD system, Kratos Analytical X-ray photoemission spectrometer (XPS) with Al Kα X-ray source (hν = 1486.8 eV) was used to recognize the functional groups in Clove-treated carbon nanostructures. CASA XPS programme with Gaussian-Lorentzian mix function

and Shirley background subtraction were used for deconvolution of the XPS spectra (Figure3.9).

Figure 3. 9: Axis Ultra-DLD system, Kratos Analytical X-ray photoemission spectrometer (XPS)

3.3.5 TEM

Transmission electron microscopy (TEM) is the primary technique to verify single particle dimensions and to identify agglomerations of the particles. The electron beam can be used to see features on the nanometer level. A major drawback to the use of TEM is that samples must be dried out of solution in order to be attached to the carbon matrix and placed in the vacuum chamber of the TEM; therefore, the particles are not exactly in the colloid state and agglomeration might occur during drying. However, TEM can be used in combination with dynamic light scattering to acquire exact sizing in nanofluid form. Hitachi HT7700 transmission electron microscope (Figure 3.10) was conducted to examine the morphological characteristics of the samples. For the TEM analysis, the samples were prepared by ultrasonically dispersing the nanoparticles in ethanol prior to collection on Lacey carbon grids.

Figure 3. 10: Hitachi HT7700 transmission electron microscope

3.3.6 Zeta potential

It is worth noting here that the stability of nanofluid is closely linked with its electro-kinetic properties. The high surface charge density of nanoparticles will generate strong repulsive forces, which helps in the attainment of well-dispersed, stable carbon nanoparticles suspensions. (L. Chen & Xie, 2010) Hence, zeta potential measurements were taken to investigate the electrophoretic behavior and further understand the dispersion behavior of MWCNTs and GNPs in water. (Bala et al., 2005; Mayer, Neveu, Secheresse, & Cabuil, 2004) Zeta potential values that are more negative than –30 mV or more positive than +30 mV are generally considered to represent sufficient mutual repulsion to ensure stability of the dispersion. The particles can no longer be strongly repelled close to the isoelectric point (i.e. point of zero charge) and therefore, they begin to aggregate and sediment over time (Ko et al., 2007). Zeta sizer Nano ZS two-angle particle and molecular size analyser (Malvern Instruments Ltd., Malvern, UK) was used to measure the zeta potential of the nanofluid samples (Figure3.11).

Figure 3. 11: Malvern Instruments Ltd Zeta sizer

3.3.7 UV-Vis

The solubility and stability of nanoparticles in the base fluids is very significant for practical application, the data from this instrument is limited on evaluating of the dispersibility of nanofluids. Shimadzu UV-1800 spectrophotometer (Figure 3.12) was used to determine the dispersibility of Clove treated carbon nanostructure-water nanofluids. For the UV-vis analysis, the sample nanofluids were diluted with DI water at a dilution ratio of 1:20 in order to ensure that the detectable wavelengths of the UV-vis spectrometer were able to pass through the samples. Following that the samples were poured into quartz cuvettes specialized for transmission of UV wavelengths and the absorbance of the samples were measured at pre-defined time intervals over the course of 63 days.

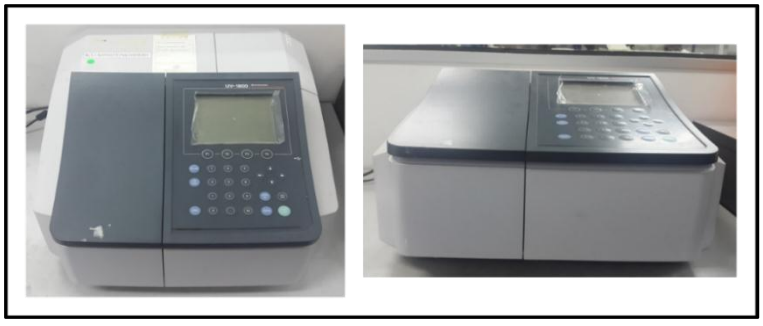

Figure 3. 12: Shimadzu UV-1800 spectrophotometer

3.3.8 KD2-PRO

The effective thermal conductivity of the samples was evaluated via KD-2 PRO portable field and laboratory thermal property analyser (Decagon Devices, USA). The KS-1 probe has a length and diameter of 60 and 1.3 mm, respectively. The accuracy of the thermal conductivity measurements is around 5%. In order to ensure equilibrium of the nanofluids, an average of 20 measurements were recorded over a 5-hrs period for each nanoparticle concentration and temperature. Calibration of the instrument was also done with DI water prior to collecting the measurements using nanofluids. Figure 3.13 shows thermal conductivity setup.

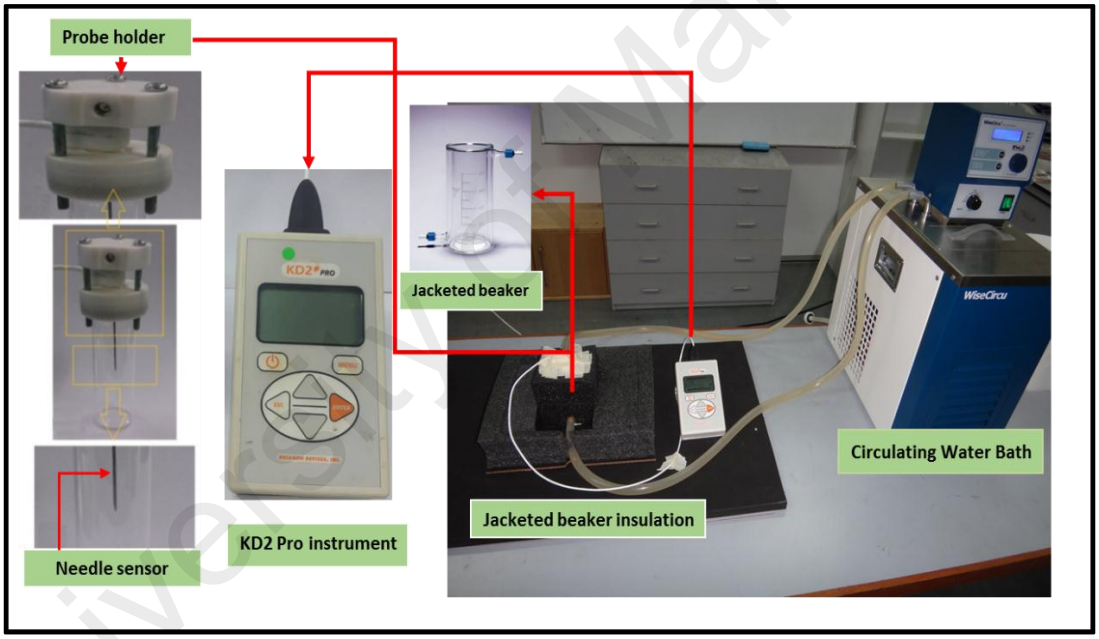

Figure 3. 13: Thermal conductivity measurements set up

3.3.9 Rheometer

Viscosity of nanofluids is one of the most critical parameters, which determines the quality of the heat transfer fluid. As in the case of simple fluids, the viscosity of a nanofluid depends largely on the temperature (Mehrali et al., 2014). Moreover, the viscosity of nanofluids is measured at different rotor RPMs to investigate if the nanofluids are Newtonian or non-Newtonian fluids. The viscosity of the nanofluid suspensions was

evaluated via Physica MCR rheometer (Anton Paar, Austria). The rotational rheometer consists of a moving cylindrical plate and a stationary cylindrical surface placed in parallel with a small gap between them (Figure 3.14).

Figure 3. 14: Anton Paar rheometer

3.3.10 Density

The density of the samples was evaluated via DE-40 density meter (Mettler Toledo, Switzerland), with an accuracy of 10^{-4} g/cm^3. The measurements were made in triplicate for each sample and temperature. Figure 3.15 depicts density meter setup.

Figure 3. 15: DE-40 density meter, Mettler Toledo

3.3.11 DSC

Differential scanning calorimetry (DSC) is a powerful tool to measure the heat capacity of the nanofluids. The difference in the amount of heat flow required for heating up a sample pan and reference pan are measured as a function of temperature. During the whole process, the sample and reference pans are maintained at nearly the same temperature throughout the experiment. The heat capacity of the reference pan is already known. By measuring the difference in heat flow, the heat capacity of the sample is obtained. If there are phase transitions happened in the sample pan, more or less heat will need to flow out of it than the reference to maintain both at the same temperature, so endothermal or exothermal peaks are shown on the DSC curves, corresponding to melting or freezing, respectively. The phase transition temperatures and latent heats are determined according to the DSC curves. The heat capacities of the nanofluids and DI water were obtained from a differential scanning calorimeter (Perkin Elmer DSC 800 differential scanning calorimeter with an accuracy of ± 1.0%).

3.4 Experimental procedure

The overall experimental set-up for convective heat transfer measurements includes an annular flow test section, a pump, a reservoir tank, a data acquisition system, a cooling unit, a heated test section, and the measuring instruments including a differential pressure transmitter (DPT) and a flow meter. The experimental heat transfer set-up is demonstrated in Figure 3.16. The aqueous suspensions were pumped using Araki EX-70 R magnetic pump from a 10 L stainless steel jacketed tank at a flow rate of 0–14 L/min. The pressure loss and flow rate were measured using PX154 wet/wet low differential pressure transmitter (OMEGA Engineering Inc., USA) and SE 32 inline paddle wheel transmitter respectively with display (Bürkert Contromatic Corp., USA). The pump flow was regulated using Hoffman Muller inverter. The concentric annular test rig consists of a

cartridge heater (OMEGA Engineering Inc., USA) with a length of 600 mm and a Diameter of 15 mm, which was inserted into the centre of a straight, seamless and horizontal tube made from stainless steel with a length of 900 mm, an outer and inner diameter of 33.4 and 26.7 mm, respectively. The heater was linked to a QPS VT2-1 variable voltage transformer (Success Electronics & Transformer Manufacturer Sdn. Bhd., Malaysia) and, voltage and current were measured to set the desired heating power. Three built-in K-type thermocouples (OMEGA Engineering Inc., USA) were cautiously installed a little away from the outside contact surface of heater surface in order to prevent disturbance in the boundary layer caused by the thermocouple probes protruding into the internal surface of the tube. The flow bulk temperature was measured using two platinum resistance temperature detectors (Pt-100 RTDs) which were placed inside the pipe at the outlet and inlet of the test section. The maximum error for thermocouples was ± 0.2℃. The thermocouples were connected to a GL220 10-channel midi logger (Graphtec Corporation, Japan) in order to monitor and record the temperature data. The test section was wrapped with thick fibreglass wool in order to reduce heat loss to the surroundings.

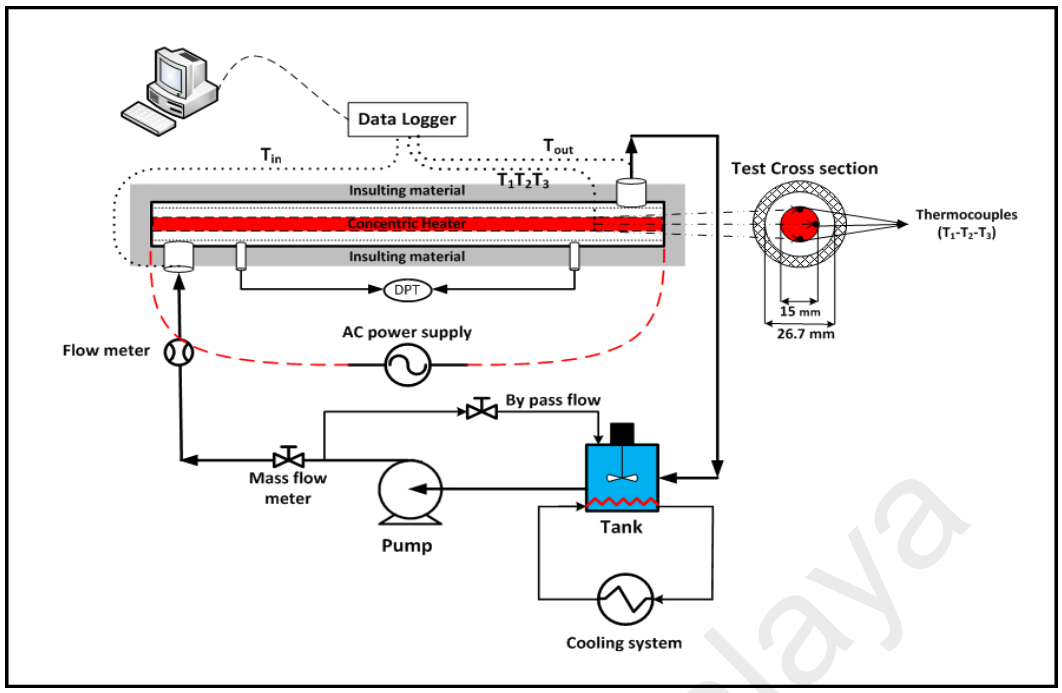

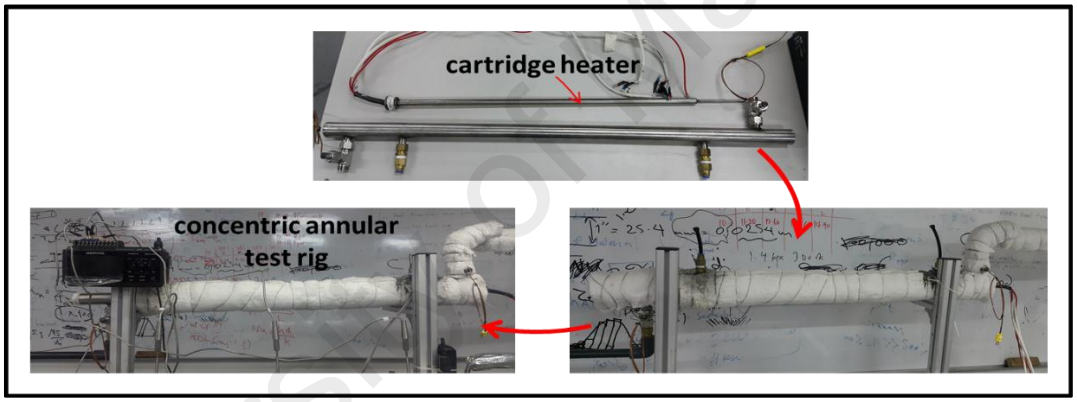

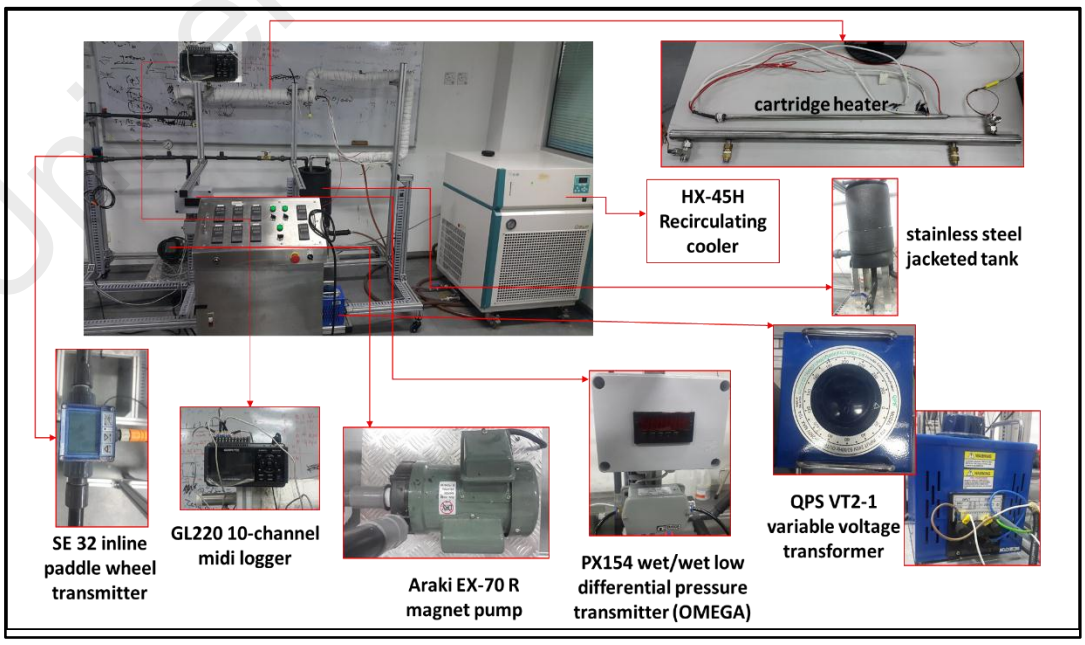

Figure 3. 16: Schematic diagram and photo of the experimental set-up

3.5 Data analysis

The experimental data were processed to assess the hydrodynamic and convective heat transfer performance of the annular heat exchanger. Taking into account conduction in the heater wall and convection heat transfer with the fluid in the test section, calibration was required to determine the temperature at the surface of the heater. Hence, an analysis based on the Wilson plot technique (Fernandez-Seara, Uhía, Sieres, & Campo, 2007) was done by equating the wall resistance. It shall be noted that there are important parameters used to determine the effect of the C-MWCNTs on the thermal properties of DI water, namely, convective heat transfer coefficient (*h*), Nusselt number (Nu) and pressure drop. The experimental heat transfer coefficient was determined from the measured bulk, surface, outlet and inlet temperatures using the Newton's law of cooling:

$$h = \frac{q^{"}}{(T_w - T_b)} \tag{3.1}$$

Where, T_w, T_b and $q^{"}$ represents the wall temperature, bulk temperature and heat flux, respectively. T_b is defined as $\frac{T_o+T_i}{2}$, where T_o and T_i are the outlet and inlet temperatures of the flow, respectively. The heat flux was determined using the following equation:

$$q^{"} = \frac{Q}{A} \tag{3.2}$$

Here, Q is the input power (VI) generated by the voltage transformer and A is the internal surface area of the pipe. Note that $A = \pi D_h L$. D_h is the annulus hydraulic diameter, which is defined as the difference between the inner annulus diameter and outer heater diameter. L is the annulus heated length. The input power (VI) was kept fixed at 900 W for the experiments. The Reynolds number (Re) was calculated using the following equation:

$$Re = \frac{\rho v \mathrm{D}_h}{\mu} \tag{3.3}$$

Here, ρ, v and μ represents the density, velocity and dynamic viscosity of the working fluid, respectively. The Nusselt number is given by:

$$Nu = \frac{h \times \mathrm{D}_h}{K} \tag{3.4}$$

Where, k and h represents the thermal conductivity and convective heat transfer coefficient, respectively. The friction factor (f) of the DI water and C-MWCNT-DI water nanofluids were determined from the pressure drop across the test section measured from experiments using the following equation (Eq.3.5):

$$f = \frac{\Delta P}{\left(\frac{L}{\mathrm{D}_h}\right)\left(\frac{\rho v^2}{2}\right)} \tag{3.5}$$

Where, ΔP and v represents the pressure drop and flow velocity, respectively.

3.6 Mathematical formulation and numerical procedure

In this study, the nanofluids are assumed to be homogeneous single-phase materials. Hence, the temperature and velocity fields are the same for the DI water and C-MWCNTs. For this reason, the nanofluids can be treated as classical Newtonian fluids and the continuity, momentum, and energy equations can be solved using the effective thermo-physical properties of nanofluids. Assuming steady-state conditions and constant thermo-physical fluid properties, the conservation equations (Chung, 2010)are given as follows:

Continuity equation:

$$\nabla.(\rho\vec{V}) = 0.0 \tag{3.6}$$

Momentum equation:

$$\nabla.\left(\rho\vec{V}\,\vec{V}\right) = -\nabla P + \mu\,\nabla^2\vec{V} + \rho g \tag{3.7}$$

Energy equation:

$$\nabla.\left(\rho C_p\,\vec{V}\right)T = K_{eff}\nabla^2 T + \mu\left\{2\left[\left(\frac{\partial u}{\partial x}\right)^2 + \left(\frac{\partial v}{\partial y}\right)^2 + \left(\frac{\partial w}{\partial z}\right)^2\right] + \left(\frac{\partial v}{\partial x} + \frac{\partial u}{\partial y}\right)^2 + \left(\frac{\partial w}{\partial y} + \frac{\partial v}{\partial z}\right)^2 + \left(\frac{\partial u}{\partial z} + \frac{\partial w}{\partial x}\right)^2\right\} \tag{3.8}$$

where K_{eff} is the effective thermal conductivity. The effective thermal conductivity is the sum of the molecular conductivity and turbulent conductivity calculated from the turbulence model.

In this study, we applied the standard *k*-*ω* turbulent model proposed by (Launder & Spalding, 1972) to model the turbulent regime.

The turbulence kinetic energy, *k*, for the *k*-*ω* model is given by:

$$\frac{\partial}{\partial t}(\rho k) + \frac{\partial}{\partial x_i}(\rho k u_i) = \frac{\partial}{\partial x_j}\left[\left(\mu + \frac{\mu_t}{\sigma_k}\right)\frac{\partial k}{\partial x_j}\right] + G_k - Y_k + S_k \tag{3.9}$$

where Y_k is the dissipation rate of kinetic energy due to turbulence, σ_k is the turbulent Prandtl number for kinetic energy, and $\mu_t = \alpha^* \frac{\rho k}{\omega}$. where, α^* is the viscosity damping coefficient, which equals to unity.

The specific rate of dissipation for kinetic energy, *ω*, for the *k*-*ω* model is given by:

$$\frac{\partial}{\partial t}(\rho\omega) + \frac{\partial}{\partial x_i}(\rho\omega u_i) = \frac{\partial}{\partial x_j}\left[\left(\mu + \frac{\mu_t}{\sigma_\omega}\right)\frac{\partial \varepsilon}{\partial x_j}\right] + G_\omega - Y_\omega + S_\omega \tag{3.10}$$

where Y_ω and σ_ω represent the turbulence dissipation rate and Prandtl number due to ω, respectively. The values of the constants are as follows: $\sigma_{\omega,1} = 2.0$, $\sigma_{k,1} = 1.176$, $\sigma_{\omega,2} = 1.168$, and $\sigma_{k,2} = 1.0$.

3.6.1 Geometric model and boundary conditions

Figure 3.17 shows the geometric model and computational domain of the concentric annular heat exchanger with length L. The inner and outer diameters of the concentric annular heat exchanger are represented by D_i and D_o, respectively. The outer tube is completely insulated from the environment whereas the inner tube is a solid electrical heater with a capacity of 50 kW/m^2. The following settings are selected for the geometric model: L = 0.55 m, D_i = 15 mm, and D_o/D_i = 1.78. The tube length is ~50 times its hydraulic diameter (D_h) in order to ensure that the turbulent flow is fully developed in the annular section.

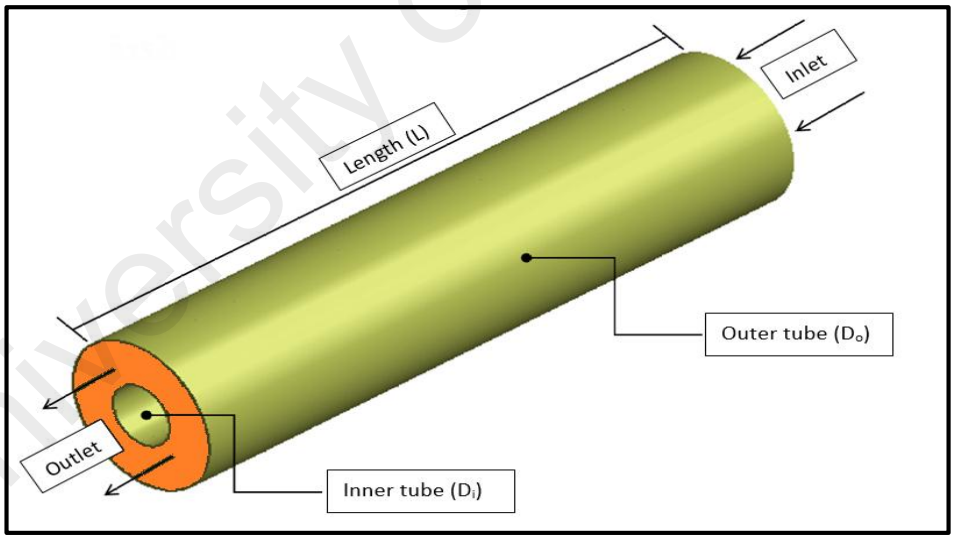

Figure 3. 17: Geometric model of the concentric annular heat exchanger

ANSYS Fluent Version 15 commercial CFD software is used to solve the governing equations. Figure 3.18 shows the computational mapped mesh for the concentric annular heat exchanger. The hexahedral cells were generated by dividing the concentric annular heat exchanger in peripheral, radial, and longitudinal directions. It will be easier to control

the number of cells by changing the number of divisions in the peripheral and radial directions and identify the parameter that has the most significant effect on the solution. We defined the inlet velocity, outlet pressure, and all of the thermo-physical properties of the fluid (including the average flow temperature) in order to solve the governing partial differential equations. These partial differential equations were converted into a system of algebraic equations using the finite volume approach. Figure 3.19 illustrates the method for finding the proper simulation data such as convective heat transfer coefficient and Nusselt number.

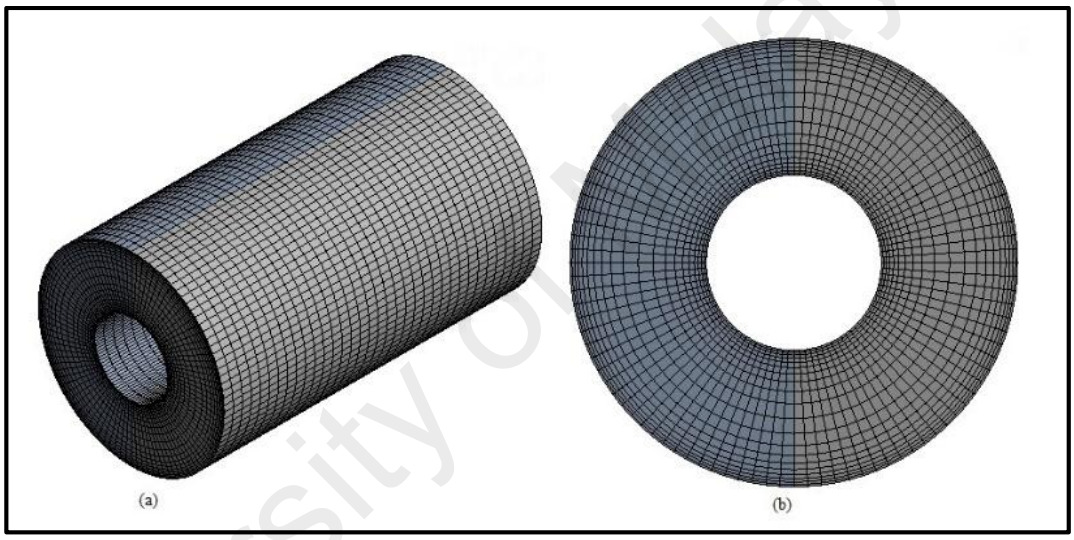

Figure 3. 18: Computational mesh of the concentric annular heat exchanger: (a) three-dimensional view and (b) front view of the geometric model. Note that the mesh is finer and more clustered near the walls of the concentric annular heat exchanger

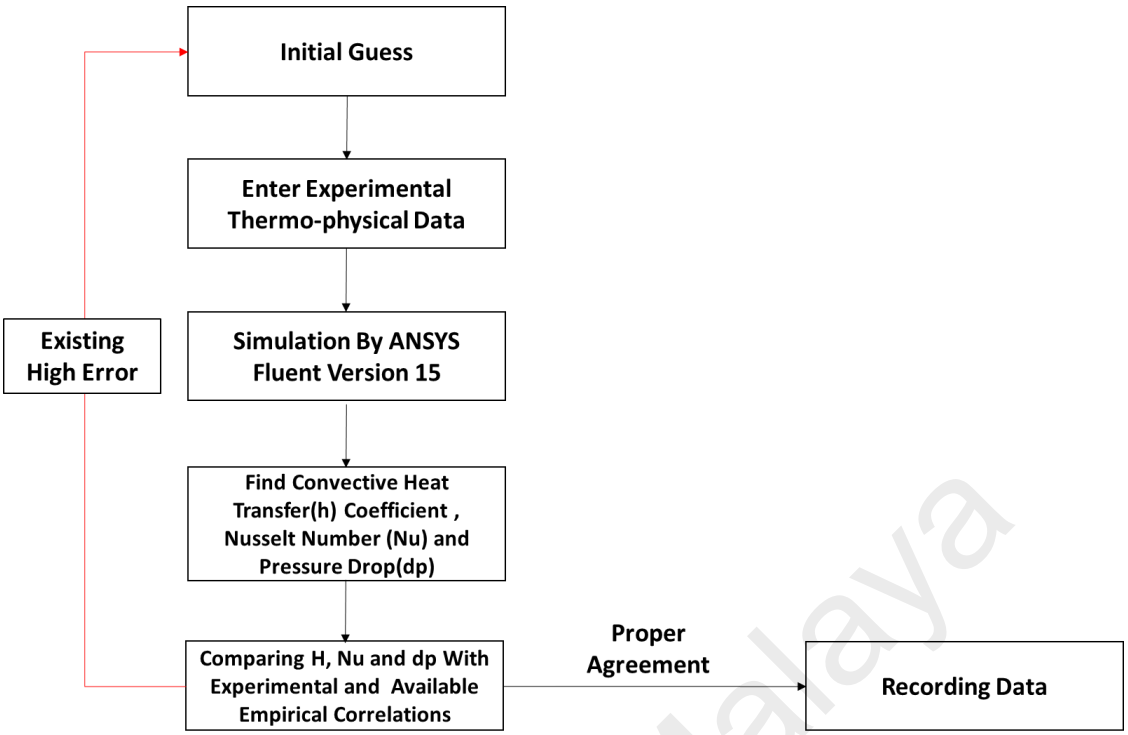

Figure 3. 19: Schematic flowchart of the trial and error procedure for finding a proper effective simulation data

Table 3. 1: The simulation parameters

Cases	Model	Changing parameters	Purpose
1	Single phase k-ω model	$\varphi = 0.075 - 0.175\ wt\%$ Fluid Velocity	Simulation data validation

3.6.2 Mesh dependency

Mesh independence test is conducted in order to determine the effect of mesh size on the simulation results and the results are shown in Figure 3.20. It can be observed that there is no significant difference in the Nusselt number when the number of mesh elements is varied at 500000, 1000000, and 1500000. Based on the results, we selected the lowest number of mesh elements (i.e. 500,000) in order to reduce computational time.

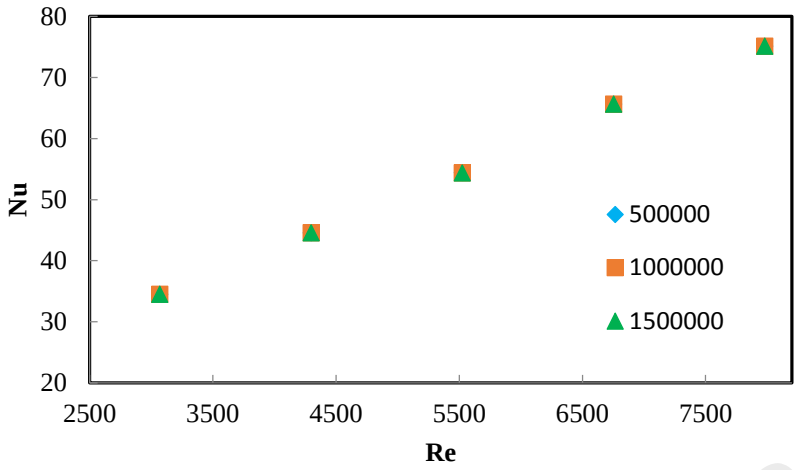

Figure 3. 20: Effect of mesh size on the Nusselt number for DI water

CHAPTER 4: RESULT AND DISCUSSION

4.1 Characterization of clove treated multi walled carbon nanotube

In this research, several characterization methods were employed to characterize the C-MWCNTs and C-GNPs. The morphology of the Clove treated MWCNTs and GNPs was examined using TEM, FTIR spectroscopy, Raman spectroscopy, X-ray photoelectron spectroscopy (XPS), transmission electron microscopy (TEM) and zeta potential measurements in order to verify the success of covalent functionalization. Figure4.1 (A) shows the FTIR spectra for the pristine MWCNTs and C-MWCNTs, which are represented by the transmittance (%) *versus* the wavenumber (cm^{-1}). It can be observed from Figure4.1 (A) that there are noticeable cues of the eugenol molecule in the C-MWCNTs compared to the pristine MWCNTs. The broad peak at 3448.19 cm^{-1} is ascribed to O–H stretching vibrations, which may be caused by the reaction between the MWCNTs and hydroxyl groups of eugenol and/or hydrogen peroxide. The symmetric and asymmetric sharp vibrations of C–H bonds are observed within a wavenumber range of 2850–3000 cm^{-1} for both MWCNTs and C-MWCNTs. A couple of peaks are observed within the wavenumber range of 1579–1639 cm^{-1}, which arise from C=C stretching vibrations of MWCNTs after opening due to the addition of electrophilic reactions between the main structure of MWCNTs and the –OH band of eugenol. The functionalization of MWCNTs by eugenol is confirmed by the peaks at 1428, 1386 and, 1077-1113 cm^{-1}, which are ascribed to CH_2 bending vibrations, out-of-plane CH vibrations and C–O stretching vibrations, respectively. The peaks within the wavenumber range of 1722–1763 cm^{-1} and the peak centred at 1621 cm^{-1} are assigned to O–C=O stretching vibrations, indicating the formation of carboxyl groups at the main structure of MWCNTs(Sadri, Hosseini, Kazi, Bagheri, Ahmed, et al., 2017).

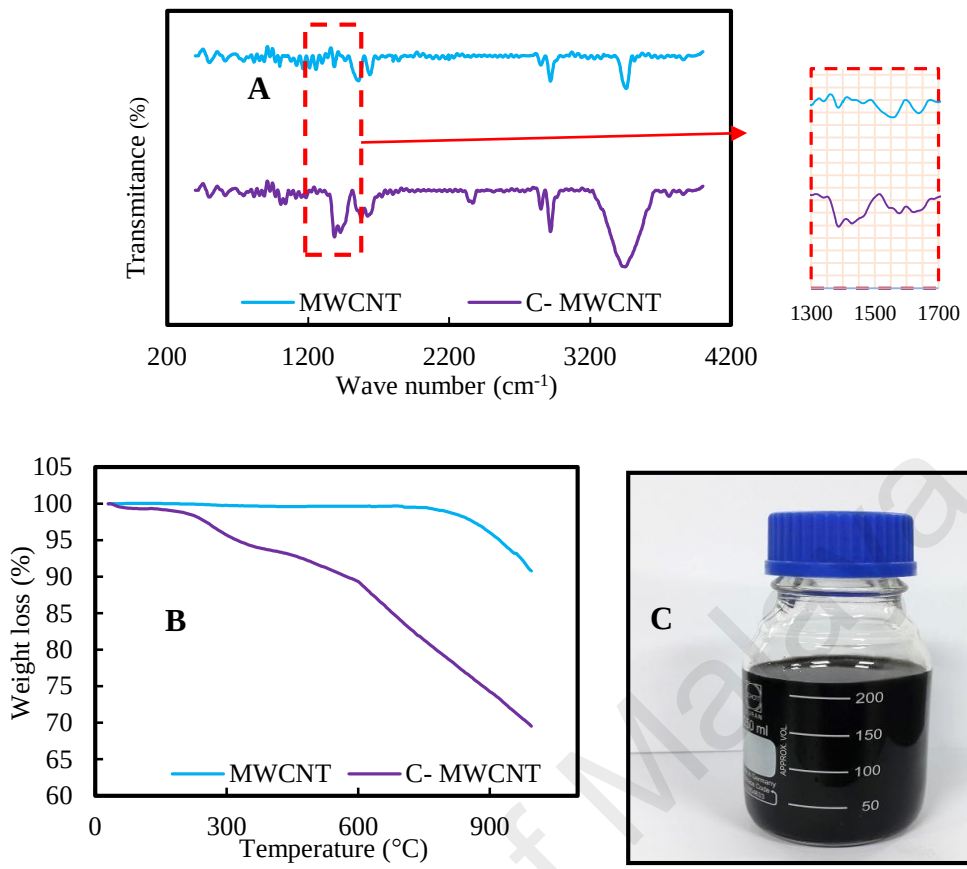

Figure 4. 1: (A) FTIR spectra of MWCNTs and C-MWCNTs, (B) TGA curves of MWCNTs and C-MWCNTs, and (C) photograph of C-MWCNTs dispersed in DI water after three months

TGA is a thermal analysis technique, whereby modifications in the structure of materials are evaluated as a function of temperature. TGA represents information about the quantitative amount of functional groups on the surface of MWCNTs, which was used to characterize the C-MWCNTs with respect to pristine MWCNTs(Sadri, Hosseini, Kazi, Bagheri, Ahmed, et al., 2017). Figure 4.1(B) shows the TGA curves for pristine MWCNTs and C-MWCNTs where it can be seen that there was no weight loss in the pristine MWCNTs up to a temperature of ~700°C, which is the temperature at which the main graphitic structures begin to decompose. However, there is a gradual weight loss for the C-MWCNTs, which confirms the decomposition of the functional groups. There were three distinctive steps of weight losses for the clove-treated MWCNTs within the temperature range of 0–600°C. The first weight loss occurred at temperature of ~100°C, which is attributed to water whereas the second weight loss occurred between 200 and

300°C, which is due to the decomposition of the functional group (*i.e.* eugenol). The third weight loss occurred after 600°C, caused by the degradation of the graphitic structures in air. The results indicate the successful covalent functionalization of the MWCNTs with eugenol, which is evidenced by the gradual weight loss observed in the TGA curve for C-MWCNTs. Digital image of C-MWCNTs dispersed in DI water after 90 days, is shown in Figure 4.1 (C).

Raman spectroscopy provides fundamental information for us to examine the structure of sp^2 and sp^3 hybridized carbon atoms in carbon-based materials and therefore, Raman spectroscopy was chosen as the first characterization technique. In addition, Raman spectroscopy elicits essential information on the covalent functionalization of MWCNTs by following the variations in holes.

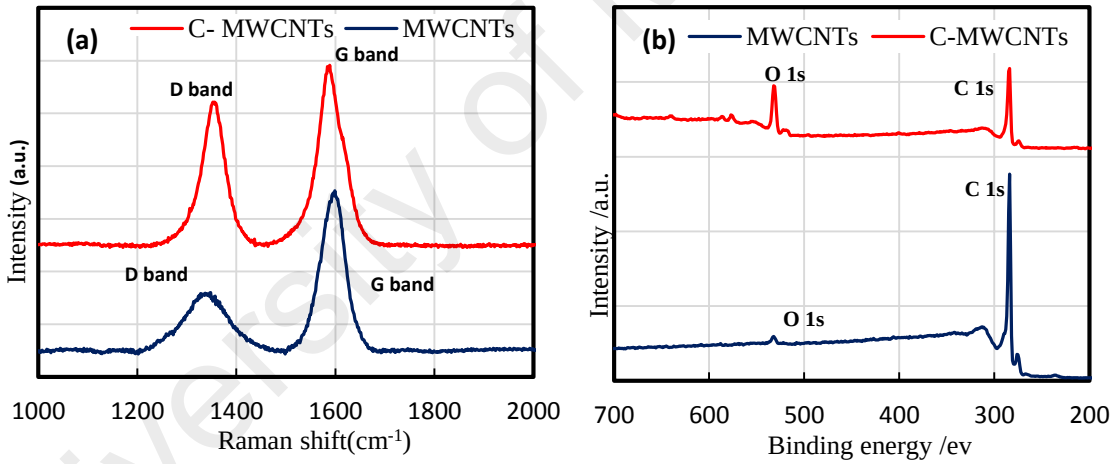

Figure 4. 2: (a) Raman spectra and (b) wide-scan O1s and C1s XPS spectra for pristine MWCNTs and CMWCNTs

Figure4.2(a) shows the Raman spectra of the MWCNT and CMWNTs. The enhancement in the Raman intensity ratio (I_D/I_G) indicates a change in hybridized carbon from sp^2 to sp^3, which is a direct evidence of covalent functionalization (R. Das et al., 2015). The pristine MWCNTs have an I_D/I_G ratio of 0.36 whereas the CMWCNTs have an I_D/I_G ratio of 0.8. The larger I_D/I_G ratio obtained for the CMWCNTs indicates the presence of a higher number of sp^3 carbons and the

occurrence of an electrophilic addition reaction, which confirms the successful covalent functionalization of MWCNTs. Raman spectra analysis data is given in Table 4.1.

Table 4. 1: Raman spectra analysis results for pristine and clove-treated MWCNTs

Sample	Peaks	Centre (cm^{-1})	Intensity (a.u.)	I_D/I_G
MWCNTs	D band	1339.63	2253.2	0.36
	G band	1595.67	6118.35	
C-MWCNTs	D band	1353.56	5454.51	0.8
	G band	1586.29	6825.58	

X-ray photoelectron spectroscopy (XPS) was used to examine the nature and elemental compositions of the MWCNTs before and after covalent functionalization with cloves and the results are shown in Figure 4.2(b). Each of the peaks were fitted to the binding energy of standard carbon, *i.e.* 284.6 eV. It is apparent from the XPS spectra for both MWCNTs and C-MWCNTs that the highest peak intensity occurs at around 284.6 eV (C1s) and 532.8 eV (O1s). Based on these results, it could be presumed that the pristine MWCNTs have a very little amount of oxygen. However, upon functionalization, the intensity of the O1s peak increases considerably, as indicated by the oxygen to carbon ratio (O/C), which increases from 0.024 (MWCNTs) to 0.241 (C-MWCNTs). This data confirms the successful free radical grafting of different oxygen functional groups onto the C-MWCNTs.

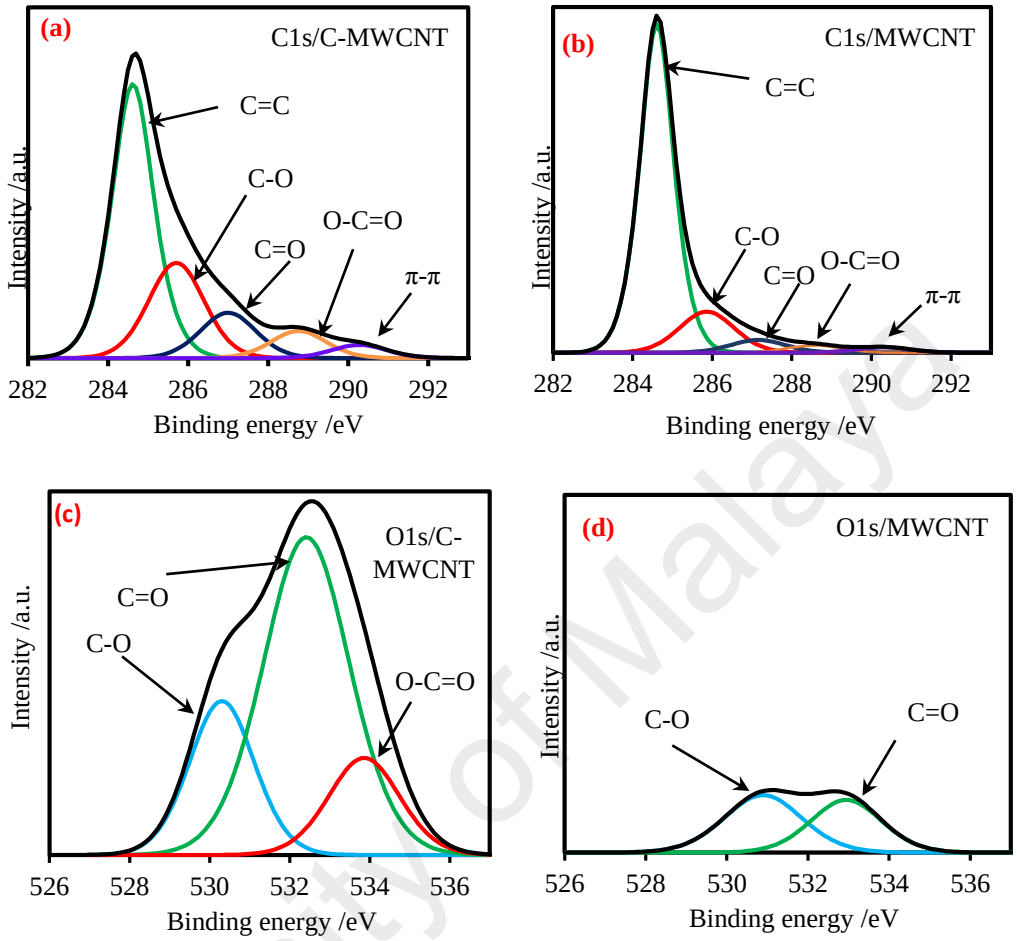

Figure 4. 3: C1s XPS spectra for (a) C-MWCNTs and (b) pristine MWCNTs, and O1s XPS spectra for (c) C-MWCNTs and (d) pristine MWCNTs

Figure4.3 shows the high resolution C1s and O1s XPS results and the deconvoluted peaks (bonding components) for both pristine MWCNTs and C-MWCNTs. The C1s XPS spectrum for the C-MWCNTs (Figure4.3 (a)) shows that the C-MWCNTs have three oxygen functional groups at 285.8, 287.02 and 288.78 eV, which is assigned to the C−O (hydroxyl and epoxy), C=O (carbonyl) and O−C=O (carboxylic acid) bonds, respectively. The C1s XPS spectrum for the MWCNTs (Figure4.3(b)) also shows these peaks but their intensities are distinctively lower than those for C-MWCNTs, indicating that large fractions of oxygen atoms are existing as either C−O and C=O for the C-MWCNTs. In

addition, the peaks at 284.6 and 290.3 eV (for both pristine MWCNTs and C-MWCNTs) are related to the C=C (aromatic) and π-π interaction bonds, respectively.

Figure4.3(c, d) shows three oxygen peaks arising from C=O (~530.3 eV), C−O (carbonyl ~532.4 eV) and O−C=O (~533.8 eV) groups for MWCNTs and two oxygen peaks arising from C=O (~530.3 eV) and O−C=O (~532.9 eV) groups for C-MWCNTs. After functionalization, the three peaks related to C−O / C=O / O−C=O increases from 1.44 %, 1.2% and 0% for MWCNTs to 4.34%, 11.89% and 3.01% for C-MWCNTs. The raw MWCNTs show generic functionalities such as O−C=O and C−O−C, as well as C=O and C−OH in O1s and C1s, respectively ((Figurw4.3(d)). It is likely that these groups were created unintentionally when the pristine MWCNTs were subjected to the environment comprising natural oxidizing agents such as hydroxyl radicals and ozone.(R. Das et al., 2015) Full XPS analysis data is given in Table4.2.

Table 4. 2: XPS analysis results for pristine and clove-treated MWCNTs

Sample	Overall Percentage (atom %)		Elemental composition (atom %)							
			C1s					O1s		
	C1s	O1s	$C=C$	$C-O$	$C=O$	$O-C=O$	$\pi-\pi$	$C-O$	$C=O$	$O-C=O$
MWCNTs	97.09	2.91	73.84	14.44	4.53	2.58	1.97	1.44	1.20	0
C-MWCNTs	80.56	19.44	43.87	19.43	9.26	5.51	2.69	4.34	11.89	3.01

Even though transmission electron microscopy (TEM) does not provide any information on the functional groups, this technique enables us to examine the surface deterioration of MWCNTs, which serves as supplementary evidence of successful functionalization. Figure4.4(A–C) shows the TEM images of the pristine MWCNTs and C-MWCNTs. Indeed, it can be seen from Figure 4.4(A) that there is presence of more aggregation in pristine MWCNTs images compared to the images of C-MWCNTs (Figure 4.4(B, C)). In addition, it is evident from

Figures 4.4(B and C) that most of the tips and ends of the C-MWCNTs are well-separated, which differs significantly from Figure 4.4(A) where it shows unscathed MWCNT tips and ends. This might have happened due to the conversion of sp^2 hybridized carbons to sp^3 hybridized carbons, which can potentially defect graphitic CNTs. It is worth noting that the stability of C-MWCNT nanofluid is closely linked with its electro-kinetic properties.

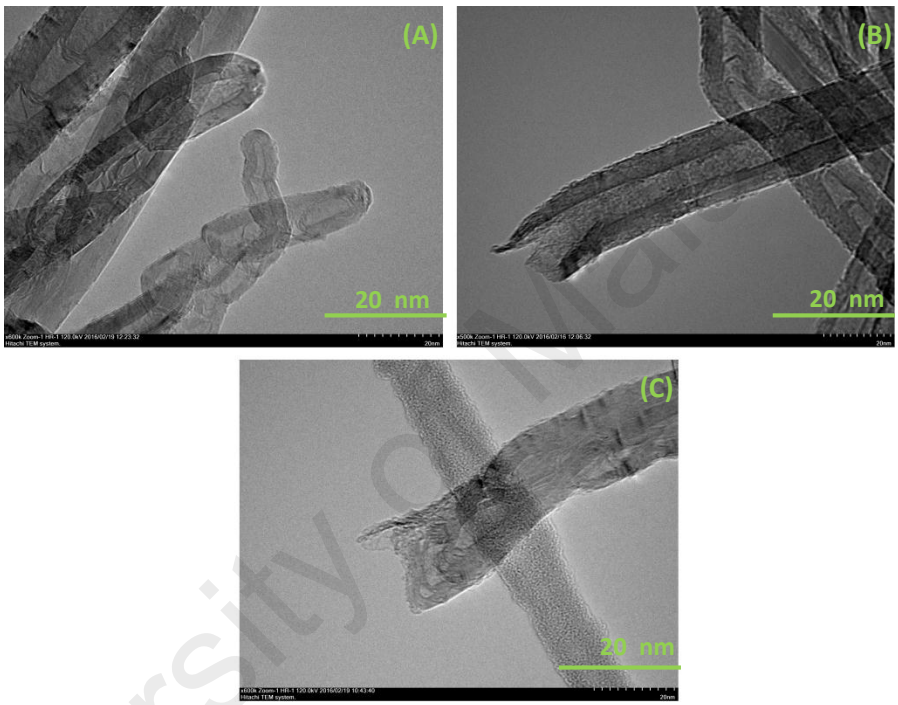

Figure 4. 4: TEM photographs of: (A) pristine MWCNTs, and (B and C) C-MWCNTs

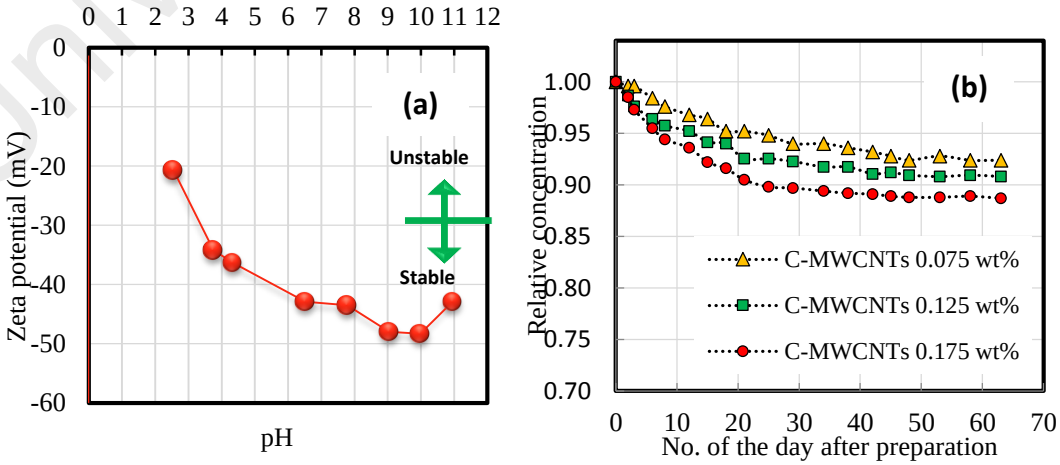

Figure 4. 5: (a) Colloidal stability of Clove-treated MWCNTs dispersed in DI water and (b) zeta potential values of the C-MWCNT nanofluid as a function of pH

The high surface charge density of MWCNTs will generate strong repulsive forces, which helps in the attainment of well-dispersed, stable MWCNT suspensions (L. Chen & Xie, 2010). Hence, zeta potential measurements were done to investigate the electrophoretic behavior and further understanding of the dispersion behavior of MWCNTs in water.

Figure 4.5(A) shows the measured zeta potential values as a function of pH for the C-MWCNT aqueous suspension. It can be observed that the C-MWCNT nanofluid has high negative values (–20.7 mV to –42.9 mV) within the pH variation from 2.55 to 10.95. More importantly, the zeta potential values for the C-MWCNT nanofluid are far from the isoelectric point (i.e. point of zero charge), which indicates that this pH range (3.5–10.95) results in strong electric repulsion forces between the particles of C-MWCNTs. This prevents aggregation of the C-MWCNTs by non-covalent interactions such as π-π interactions or H-bonding. We attribute this phenomenon to the oxygen functionalities at the surface of the C-MWCNTs. Hence, the C-MWCNT aqueous suspension is stable when the pH is more than 3.5 (where the corresponding zeta potential is around –30.6 mV). Thus, it could be highlighted, the C-MWCNT aqueous suspension is stable even in weak acidic conditions.

In stronger acidic solutions (pH < 3.5), the material tends to agglomerate and undergo intermolecular dehydration catalyzed by H+, leading to the coupling of C-MWCNTs via ether linkages.It could be noted that the C-MWCNT nanofluid became more stable by adding alkali to the aqueous suspension, which lead to the generation of additional negative charges in the nanoparticles. UV-Vis spectroscopy is a technique used to study dispersibility of nanofluids with respect to the sedimentation time.

Figure 4.5(b) shows the colloidal stability of the C-MWCNT-DI water nanofluids with respect to the number of days after preparation. It is obvious that the relative concentration of the aqueous suspensions reduces with the number of days. However, all of the samples have a fairly constant concentration after Day 63. The maximum amount of sedimentations is 7.6, 9.2 and 11.3% for a nanoparticle concentration of 0.075, 0.125 and 0.175 wt.% respectively which confirms the colloidal stability of the nanofluids containing C-MWCNTs.

4.2 Characterization of clove treated graphene nanoplatelets

Figure 4.6(A) shows the FTIR spectra for the pristine GNPs and CGNPs, which are represented by the transmittance (%) *versus* the wavenumber (cm^{-1}). It can be observed from Figure 4.6 (A) that there are noticeable cues of the eugenol molecule in the CGNPs compared to the pristine GNPs. The broad peak at 3436.92 cm^{-1} is ascribed to O–H stretching vibrations, which may be caused by the reaction between the GNPs and hydroxyl groups of eugenol and/or hydrogen peroxide. The symmetric and asymmetric sharp vibrations of C–H bonds are observed within a wavenumber range of 2849.68–2917.09 cm^{-1} for both GNPs and CGNPs.

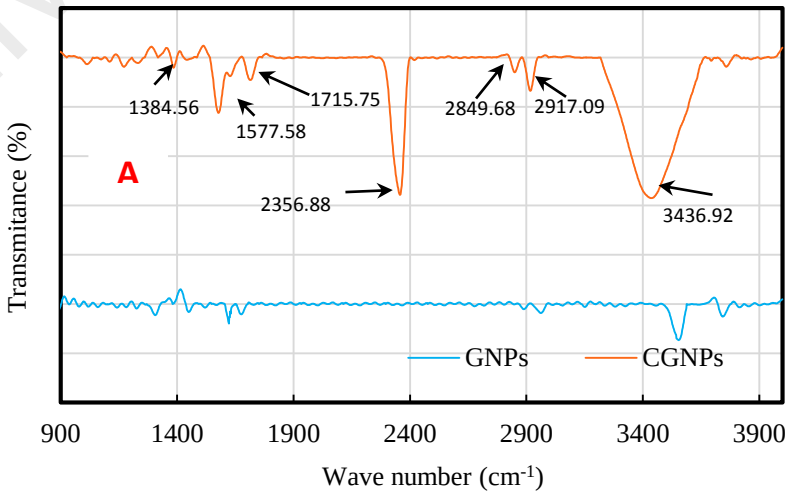

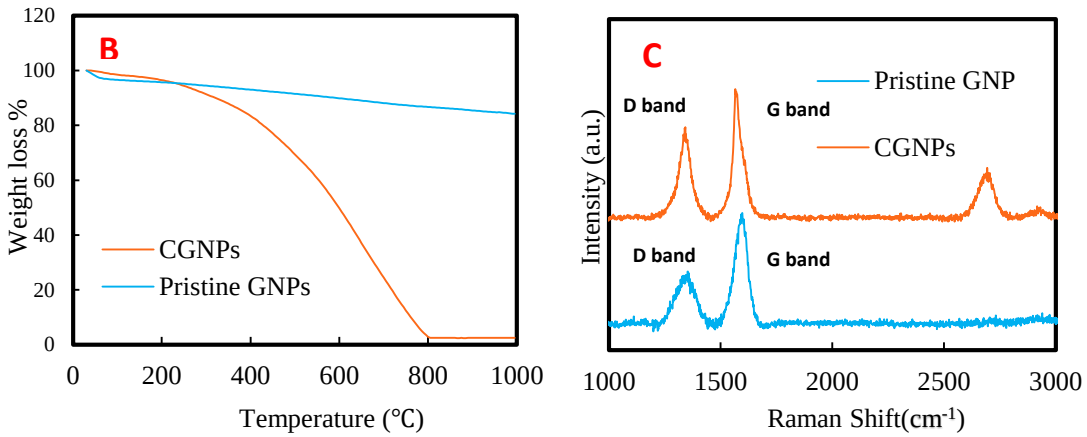

Figure 4. 6: FTIR spectra of pristine GNPs and C-GNPs, (B) TGA curves, and (C) Raman spectra of pristine GNPs and CGNPs

A couple of peaks are observed within the wavenumber range of 1577.58 cm^{-1}, which arise from C=C stretching vibrations of GNPs after opening due to the addition of electrophilic reactions between the main structure of GNPs and the –OH band of eugenol. The functionalization of GNPs by eugenol is confirmed by the peaks at 1384.56, and 1178 cm^{-1}, which are out-of-plane CH vibrations and C–O stretching vibrations, respectively. The peaks within the wavenumber range of 1715.75cm^{-1} and the peak centred at 1631 cm^{-1} are assigned to O–C=O stretching vibrations, indicating the formation of carboxyl groups at the main structure of GNPs.

TGA provides information about the quantitative amount of each functional groups on the surface of GNPs, which were used to characterize the pristine GNPs and CGNPs. Figure 4.6(B) shows the TGA curves for pristine GNPs and CGNPs and it can be seen that there was feeble weight loss in the pristine GNPs up to the temperature of ~800°C, which is the temperature at which the main graphitic structures began to decompose. However, there was a significant weight loss for the CGNPs, which confirms the decomposition of the functional groups. There are two distinctive steps of weight loss for the clove-treated GNPs within a temperature range of 0–800°C. The first weight loss occurred at ~100°C, which was attributed to water whereas the second weight loss happened between 160 and 800°C, which is due to the decomposition of the functional

group (*i.e.* eugenol) and the degradation of the graphitic structures in air (after 600°C). The results indicate the successful covalent functionalization of GNPs with eugenol, which is evidenced by the gradual weight loss observed in the TGA curve of CGNPs.

Raman spectroscopy provides fundamental information for us to examine the structure of sp^2 and sp^3 hybridized carbon atoms in carbon-based materials and therefore, Raman spectroscopy was chosen as the first characterization technique. In addition, Raman spectroscopy elicits essential information on the covalent functionalization of GNPs by following the variations in holes. Figure4.6(C) shows the Raman spectra of the MWCNT and CGNPs. The enhancement in the Raman intensity ratio (I_D/I_G) indicates a change in hybridized carbon from sp^2 to sp^3, which is a direct evidence of covalent functionalization (R. Das et al., 2015). The pristine GNPs have an I_D/I_G ratio of 0.57 whereas the CGNPs have an I_D/I_G ratio of 0.85. The larger I_D/I_G ratio obtained for the CGNPs indicates the presence of a higher number of sp^3 carbons and the occurrence of an electrophilic addition reaction, which confirms the successful covalent functionalization of GNPs. Raman spectra analysis data are presented in Table 4.3.

Table 4. 3: Raman spectra analysis results for pristine and clove-treated GNPs

Sample	Peaks	Centre (cm^{-1})	Intensity (a.u.)	I_D/I_G
GNPs	D band	1353.94	593.47	0.57
	G band	1597.43	1036.38	
CGNPs	D band	1341.82	1682.44	0.85
	G band	1566.24	1970.01	

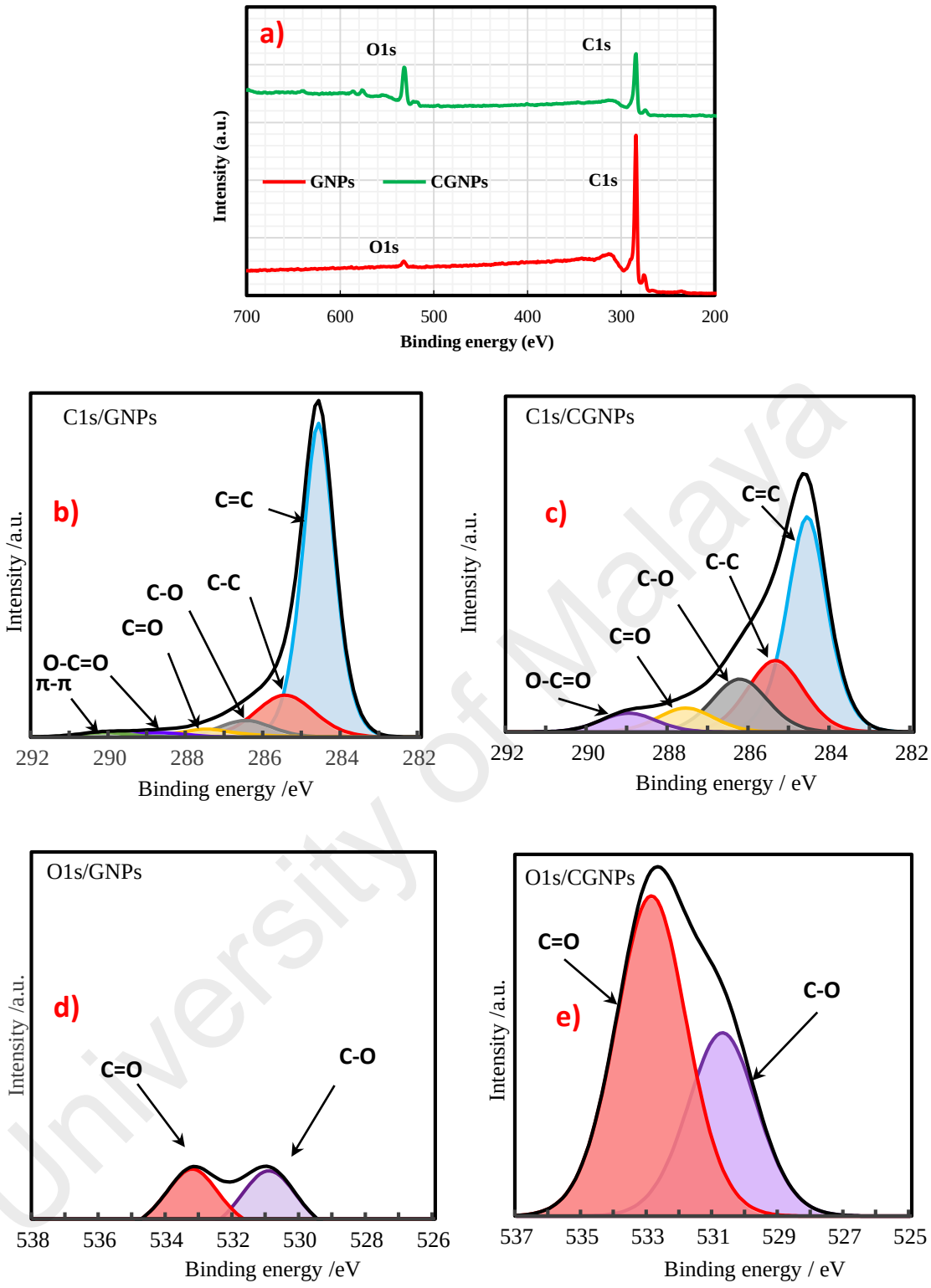

Figure 4. 7: (a) Wide-scan XPS spectra for the GNPs and CGNPs; High-resolution XPS spectra of the deconvoluted peak components for C1s: (b) GNPs, (c) CGNPs; High-resolution XPS spectra of the deconvoluted peak components for O1s: (d) GNPs, (e) CGNPs

The elemental compositions of the surfaces of the GNPs were examined before and after functionalization with cloves using XPS. Each of the peaks were fitted to the binding energy of standard carbon, *i.e.* 284.6 eV. It can be observed from the wide-scan XPS

spectra for GNPs and CGNPs (Figure 4.7(a)) that the C1s and O1s peaks are centred at ~284.6 and 532.8 eV, respectively. Unlike GNPs, the CGNPs have a higher O1s peak intensity since the oxygen-to-carbon ratio (O/C) increases from 0.029 (GNPs) to 0.247 (CGNPs). This proves the prospering oxidizing amorphous carbon impurities and free radical grafting of different oxygen functional groups onto the CGNPs. It is very likely that the oxygenated groups such as C–O (in hydroxyl and epoxy), C=O (in carbonyl derivatives) and COO (in carboxylic acids) are attached to the edge and surface of the GNPs after functionalization. Curve fittings of high-resolution were done for C1s and O1s spectra in order to assess the contributions of these groups.

Figure 4.7(b) and (c) shows the high-resolution XPS spectra of the C1s deconvoluted peak components for GNPs and CGNPs, respectively. Current results confirm the presence of an aromatic group (C=C) at 284.6 eV, an aliphatic group (C−C) at 285.39 eV, hydroxyl and epoxy groups (C−O) at 286.27 eV, carbonyl group (C=O) at 287.61 eV, carboxyl group (O–C=O) at 289.02 eV as well as π-π interaction bonds at 290.13 eV. After oxidative treatment, the intensity of the C–O, C=O and O–C=O bonds increases from 5.75, 4.04 and 1.62% (pristine GNPs) to 13.04, 5.95 and 4.7% (CGNPs), respectively, while the π-π interaction bonds vanished completely. The higher peak intensities at 530.7 and 533 eV in the O1s spectrum (Figure 4.7(d) and (e)) confirm the presence of large fractions of oxygen atoms in the form of C=O and C−O functional groups in the CGNPs. In contrast, the pristine GNPs show the presence of feeble and generic functional groups such as C–O and C=O (R. Das et al., 2015). These functional groups were created unintentionally when the pristine GNPs were subjected to the environment comprising natural oxidizing agents such as hydroxyl radicals and zone. The results of XPS analyses are presented in Table 4.4.

Table 4. 4: XPS analysis results for GNPs and CGNPs

Sample	Overall percentage (atom %)		Elemental composition (atom %)							
			C1s						O1s	
	C1s	O1s	C = C	C − C	C − O	C = O	O − C = O	π − π	C − O	C = O
GNPs	97.09	2.91	68.15	16.19	5.75	4.04	1.62	1.52	1.32	1.41
CGNPs	80.15	19.85	39.63	17.63	13.04	5.95	4.7	0	6.84	12.21

Even though TEM highlights the surface deterioration (morphology) and wrinkling of GNPs, this technique does not provide any information on the functional groups. Figure 4.8 (a) and (b) shows the TEM image of the GNPs and CGNPs, respectively. It can be observed from Figure 4.8 (a) that the GNPs have a multi-layered structure with relatively smooth surface and edges (low edge defects) as well as higher presence of aggregation. In contrast, the surface of the CGNPs appears very rough with higher defects and wrinkles resulting from covalent functionalization. The presence of wrinkles and lines on the surface of the CGNPs are responsible for the inherent instability of the two-dimensional structures as well as improved flexibility of the GNPs after covalent functionalization with cloves.

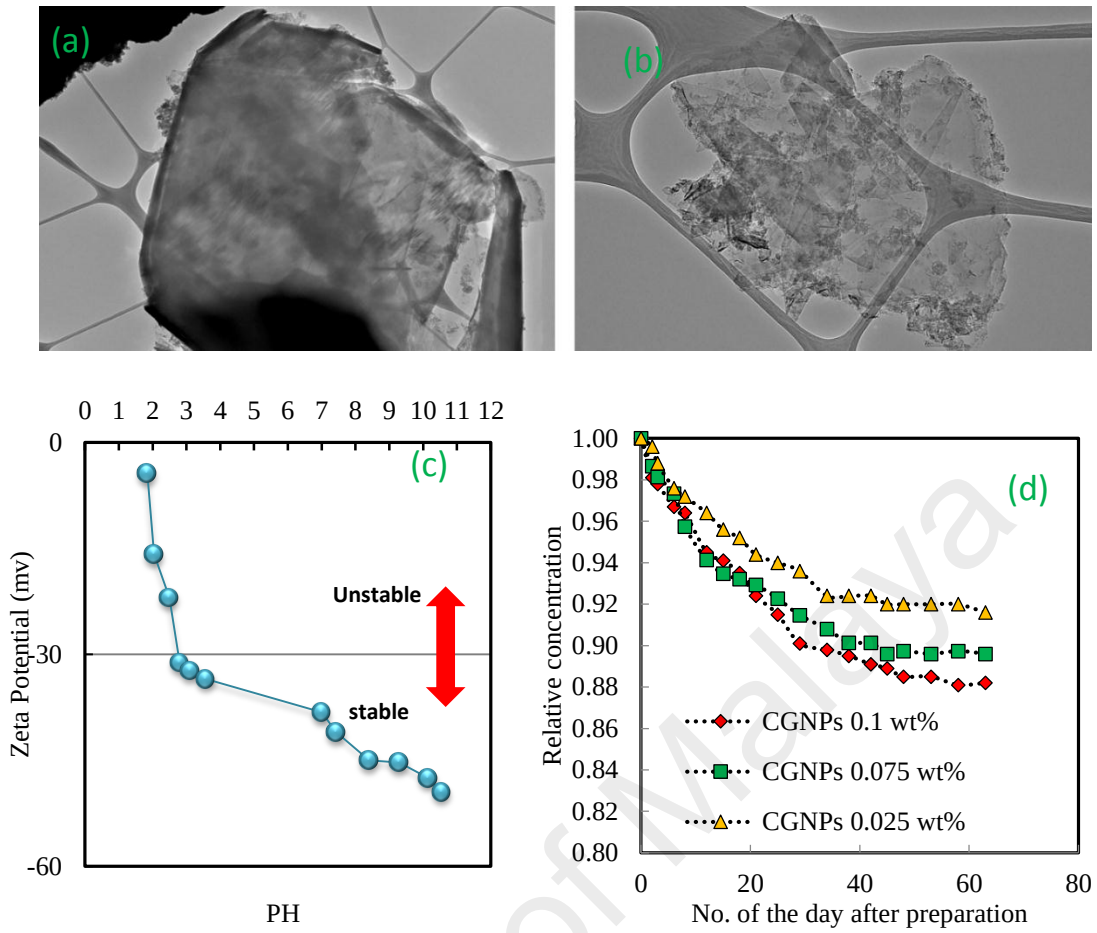

Figure 4. 8: TEM image of (a) GNPs and (b) CGNPs (c) zeta potential values of the CGNP nanofluid as a function of pH (d) Colloidal stability of Clove-treated GNPs dispersed in DI water

Figure 4.8(C) shows the measured zeta potential values as a function of pH for the CGNP aqueous suspension. It can be observed that the CGNP nanofluid has high negative values (–4.42 mV to –49.5 mV) within the pH variations from 1.84 to 10.55. More importantly, the zeta potential values for the CGNP nanofluids are far from the isoelectric point (*i.e.* point of zero charge), which indicates that this pH range (2.8–10.55) results in strong electric repulsion forces between the particles of CGNPs. This prevents aggregation of the CGNPs by non-covalent interactions such as π-π interactions or H-bonding. This phenomenon is attributed to the oxygen functionalities at the surface of the CGNPs. Hence, the CGNP aqueous suspension is stable when the pH is more than 2.8 (where the corresponding zeta potential is around –30.6 mV). In this study it could be highlighted that the CGNP aqueous suspension is stable even in weak acidic conditions.

In strong acidic solutions (pH < 2.8), the material tends to agglomerate and undergo intermolecular dehydration catalyzed by H^+, leading to the coupling of CGNPs via ether linkages. It was identified that the CGNP nanofluid became more stable by adding alkali to the aqueous suspension, which lead to the generation of additional negatively charged in the nanoparticles.

UV-vis spectroscopy is a common technique used to study the dispersibility of nanofluids as a function of the sedimentation time. Figure 4.8(d) indicates the stability of CGNP-water nanofluids with respect to the number of days after preparation. It was seen that the relative concentration of the nano-coolants decreased with the passage of days after sample preparation. However, the relative concentrations of the nanofluids were almost constant after Day 63 for all the tested samples. It was observed that the highest sedimentation data were 8.4, 10.4 and 11.8% for the samples containing of 0.025, 0.075 and 0.1 wt% of CGNPs, respectively. This confirms the stability of the CGNP-water nanofluids.

4.3 Thermophysical properties C-MWCNTs-DI water nanofluids

The effective viscosity of nanofluids containing C-MWCNTs and DI water were measured experimentally and the results are shown in Figures 4.9. The dynamic viscosity is shown as a function of the nanoparticle concentration and temperature at a fixed shear rate of 150 s^{-1}. It can be observed that there was a slight increase in the dynamic viscosity of the C-MWCNT-DI water nanofluids relative to that of DI water. This indicates that the C-MWCNTs remain suspended in the base fluid, which ensures the successful covalent functionalization. It can also be observed from Figure 4.9 that the dynamic viscosity of the C-MWCNTs aqueous nanofluids declines by increasing temperature, which may be attributed to weakening of intermolecular forces (Aravind et al., 2011). This observation corroborates well the findings of Aravind *et al.* (Aravind et al., 2011),

Ko et al. (Ko et al., 2007) and Sadri et al. (Sadri et al., 2016), who observed that the decrease in viscosity with the increase of fluid temperature. The mild increase in the effective viscosity with the increase of nanoparticle concentration is an important advantage, since the increase in viscosity could undermine the overall positive impact of enhanced conductivity in heat transfer due to the pumping penalty of the working fluids.

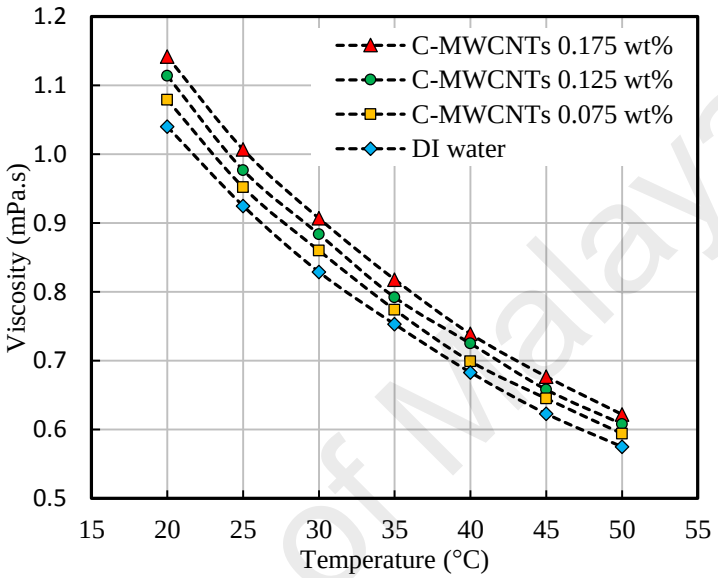

Figure 4. 9: Dynamic viscosity of nanofluids containing C-MWCNTs and DI water at a shear rate of 150 s^{-1} (mPa·s)

The density was measured for the C-MWCNT aqueous suspensions and base fluid at various temperatures and the results are presented in Table 4.5. It can be seen that there was a decrease in the density of the C-MWCNT-DI water nanofluids and DI water with the increase in fluid temperature, which could be attributed to the liquid thermal expansion. There is a slight increment in the density for the C-MWCNT-DI water nanofluids with the increase in nanoparticle concentrations. The increase in nanofluid density can be attributed to the density of the C-MWCNTs particles, which is higher than that of the base fluid. The maximum increase in density of the C-MWCNT-DI water nanofluid is 0.08% for a nanoparticle concentration of 0.175 wt.% at 20℃. However, the density was decreased by approximately 0.6% when the temperature was increased from 20 to 40℃ for the same nanoparticle concentration.

Table 4. 5: Density of C-MWCNT-DI water nanofluids and DI water as a function of temperature

	Density (kg/m^3)				
Concentration/temperature (℃)	20	25	30	35	40
DI water	998.00	996.85	995.50	993.90	992.00
0.075 wt%	998.30	997.20	995.85	994.15	992.25
0.125 wt%	998.55	997.50	996.15	994.45	992.50
0.175 wt%	998.80	997.75	996.45	994.65	992.70

The thermal conductivity of a coolant is one of the parameters that play a significant role in increasing the heat transfer rate of heat exchangers. Hence, the thermal conductivity of the C-MWCNT-DI aqueous suspensions was measured experimentally in this study and the results are shown in Figure 4.10. The thermal conductivity of the C-MWCNT-DI water nanofluids are plotted as a function of temperature and nanoparticle concentration. It shall be noted that only nanofluids with low concentrations of C-MWCNTs were considered in this study in order to prevent a drastic increase in viscosity. The thermal conductivity of the base fluid was compared with that from the National Institute of Standards and Technology (NIST) database and there is good agreement between these values (Ramires et al., 1995), whereby the error is less than 1% at 20℃. It is evident from Figure 4.10 that the thermal conductivities of the C-MWCNT-DI water nanofluids are markedly greater than that for the DI water. Moreover, it is evident that the thermal conductivity of the C-MWCNT aqueous suspensions and base fluid increases with an increase in fluid temperature. Nonetheless, the thermal conductivity enhancement is higher for the C-MWCNT-DI water nanofluids at higher nanoparticle concentrations. Based on Figure 4.10, it can be deduced that temperature plays a vital role on enhancing the effective thermal conductivity of nanofluids, which is due to the Brownian motion of

the C-MWCNTs particles dispersed in the base fluid (Aravind et al., 2011). The maximum thermal conductivity enhancement obtained was 7.29, 13.02, 20.15%, for the nanoparticle concentration of 0.075, 0.125, 0.175 wt.% respectively at 50℃.

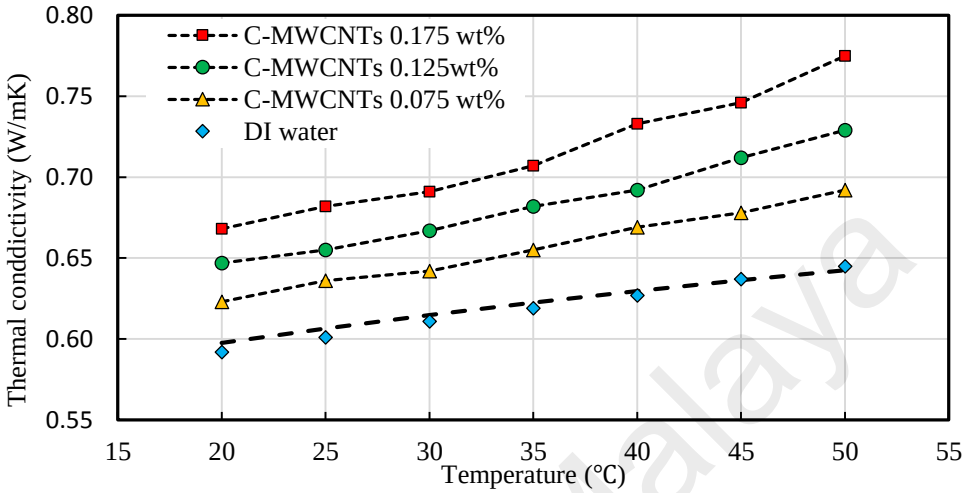

Figure 4. 10: Thermal conductivity of C-MWCNT-DI water nanofluids and DI water

4.4 Thermophysical properties CGNPs-DI water nanofluids

The effective dynamic viscosity, thermal conductivity and specific heat capacity of the CGNP-water nanofluids and DI water were measured experimentally and the results are presented as functions of temperature and weight concentration in Figures 4.11(a)–(c). The thermal conductivity of a coolant is one of the significant factors in raising the heat transfer rate (and thus, heat dissipation efficiency) of heat exchangers. The thermal conductivity of the DI water was used as the base fluid in the present study and found similar to those in the NIST database (Ramires et al., 1995) with a maximum error of 1%. It is apparent from Figure 4.11(a) that the effective thermal conductivity is significantly higher for the CGNP-water nanofluids compared to the DI water. In addition, the thermal conductivities of CGNP-water nanofluids are increased with the increase of the fluid temperature. Interestingly, the rate of increment in thermal conductivity for the CGNP-water nanofluids is greater at higher particle concentrations. Temperature plays a pivotal role in increasing the thermal conductivities of nanofluids, as evidenced from Fig 4.11(a).

This is due to the increase in Brownian motion of the CGNPs dispersed in the DI water. The maximum thermal conductivity enhancement of 5.96, 15.8 and22.9% for a particle concentration of0.025, 0.075 and 0.1 wt% respectively at 45℃ was obtained.

One of the goals of this study was to prevent a radical increase in the viscosity of the coolant, since the increase of viscosity increases the pumping power. Here, the effective dynamic viscosity of the CGNP-water nanofluids (particle concentrations: 0.025, 0.075 and 0.1 wt.%) and DI water are presented at a shear rate of 150 s^{-1} and temperature range of 20–50℃ in Figure 4.11(b). It is clear that when the weight concentration of CGNPs in DI water was increased then there was only a slight increase in the dynamic viscosity of the nanofluids relative to that of DI water. This is indeed expected since low concentrations of CGNPs were used in the samples. Fig 4.11(b) also shows the benefit of covalent functionalization using cloves since the CGNPs remain suspended in the DI water. It can also be observed that the dynamic viscosity of the CGNP-water nanofluids and DI water reduces with an increase in temperature which is assigned to the weakening of the intermolecular forces (Aravind et al., 2011). Interestingly, the samples used show the same declining trend for the dynamic viscosities. Present results conform well with those of Ko et al. (Ko et al., 2007), Sadri et al. (Sadri et al., 2016) and Aravind et al. (Aravind et al., 2011). Furthermore, it is important to consider the low weight concentration of the nanoparticles dispersed in the base fluid, especially if the nanofluid are taken as coolant in heat transfer systems. A higher particle concentration may increase the dynamic viscosity of the nanofluid which negates the positive impact of using nanofluids for heat transfer enhancement. This is due to the fact that a higher fluid viscosity will result the pumping penalty of the fluid.

The specific heat capacities of the CGNP-water nanofluids and DI water as function of temperature are presented in Fig 4.11(c). It can be clearly seen that the specific heat capacity elevates when the temperature is increased for all the samples. The slope is

similar for the specific heat capacity curves, which agrees well with the findings of Pak and Cho (Pak & Cho, 1998).

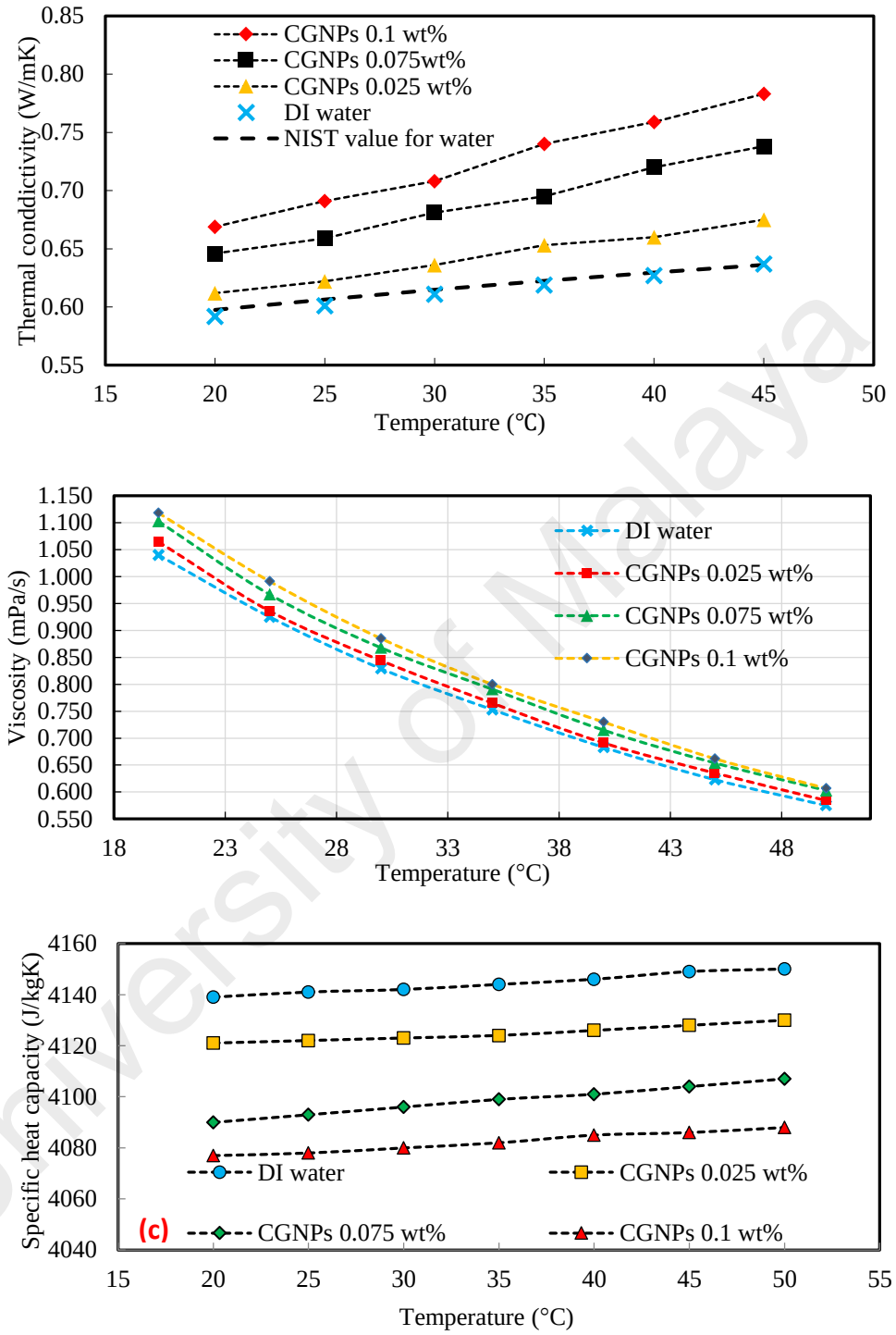

Figure 4. 11: Variation of (a) thermal conductivity, (b) dynamic viscosity and (c) specific heat capacity of CGNP-water nanofluids as a function of temperature and particle concentration

The density of the CGNP-water nanofluids and DI water were measured experimentally within a temperature range of 20–40°C and the results are present in Table 4.6. It can be observed that the density for all the samples reduces with an increase in the fluid temperatures due to the thermal expansion of the fluid. Furthermore, the density of the CGNP-water nanofluid increases with the increase in particle concentration, though the increase is rather minor. The higher density of the CGNP-water nanofluids is attributed to the density of the CGNPs, which is higher than the density of water. The density of the CGNP-water nanofluid increases by only 0.04% for a particle concentration of 0.1 wt.% at 20°C. However, the density of this nanofluid decreases by approximately 6% when the fluid temperature is increased from 20 to 40°C, representing the influence of temperature.

Table 4. 6: Density of CGNP-water nanofluids and DI water as the function of temperature and particle concentration

	Density (kg/m^3)				
Concentration/Temperature (℃)	20	25	30	35	40
DI water	998.00	996.85	995.50	993.90	992.00
0.025 wt%	998.10	997.00	995.60	994.00	992.05
0.075 wt%	998.30	997.20	995.80	994.15	992.15
0.1 wt%	998.40	997.30	995.90	994.20	992.25

4.5 Thermal performance of C-MWCNT-DI water nanofluids

To evaluate the reliability and accuracy of the experimental set-up, preliminary experiments were carried out for the base fluid prior to systematic experiments involving nanofluids in the annular heat exchanger. The results from the base fluid flowing through the experimental set-up at constant heat flux boundary conditions were compared with the data calculated using empirical correlations proposed by Petukhov (Petukhov, 1970)

,Gnielinski(Gnielinski, 2015), McAdams(McAdams, 1954) for the turbulent flow regime. These empirical correlations are given by Eq. (4.1) , (4.2), and (4.9) respectively.

$$Nu = \frac{(\frac{f}{8})RePr}{1.07 + 12.7\left(\frac{f}{8}\right)^{0.5}(Pr^{2}/_{3} - 1)} \quad (4.1)$$

It shall be noted Eq. (4.1) is applicable for a Reynolds number range of 3000 < Re < $5(10^6)$ and Prandtl number range of 0.5 < Pr < 2000.

$$Nu = \frac{(f_{ann}/8)RePr}{k_1 + 12.7\sqrt{f_{ann}/8(Pr^{2/3}-1)}}\left[1 + \left(\frac{D_h}{L}\right)^{2/3}\right]F_{ann}\mathrm{K} \quad (4.2)$$

With

$$k_1 = 1.07 + \frac{900}{Re} - \frac{0.63}{(1 + 10Pr)} \quad (4.3)$$

Eq. (4.2) is used for a Reynolds number range of Re >4000, Prandtl number range of $0.1 \leq \mathrm{Pr} \leq 1000$ and$(D_h/L) \leq 1$.

The factor " F_{ann}" in Eq.(4.2) representing the boundary condition of "heat transfer at the inner wall with the outer wall insulated" and the factor "K" for liquids as variation of fluid properties with temperature can be calculated by Equations (4.4) and (4.5) respectively.

$$F_{ann} = 0.75a^{-0.17} \quad (4.4)$$

Where, a is annular diameter ratio, D_o/D_i

$$K = \left(\frac{Pr_b}{Pr_w}\right)^{0.11} \quad (4.5)$$

The friction factor (f_{ann}) in Eq. (4.2) is given by Gnielinski (Gnielinski, 2015) as:

$$f_{ann} = (1.8 \log_{10} Re^{*} - 1.5)^{-2} \tag{4.6}$$

$$Re^{*} = Re \, \frac{(1 + a^2) \ln a + (1 - a^2)}{(1 - a)^2 \ln a} \tag{4.7}$$

McAdams (McAdams, 1954) presented correlation of Nu for turbulent flow through concentric annulus and α in the range of 1.18–6800 as shown by equation (4.8).

$$Nu = 0.03105 \, a^{0.15} (a - 1)^{0.2} Re^{0.8} Pr^{1/3} \left(\frac{\mu}{\mu_w}\right)^{0.14} \tag{4.8}$$

Figure 4.12 shows the comparison between the experimentally measured average Nusselt number and those calculated using the aforementioned empirical correlations for the base fluid at a fixed water inlet temperature of 30ºC. Indeed, the Nusselt number increases by elevating Reynolds number, as expected. The maximum errors between the values obtained from experiments and Petukhov (Petukhov, 1970) and Gnielinski (Gnielinski, 2015) empirical correlations are found to be approximately 3.5 and 9.5%, respectively. In general, the results obtained from the experiments are in good agreement with those from empirical correlations within the range of Reynolds number (Re 3000-8000) investigated in this study. Hence, it could be deduced that the experimental set-up was reliable to assess the heat transfer properties of the C-MWCNT aqueous suspensions.

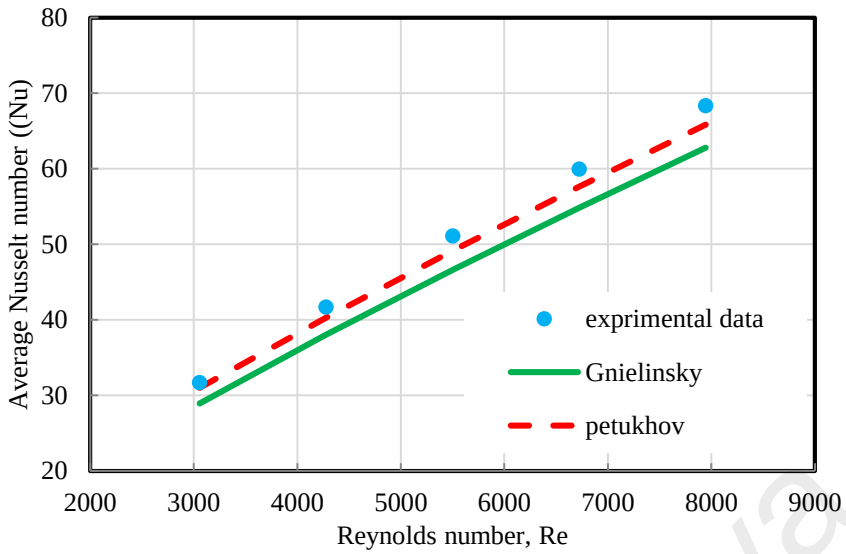

Figure 4. 12: Comparison between the measured Nusselt numbers of DI water with those calculated from empirical correlations

A series of experiments were conducted for the C-MWCNT-DI water nanofluids (nanoparticle concentrations: 0.075, 0.125 and 0.175 wt.%) by varying the Reynolds number from 3055 ± 5 to 7944 ± 5 in order to determine the convective heat transfer of the aqueous suspensions in turbulent flow regime. The input power was kept fixed at 900 W. The results are shown in Figure 4.13 for a constant inlet temperature of 30℃. It can be observed that the convective heat transfer coefficient increases when the Reynolds number is increased for both the base fluid and C-MWCNT-DI water nanofluids. It can also be observed that the nanoparticle concentration affects the heat transfer coefficient of the nanofluids suspensions. The remarkable enhancement in convective heat transfer coefficient of the C-MWCNT-DI water nanofluids is mainly due to the thermal conductivity enhancement of nanofluids, narrow thermal boundary layer as well as a decrease in thermal resistance between the flowing nanofluids and inner wall surface of the annular tube at higher Reynolds number. According to (Aravind et al., 2011; Ding et al., 2006), carbon nanomaterials (*e.g.* carbon nanotubes and graphene nanoplatelets) tend to reduce the thickness of the thermal boundary layer. The specific surface area and Brownian motion of the nanoparticles also play an important role in influencing the

convective heat transfer coefficient. In this study, the convective heat transfer coefficient of the nanofluids increases by 12.38, 24.1 and 35.89% for the nanoparticle concentrations of 0.075, 0.125 and 0.175 wt.%, respectively.

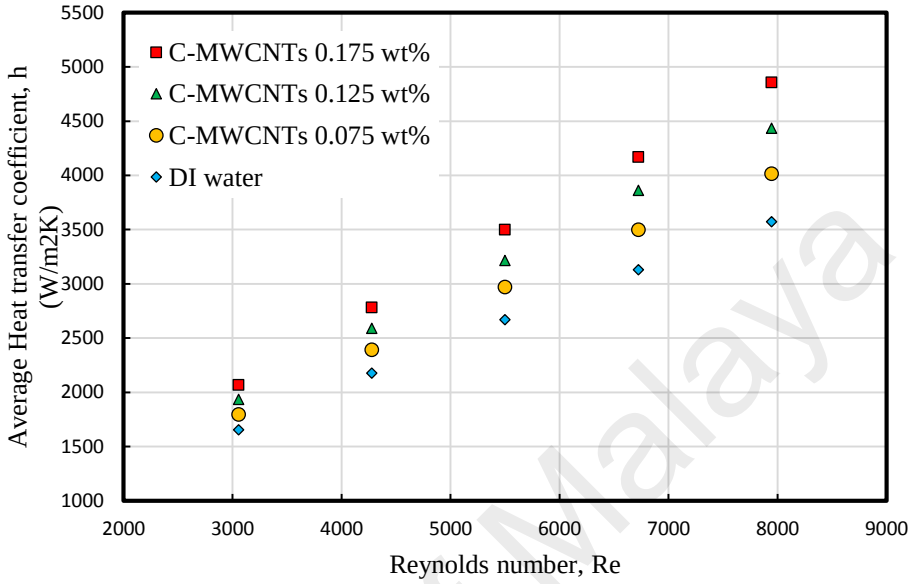

Figure 4. 13: Variation of the average heat transfer coefficient for C-MWCNT/ DI water nanofluids versus Reynolds number

To assess the convective-to-conductive heat transfer ratio of C-MWCNT aqueous suspensions, the average Nusselt number determined from Eq.3.4 was evaluated along with the Reynolds number and nanoparticle concentrations. The data are represented in Figure 4.14 and it can be observed that there is a significant increase in the Nusselt number with the increase of the Reynolds number as well as concentration of C-MWCNTs relative to the DI water. The greater Nusselt number for the C-MWCNT nanofluids is attributed to the higher thermal conductivity of the nanofluids suspensions, as well as the Brownian motion of the C-MWCNTs (Sundar, Singh, & Sousa, 2014). The maximum increase in the Nusselt number of the C-MWCNT-DI water nanofluids is found to be 6.96, 13.66 and 20.15% for the nanoparticle concentrations of 0.075, 0.125 and 0.175 wt.%, respectively. The maximum increase has achieved at the Re = 7944 ± 5.

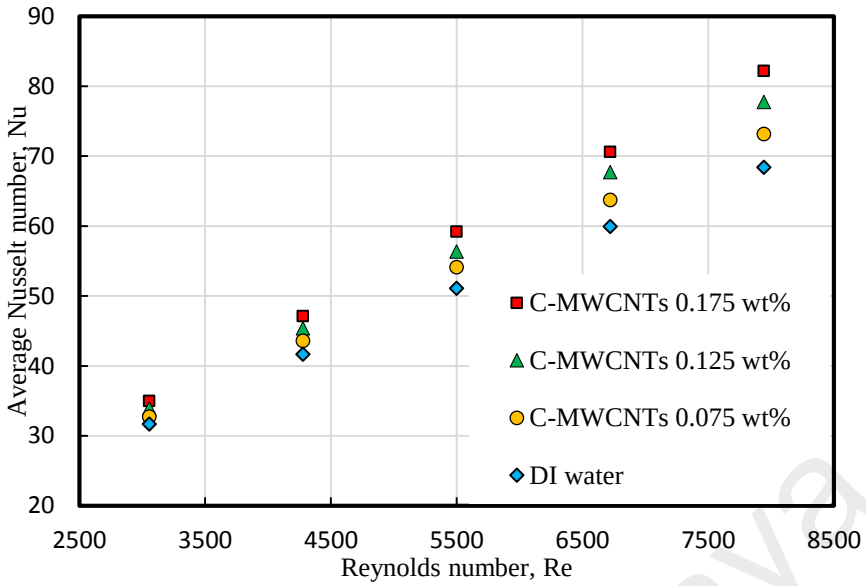

Figure 4. 14: Variation of the Nusselt number for C-MWCNT-DI water nanofluids as the function of Reynolds number

In order to validate the pressure drop accuracy in the experimental set-up, the variation of the measured friction factor for the DI water was compared with the values calculated from empirical correlations proposed by Gnielinski (Gnielinski, 2015), (Eqs.4-6) and the data are illustrated in Figure 4.15. It can be clearly seen that there is only a slight deviation between the data obtained from experiments and those calculated from the empirical models. The deviation between the experimental friction factor values and those calculated using the Gnielinski empirical correlation is less than 4.15%. Hence, it can be stated that the experimental set-up used to measure the pressure drop is validated for the range of Reynolds number investigated in this study.

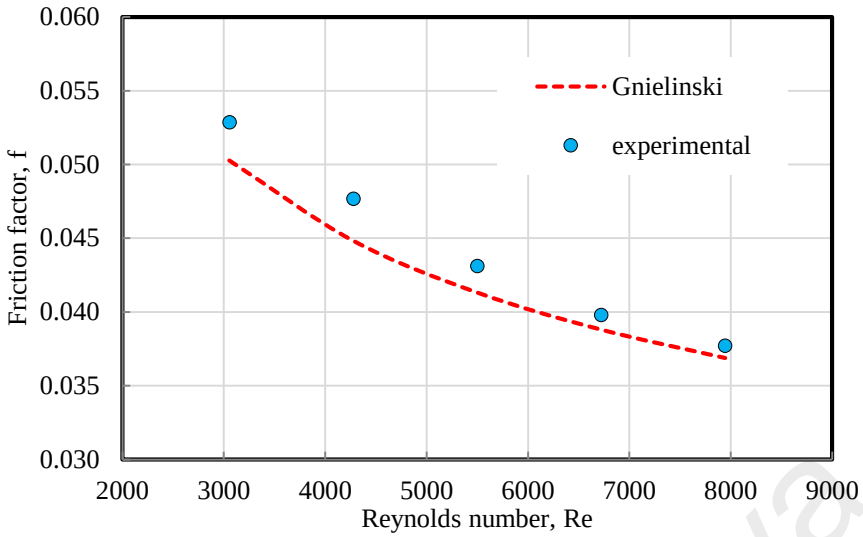

Figure 4. 15: Plot of the friction factor as a function of Reynolds number for DI water obtained from experiments and empirical correlations

The pressure drop of the C-MWCNT-DI water nanofluids flowing through the test section recorded over a range of Reynolds number is shown in Figure 4.16(a). The corresponding friction factor values were calculated using Eq. (3.5) and the data are represented in Figure 4.16(b). The data indicate that there is a small increment in both the pressure drop and friction factor for the C-MWCNT-DI water nanofluids relative to those for DI water. The maximum increase in the friction factor and pressure drop is found to be ~3% and 23%, respectively, for the nanoparticle concentration of 0.175 wt.%. The enhancement in friction factor is largely attributed to the increase in the viscosity of nano-coolants. Note that for a constant Reynolds number, an increase in viscosity requires a small increase in fluid velocity. Therefore, the increase in the velocity of working fluid can be considered as the reason for increase of the friction factor of the nano-coolants in convective heat transfer systems. This matter can be acknowledged by revisiting Eq. (3.5) for the pressure drop and friction factor, and Eq. (3.3) for the Reynolds number.

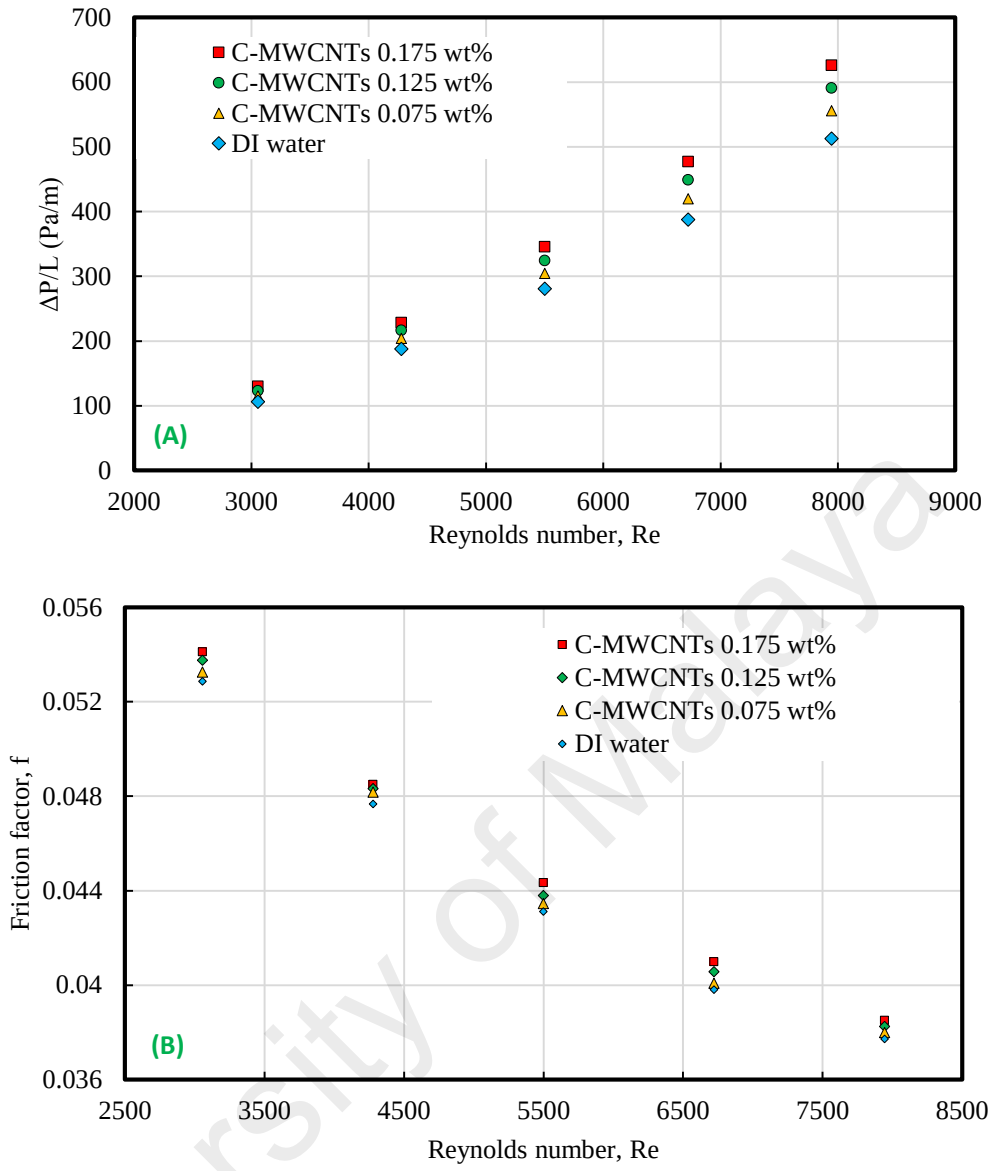

Figure 4. 16: Plot of (A) pressure drop and (B) friction factor versus the Reynolds number for C-MWCNT-DI water nanofluids in the annular test section

The performance index (ε) was calculated using Eq. (4.9) to evaluate the economic performance of the novel, eco-friendly C-MWCNT-DI water nanofluids synthesized in this study as potential fluids in heat transfer systems such as solar collectors and heat exchangers.

$$\varepsilon = \frac{h_{nf}/h_{bf}}{\Delta P_{nf}/\Delta P_{bf}} = \frac{R_h}{R_{\Delta P}} \tag{4.9}$$

Where, $R_{\Delta P}$ is the ratio of pressure drop of the C-MWCNs aqueous suspensions to the base fluid, and R_h is the ratio of heat transfer enhancement of C-MWCNTs nanofluids

relative to the base fluid. Figure 4.17 indicates the performance index of the C-MWCNT aqueous suspensions over a range of Reynolds number and various nanoparticle concentrations. It can be observed that the performance index is higher than 1 for all the samples, which shows the advantage of using these novel nanofluids in heat transfer systems. It is apparent that the performance index increases with increasing the concentration of C-MWCNTs in the base fluid. This implies that these eco-friendly nanofluids have higher effectiveness when the particle loading is increased. Figure 4.17shows that the performance index of the C-MWCNT nanofluids tends to increase with the increase in the Reynolds number (regardless of the nanoparticle concentration), indicating that the C-MWCNT-DI water nanofluids are suitable alternative coolants for heat transfer applications.

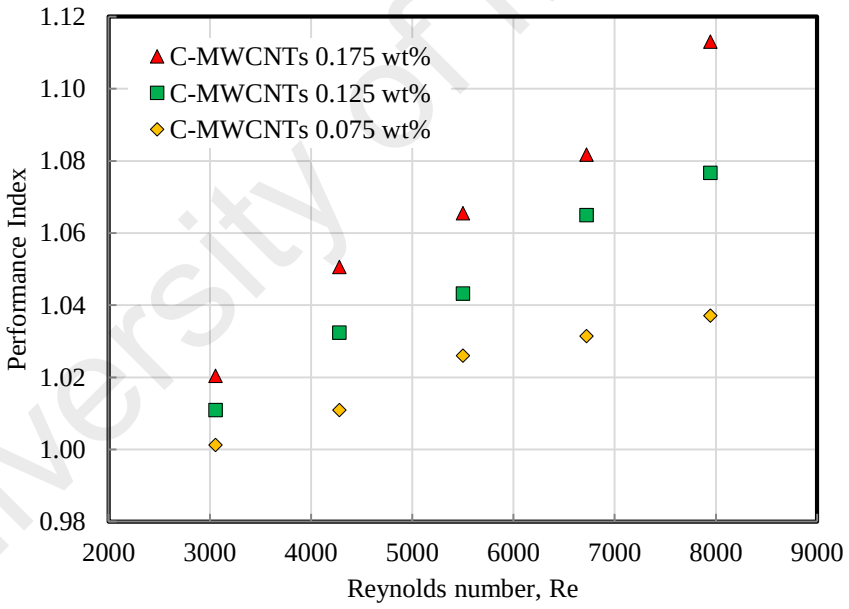

Figure 4. 17: Plot of performance index versus Reynolds number for the C-MWCNT-DI water nanofluids

The power consumption of a heat transfer set-up is a significant parameter in terms of economy and energy saving in various thermal applications. The pumping power for turbulent flow regime can be measured using following Equation (Mansour, Galanis, & Nguyen, 2007) :

$$\dot{W} = 0.158\left(\frac{4}{\pi}\right)^{1.74}\left(\frac{L\dot{m}^{2.75}\mu^{0.25}}{\rho^2 D^{4.75}}\right) \tag{4.10}$$

Where, $\dot{m}$ is mass flow rate. Using $\rho = \frac{\dot{m}}{\dot{V}}$ and $v = \frac{\dot{V}}{A}$ for a fixed $Re = \frac{\rho v D}{\mu}$ and substituting $\dot{m}$ into the Eq. (4.10), the relative pumping power $(\frac{\dot{W}_{nf}}{\dot{W}_{bf}})$ for constant Reynolds number is given as,

$$\frac{\dot{W}_{nf}}{\dot{W}_{bf}} = \left(\frac{\rho_{bf}}{\rho_{nf}}\right)^2\left(\frac{\mu_{nf}}{\mu_{bf}}\right)^3 \tag{4.11}$$

Where $\dot{W}_{bf}$ and $\dot{W}_{nf}$ is the pumping power of the base fluid and nano-coolants, respectively. The relative pumping power of the nano-coolants is calculated employing the equation (4.11) and the results are presented in Figure 4.18 for various weight concentrations. It can be clearly seen that the efficiency of loop is greater than 1 for the range of Reynolds numbers and weight concentrations studied, showing the potential of C-MWCNTs aqueous suspensions as a novel environmentally friendly alternative coolant in heat transfer equipment.

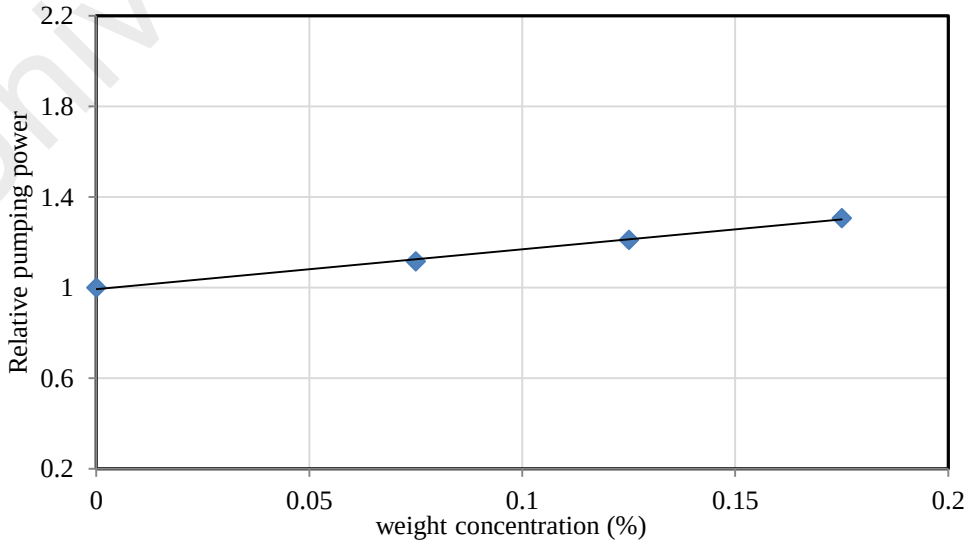

Figure 4. 18: Relative pumping power of the clove treated MWCNTs-water nanofluids and distilled water

4.6 Thermal performance of C-GNPs-DI water nanofluids

A series of experiments were conducted for the CGNPs-DI water nanofluids (nanoparticle concentrations: 0.025, 0.750 and 0.1 wt.%) by varying the Reynolds number from 3055 ± 5 to 7944 ± 5 in order to determine the convective heat transfer of the aqueous suspensions in turbulent flow regime. The input power was kept fixed at 900 W. The results are shown in Figure 4.19 for a constant inlet temperature of 30℃. It can be observed that the convective heat transfer coefficient increases when the Reynolds number is increased for both the base fluid and CGNP-DI water nanofluids. It can also be observed that the nanoparticle concentration affects the heat transfer coefficient of the CGNP aqueous suspensions. The remarkable enhancement in convective heat transfer coefficient of the CGNP-DI water nanofluids is mainly due to the thermal conductivity enhancement of nanofluids, narrow thermal boundary layer as well as a decrease in thermal resistance between the flowing nanofluids and inner wall surface of the annular tube at higher Reynolds number. According to some researchers (Aravind et al., 2011; Ding et al., 2006), carbon nanomaterials (*e.g.* carbon nanotubes and graphene nanoplatelets) tend to reduce the thickness of the thermal boundary layer. The specific surface area and Brownian motion of the nanoparticles also play a significant role in influencing the convective heat transfer coefficient. In this study, the convective heat transfer coefficient of the nanofluids increased by 10.48, 28.56 and 41.25% for the nanoparticle concentrations of 0.025, 0.75 and 0.1 wt.%, respectively.

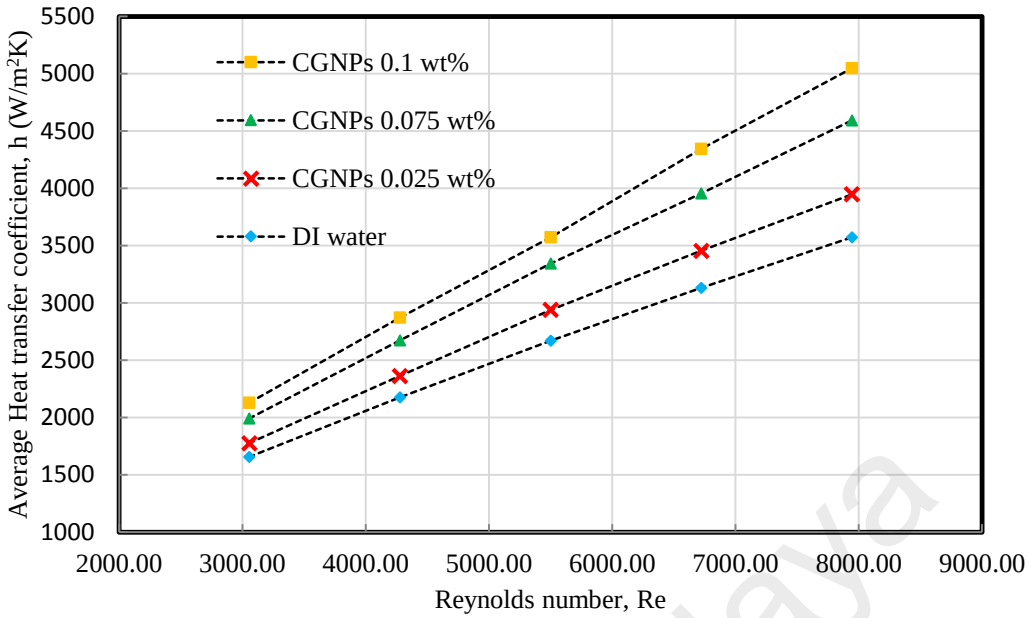

Figure 4. 19: Variation of the average heat transfer coefficient for CGNP/ DI water nanofluids versus Reynolds number

To assess the convective-to-conductive heat transfer ratio of CGNP aqueous suspensions, the average Nusselt number determined from Eq.3.4 was plotted as a function of Reynolds number and nanoparticle concentration. The results are shown in Figure 4.20 and it can be seen that there is a significant increase in the Nusselt number with the increase in the Reynolds number as well as concentration of CGNPs relative to that for the DI water. The greater Nusselt number for the CGNP nanofluids is attributed to the higher thermal conductivity of nanofluids, as well as the Brownian motion of the CGNPs (Sundar et al., 2014). The maximum increase in the Nusselt number of the CGNP-DI water nanofluids were found as 6.14, 15.34 and 21.90% for the nanoparticle concentrations of 0.025, 0.75 and 0.1 wt.%, respectively. This maximum increase was achieved at Re = 7944 ± 5.

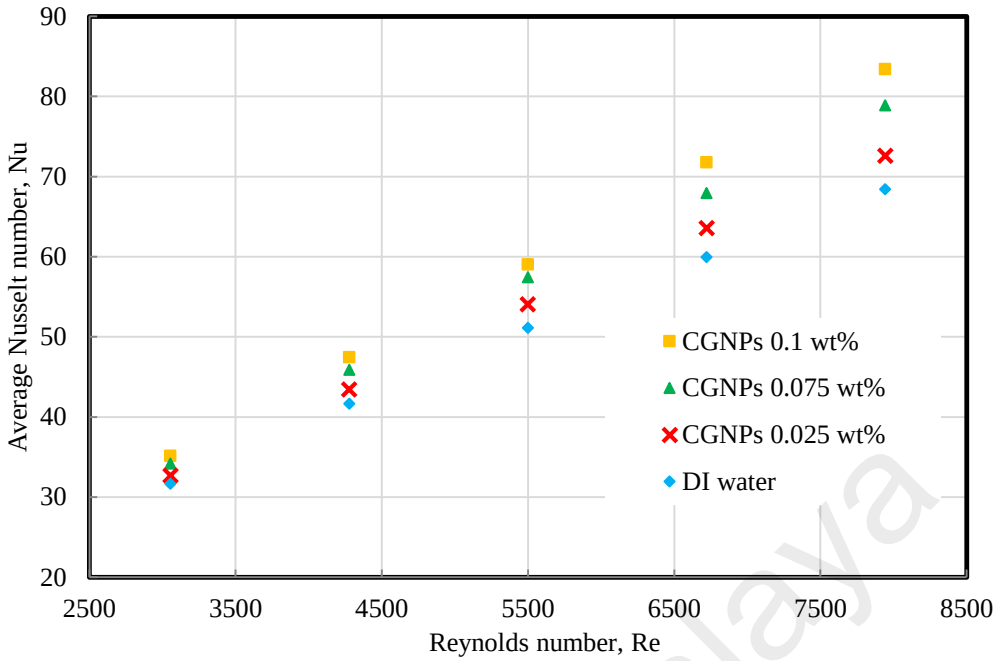

Figure 4. 20: Variation of the Nusselt number for CGNP-DI water nanofluids as a function of Reynolds number

The pressure drop of the CGNP-DI water nanofluids flowing through the test section recorded over a range of Reynolds number is shown in Figure 4.21(a). The corresponding friction factor values were calculated using Eq. (3.5) and the results are shown in Figure 4.21(b). The results show that there was a small increment in both the pressure drop and friction factor for the CGNP-DI water nanofluids relative to those for DI water. The maximum increase in the friction factor and pressure drop was found to be ~2.4% and 16.65%, respectively, for the nanoparticle concentration of 0.1 wt.%. The enhancement in friction factor is largely attributed to the increase in the viscosity of CGNP nano-coolants. Note that for a constant Reynolds number, an increase in viscosity requires a small increase in fluid velocity. Therefore, the increase in the velocity of working fluid can be considered as the reason for increase of the friction factor of the nano-coolants in convective heat transfer systems.

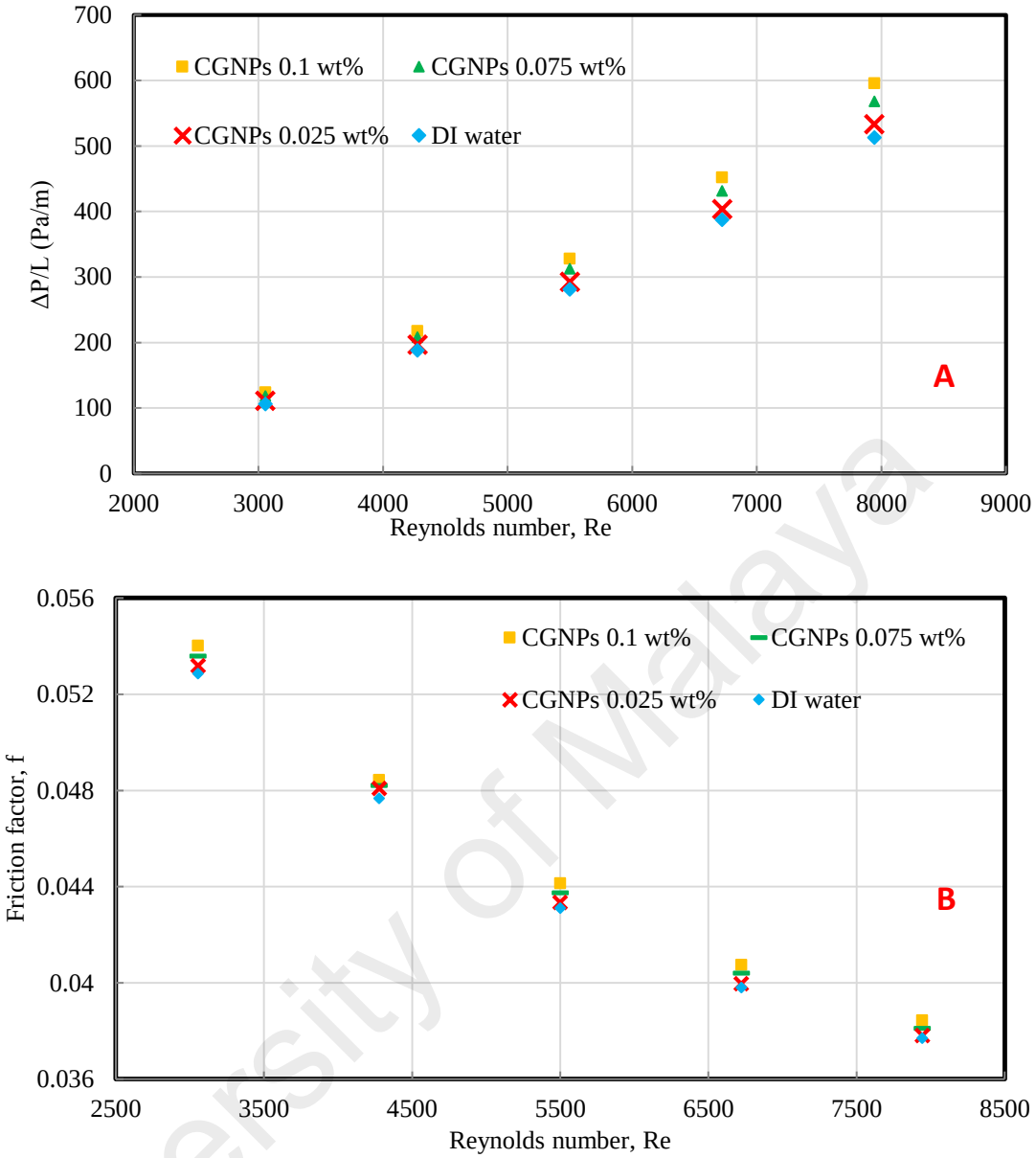

Figure 4. 21: Plot of (A) pressure drop and (B) friction factor versus the Reynolds number for CGNP-DI water nanofluids in the annular test section

Figure 4.22 indicates the performance index of the CGNP aqueous suspensions over a range of Reynolds number and various nanoparticle concentrations. It can be observed that the performance index is higher than 1 for all the samples, which show the advantage of using these novel nanofluids in heat transfer systems. It is apparent that the performance index increases with the increasing of the concentration of CGNPs in the base fluid. This implies that these eco-friendly nanofluids have higher effectiveness when the particle loading is increased. Figure 4.22 shows that the performance index of the

CGNP nanofluids tends to increase with the increase of the Reynolds number (regardless of the nanoparticle concentration), indicating that the CGNP-DI water nanofluids are suitable alternative coolants for heat transfer applications.

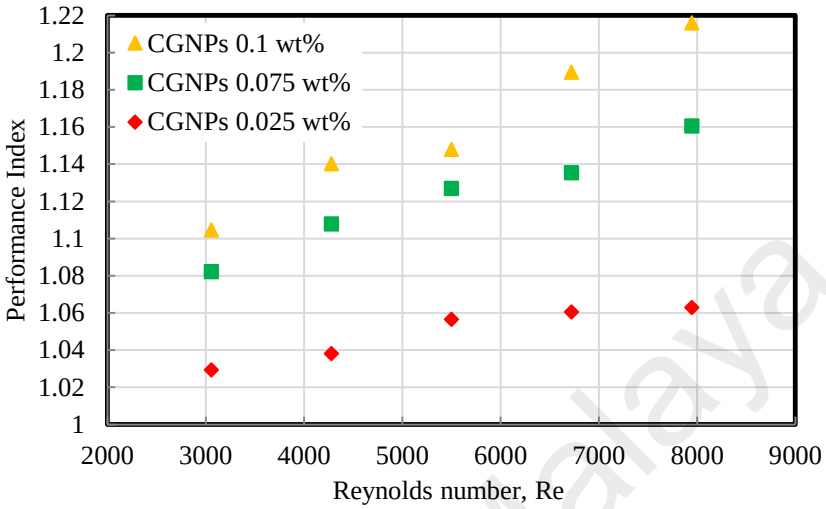

Figure 4. 22: Plot of performance index versus Reynolds number for the CGNP-DI water nanofluids

While the performance index evaluates the efficiency in terms of heat transfer rate and pressure drop, the increase in the required pumping power is of more concern in certain applications. In Eq. (4.11) η must be higher than 1 for the new heat transfer fluid to be cost effective. Variations of loop efficiency with concentration for a range of Re are plotted in Figure4.23. It is seen that the efficiency of the loop is greater than 1 for the range of Reynolds numbers and weight concentrations studied, showing the potential of CGNPs aqueous suspensions as a novel environmentally friendly alternative coolant in heat transfer equipment.

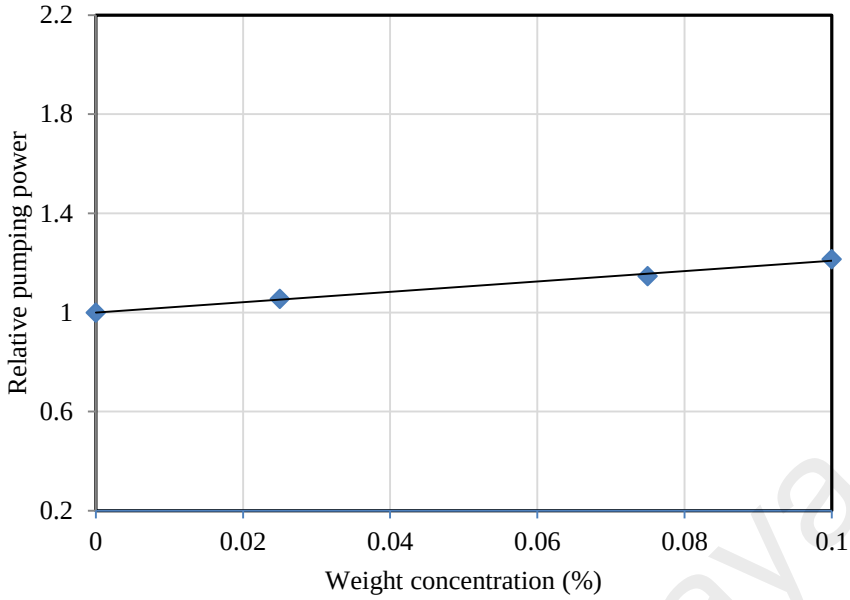

Figure 4. 23: Relative pumping power of the CGNP-water nanofluids and distilled water

4.7 Numerical study of heat transfer to Clove treated MWCNT nanofluids

4.7.1 Temperature distributions of nanofluids

Figure 4.23 shows the inner wall temperature distribution of the concentric annular heat exchanger. It can be observed that the inner wall temperature decreases when the C-MWCNT/DI water nanofluids are used as the working fluids instead of DI water. This is attributed to the higher convective heat transfer enhancement, which promotes heat transfer from the higher-temperature surface (i.e. inner wall of the tube) to the fluid.

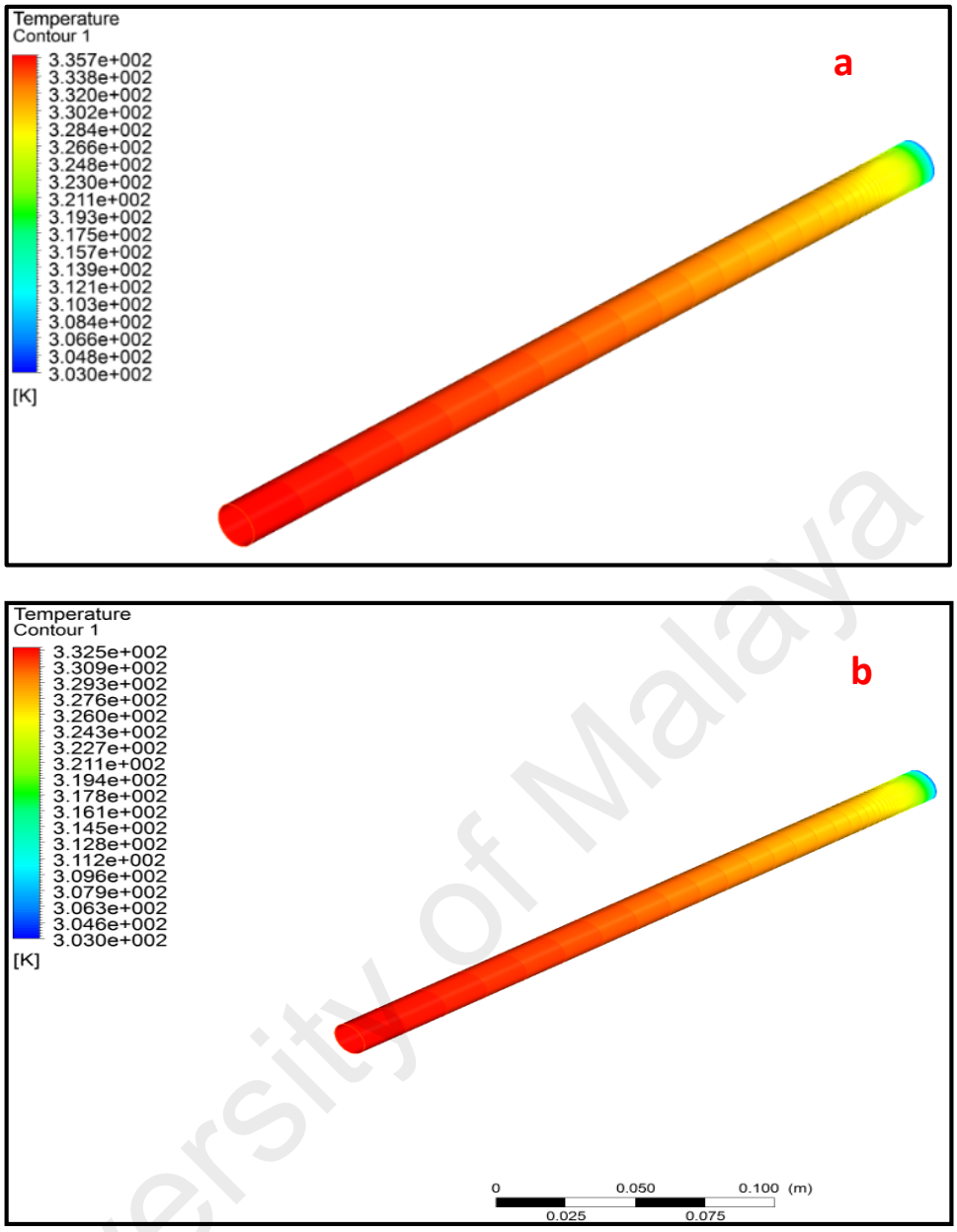

Figure 4. 24: Inner wall temperature distribution of the concentric annular heat exchanger with (a) DI water and (b) C-MWCNT/DI water nanofluid containing 0.175 wt.% of C-MWCNTs

Figure 4.25 shows the velocity contours of the concentric annular heat exchanger with DI water and C-MWCNT/DI water nanofluid containing 0.175 wt.% of C-MWCNTs. It can be observed that the flow becomes fully developed within a short axial distance from the inlet because of the narrow annulus. In addition, the maximum velocity is higher for the nanofluid compared with that for DI water even though the Reynolds number is constant. As shown in Equation 3.3, the flow velocity will increase if the viscosity increases at a

higher rate compared with density, provided that the tube diameter and Reynolds number are constant.

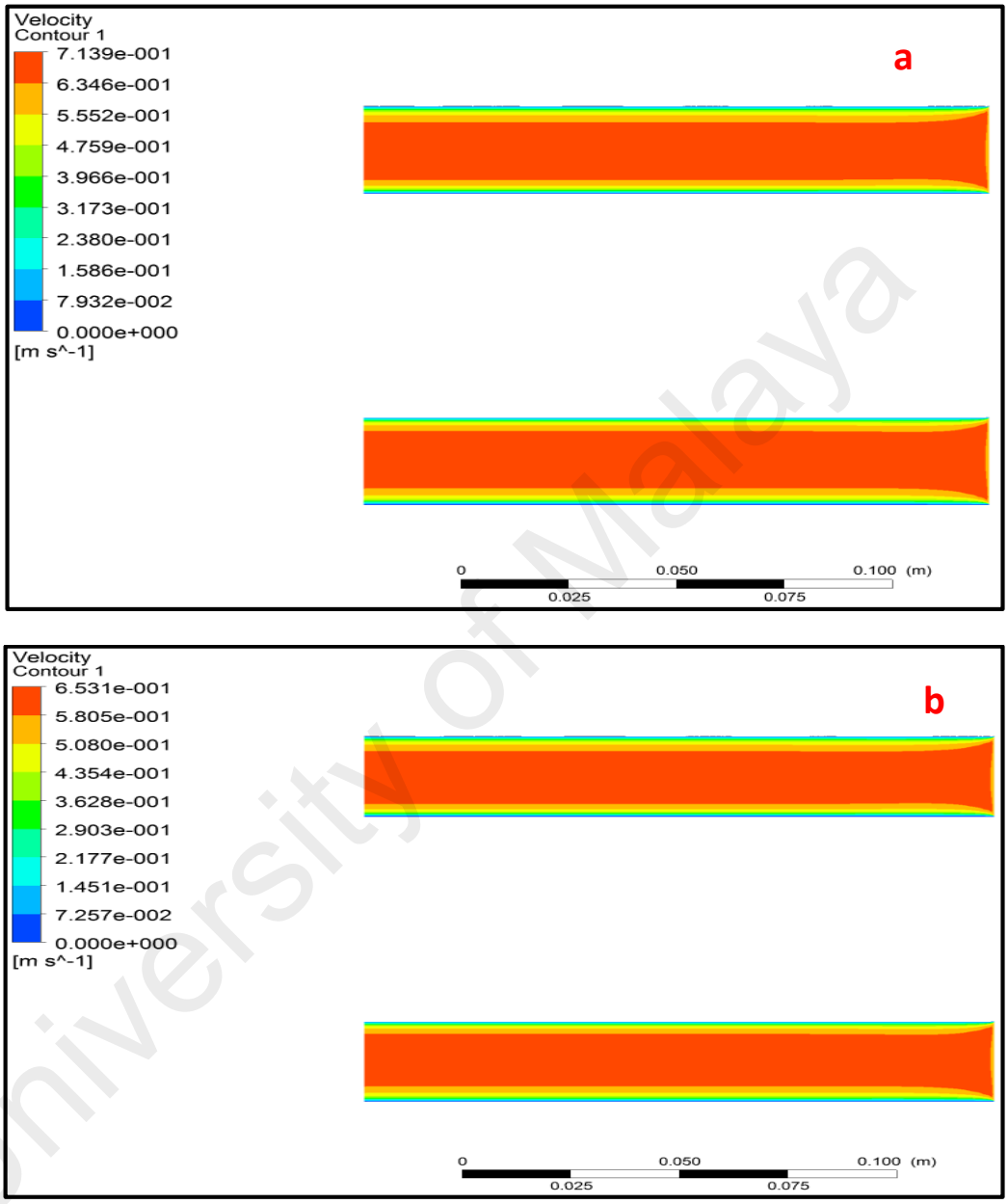

Figure 4. 25: Velocity contours of the concentric annular heat exchanger with (a) C-MWCNT/DI water nanofluid containing 0.175 wt.% of C-MWCNTs and (b) DI water

4.7.2 Validation of the present discussion

To validate the accuracy of the numerical analysis, the Nusselt number (Nu) and the pressure drop (ΔP)of the DI water are compared with the theoretical data under fully developed periodic condition (Shown in Fig 4.26). The present numerical results of Nusselt number show a good agreement with the experimental data, indicating the accuracy of the numerical model. The average relative error between experimental data and values from the McAdams correlation (Eq.4.8) with the average deviation of 8.42% and 7.28% respectively, whereas the Gnielinski correlation(Eq.4.2) shows higher deviation from simulation values of Nusselt number at lower Reynolds number and escalates with the increase of Reynolds number with average error of 18%.

Fig. 9(b) shows the numerical results of the pressure drop (ΔP)of the DI water. It is observed that the numerical results agree fairly well with the experimental data Eq. (3.5) and correlation of Gnielinski Eq. (4.6). The maximum error between the values obtained from experiments and Gnielinski empirical correlation is found to be approximately 7.32and 11.78%, respectively. As a result, the numerical output by the ANSYS-fluent is in good agreement with analytical and experimental data for clove treated multi walled carbon nanotube-DI water nanofluids in an annular heat exchanger.

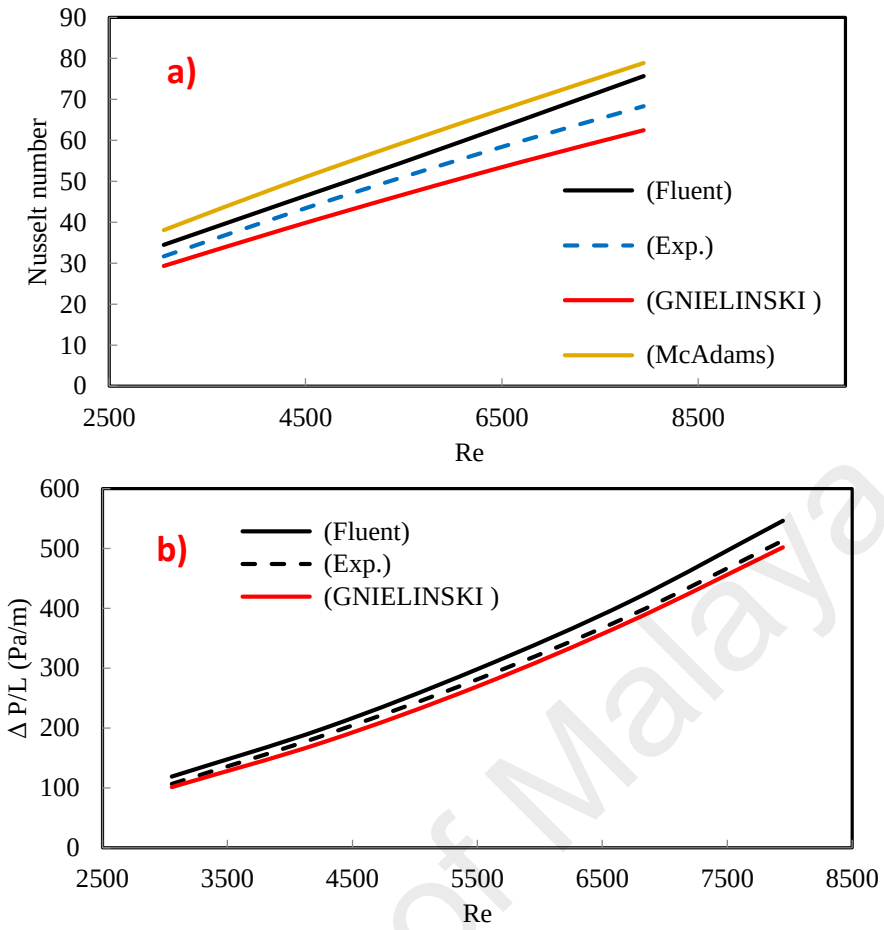

Figure 4. 26: Comparison of the (a) Nusselt number and (b) pressure drop for DI water obtained from numerical simulations with those from experiments and empirical correlations

4.7.3 Thermal analysis of C-MWCNT-DI water nanofluid

Figure 4.27 gives axial profile of local heat transfer coefficient of nanofluids for heat flux of 38346W/m^2 and various nanoparticle weight concentrations (0.075.0.125,0.175 wt%) of clove treated MWCNT nanofluids at three Reynolds numbers, respectively. As shown in this figure heat transfer coefficients decreased with increasing the axial location. The simulation results clearly show an initial drop in the local heat transfer coefficient. After placing at the minimum position, the local heat transfer coefficient remains constant in the axial direction due to the fully developed turbulent flow. It is shown that the C-MWCNTs loading in the basefluid improves the thermal conductivity of the nanofluid, and decreases the wall temperature as compared to the data of the conventional basefluid. Consequently, there is a decrease in the temperature difference between the wall and bulk

temperature and with the heat flux on the wall being constant, there is an increase in the heat transfer coefficient, as shown in Figure 4.27 a,b and c.

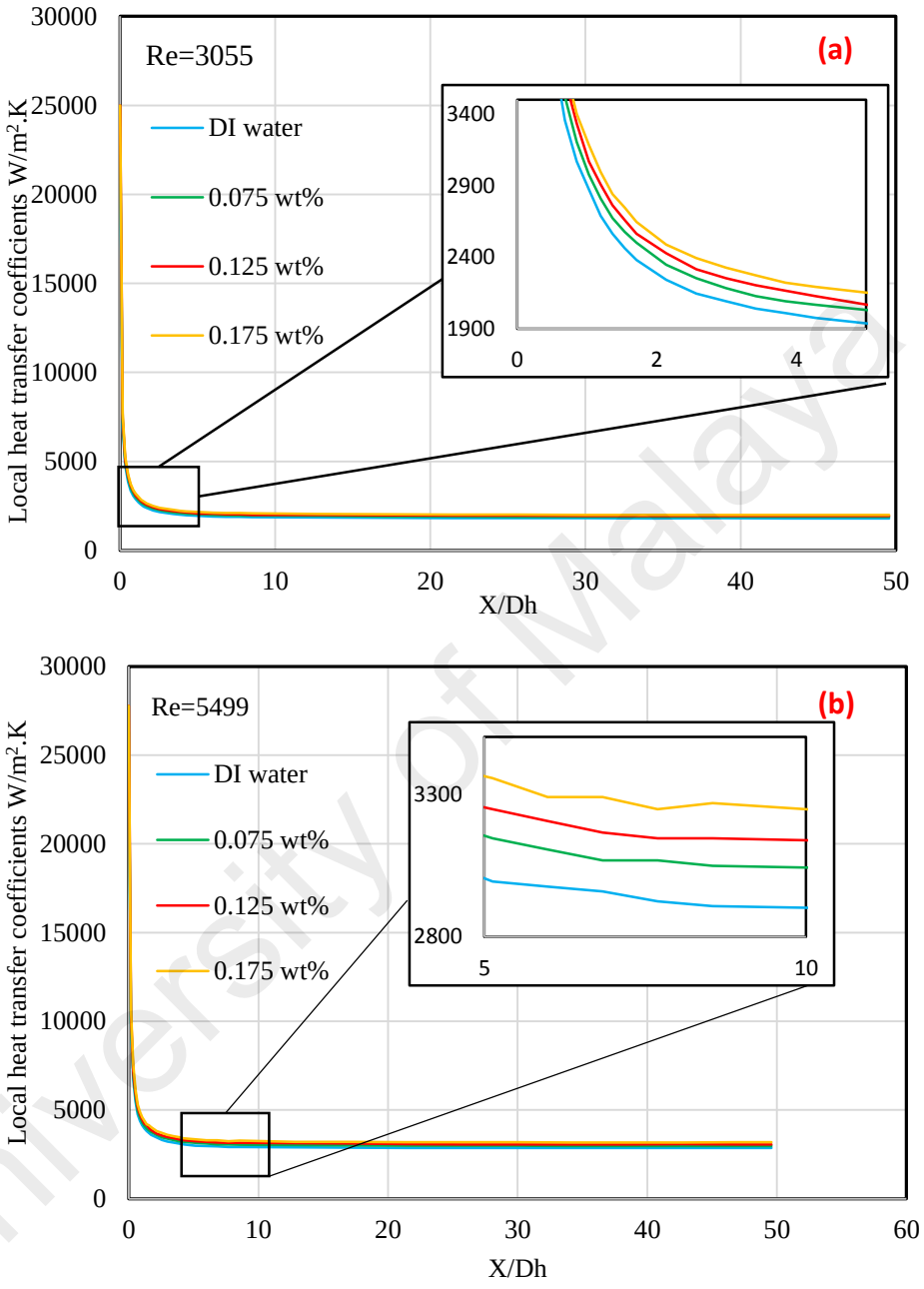

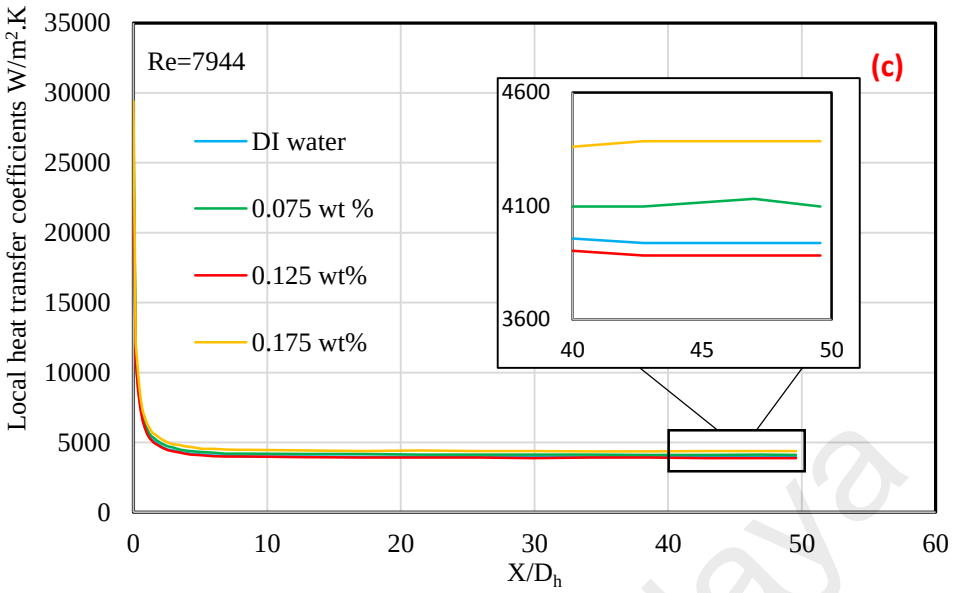

Figure 4. 26: Variation of the local convective heat transfer coefficient obtained numerically for C-MWCNT/DI water nanofluids with different C-MWCNT concentrations for three Reynolds numbers: (a) Re = 3055, (b) Re = 5499 and (c) Re = 7944

The average heat transfer coefficient characteristics with respect to nanoparticle weight concentration and Re for the Clove treated MWCNTs-DI water nanofluid at constant heat flux are shown in Figure 4.28. It is realized that, the average heat transfer coefficient increases with the increase in Re and nanoparticle concentration. The significant enhancement in convective heat transfer coefficient of the C-MWCNT-DI water nanofluids is mainly due to the narrow thermal boundary layer resulting from the thermal conductivity enhancement of C-MWCNT-DI water nanofluids as well as a decrease in thermal resistance between the flowing nanofluids and inner wall surface of the annular tube at higher Reynolds numbers. Noticeably, as reported by researchers (Aravind et al., 2011; Ding et al., 2006), carbon nanomaterials such as graphene and CNTs decrease thickness of thermal boundary layer. The specific surface area and Brownian motion of the nanoparticles also play a role in influencing the convective heat transfer coefficient. Convective heat transfer coefficient increased up to 4.32, 7.68 and 11.26 %, respectively, for the weight fractions of 0.075, 0.125 and 0.175 wt% at the

constant heat flux of 38346 W/m^2 and fixed Reynolds number of 7944±5. Furthermore, simulated data for nanofluids shows good agreement with the experimental data with the average deviation percentages of 2.15, 3.45, 7.7% at the concentrations of 0.75, 0.125, and 0.175 respectively.

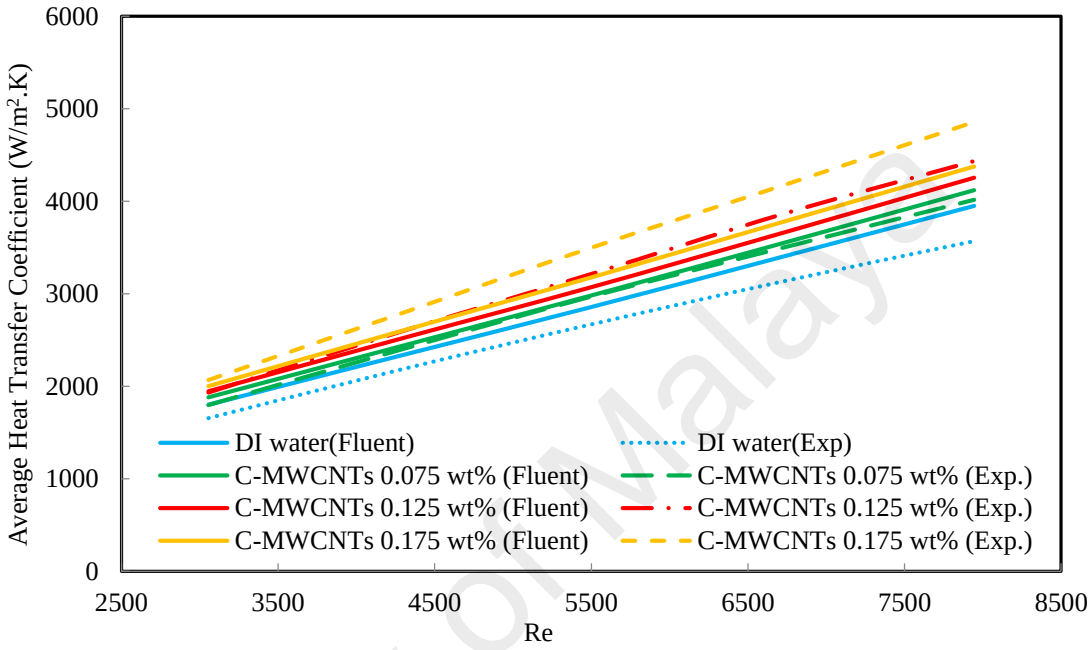

Figure 4. 27: Variation of the average heat transfer coefficient with respect to the Reynolds number for C-MWCNT/DI water nanofluids in the concentric annular heat exchanger

Figure 4.29 depicts the friction factor and pressure drop of clove treated MWCNTs in the concentric annular heat exchanger versus Reynolds numbers, at various weight concentrations. It can be clearly seen that the friction factor and pressure drop of both the numerical and experimental results are declining and increasing respectively, with the increment of the Reynolds number. In addition, the results show that there is a small increment in both the pressure drop and friction factor for the C-MWCNT-DI water nanofluids relative to those data of DI water.

The average increase in the friction factor and pressure drop are 0.028% and 20.41 %, respectively, for a nanoparticle concentration of 0.175 wt.%. The enhancement in friction factor is largely attributed to the increase in the viscosity of nanofluid. Note that

for a constant Reynolds number, an increase in viscosity requires a small increase in fluid velocity. Therefore, the increase in the velocity of working fluid can be considered as the reason for increase of the friction factor of the nanofluid in convective heat transfer systems. The CFD predictions of pressure drop and friction factor show a good agreement with the experimental data, while the average error less than 5.54 % and 1.79% for the concentration of 0.175 wt.%.

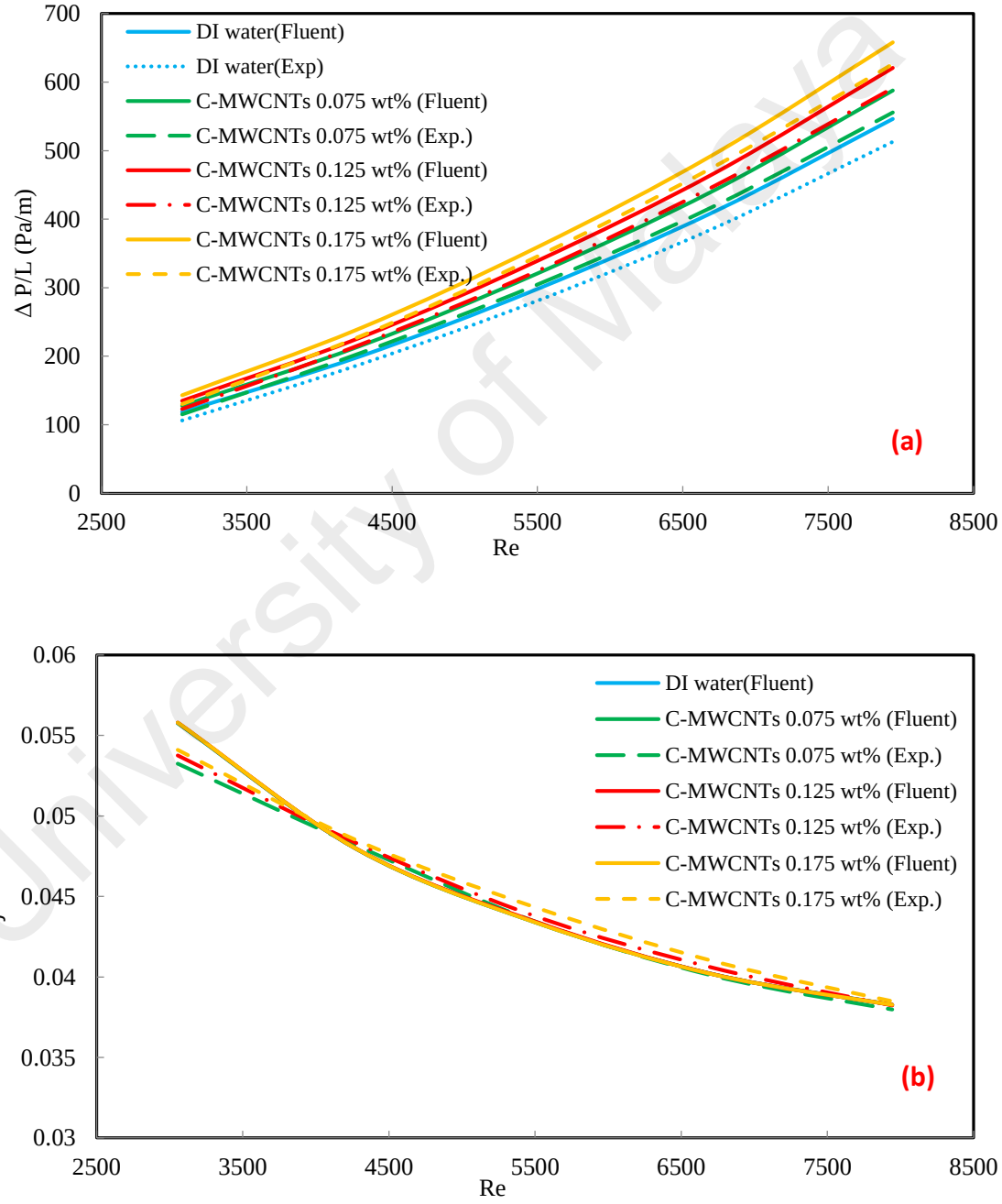

Figure 4. 28: Variation of (a) pressure drop and (b) friction factor of the C-MWCNT/DI water nanofluids with respect to the Reynolds number

CHAPTER 5: CONCLUSIONS

An environmentally friendly and cost-effective procedure for synthesizing covalently functionalized multi-walled carbon nanotubes and graphene nanoplatelets with cloves (C--MWCNTs and CGNPs) has been developed in this study. C-MWCNTs and CGNPs nanofluids were prepared by adding adequate amount of respective nanoparticles in the base fluid with adequate sonication. The potential of these nanofluids suspensions as heat transfer working fluids is investigated by convective heat transfer experiments in an annular heat exchanger at turbulent flow regime. The exceptional performance of the functionalization method has been confirmed by FTIR, RAMAN and XPS spectroscopy as well as TGA, and TEM. The stability of colloidal suspensions was examined with UV-vis spectroscopy and the maximum sedimentation of 11.3 and 11.8% is obtained for the C-MWCNT-DI water and CGNP-DI water nanofluids, respectively, at the corresponding highest concentration over the course of 63 days. Based on the thermo-physical properties of the CMWCNT-DI water and CGNP-DI water nanofluids, it can be deduced that these nanofluids are potential working fluids in heat transfer systems. Thus it can be deduced that these nanofluids are potential working fluids in heat transfer systems. Heat transfer analysis data reveals that there was significant enhancement in the convective heat transfer coefficient and Nusselt number about 20.15% for C-MWCNT-DI water nanofluids and 41.25% for CGNP-DI water nanofluids. These enhancements were observed at a Reynolds number of 7944 ± 5, constant heat flux of 38346 W/m^2 and nanoparticle concentration of 0.175 wt. % (*i.e.* C-MWCNTs) and 0.1 wt. % (*i.e.* CGNPs).

Simultaneous study of friction factor of the C-MWCNT-DI water and CGNP-DI water nanofluids experienced enhancement about 3 and 2.4%, respectively, relative to that of the base fluid, at the investigated highest nanoparticle concentrations. The observed insignificant increase in pumping power for both the C-MWCNT-DI water and CGNP-DI water nanofluids show their suitability for industrial applications. In addition,

it is found that the performance indexes of both the C-MWCNT-DI water and CGNP-DI water nanofluids are more than 1 (regardless of the nanoparticle concentration investigated in this study), indicating that these nanofluids are potential working fluids in heat transfer systems in terms of overall thermal performance and energy savings.

The experimental thermo-physical properties data were used as the raw data for ANSYS-Fluent for evaluation of heat transfer and pressure loss performances in single-phase approach. The validation results confirmed the applicability of Fluent to simulate heat transfer phenomena in the presence of nanofluids and turbulent flow condition. The experimental results of the average heat transfer coefficient of C-MWCNTs-DI water nanofluids were in good agreement with the data obtained form simulation with an average deviation of 7.7%.

5.1 Suggestion for further works

The research works presented in this thesis have opened new insights into the flow behavior and heat transfer to clove treated carbon based nanofluids through concentric annular heat exchanger. Based on the present findings the following recommendations could be made:

1- Study of the flow behavior of carbon based nanofluids at high velocities to investigate effect at high turbulent region.

2- Study on the laminar flow behavior of metal oxides and carbon based nanofluids which could extend the research avenues.

3- The present numerical approach can be extended by applying two phase method of simulation

4- In this study only two types of nanofluids were investigated, hence other different types of nanofluids could be incorporated in the investigations.

REFERENCES

Abu-Nada, E., Masoud, Z., & Hijazi, A. (2008). Natural convection heat transfer enhancement in horizontal concentric annuli using nanofluids. *International Communications in Heat and Mass Transfer, 35*(5), 657-665.

Abu-Nada, E., & Oztop, H. F. (2009). Effects of inclination angle on natural convection in enclosures filled with Cu–water nanofluid. *International Journal of Heat and Fluid Flow, 30*(4), 669-678.

Ahuja, A. S. (1975a). Augmentation of heat transport in laminar flow of polystyrene suspensions. I. Experiments and results. *Journal of Applied Physics, 46*(8), 3408-3416.

Ahuja, A. S. (1975b). Augmentation of heat transport in laminar flow of polystyrene suspensions. II. Analysis of the data. *Journal of Applied Physics, 46*(8), 3417-3425.

Akbarinia, A., & Behzadmehr, A. (2007). Numerical study of laminar mixed convection of a nanofluid in horizontal curved tubes. *Applied Thermal Engineering, 27*(8), 1327-1337.

Allen, M. J., Tung, V. C., & Kaner, R. B. (2009). Honeycomb carbon: a review of graphene. *Chemical reviews, 110*(1), 132-145.

Amrollahi, A., Hamidi, A., & Rashidi, A. (2008). The effects of temperature, volume fraction and vibration time on the thermo-physical properties of a carbon nanotube suspension (carbon nanofluid). *Nanotechnology, 19*(31), 315701.

Anoop, K., Sundararajan, T., & Das, S. K. (2009). Effect of particle size on the convective heat transfer in nanofluid in the developing region. *International Journal of Heat and Mass Transfer, 52*(9), 2189-2195.

Aravind, S. J., Baskar, P., Baby, T. T., Sabareesh, R. K., Das, S., & Ramaprabhu, S. (2011). Investigation of structural stability, dispersion, viscosity, and conductive heat transfer properties of functionalized carbon nanotube based nanofluids. *The Journal of Physical Chemistry C, 115*(34), 16737-16744.

Assael, M., Chen, C.-F., Metaxa, I., & Wakeham, W. (2004). Thermal conductivity of suspensions of carbon nanotubes in water. *International Journal of Thermophysics, 25*(4), 971-985.

Assael, M., Metaxa, I., Arvanitidis, J., Christofilos, D., & Lioutas, C. (2005). Thermal conductivity enhancement in aqueous suspensions of carbon multi-walled and double-walled nanotubes in the presence of two different dispersants. *International Journal of Thermophysics, 26*(3), 647-664.

Avsec, J., & Oblak, M. (2007). The calculation of thermal conductivity, viscosity and thermodynamic properties for nanofluids on the basis of statistical nanomechanics. *International Journal of Heat and Mass Transfer, 50*(21), 4331-4341.

Azizi, M., Hosseini, M., Zafarnak, S., Shanbedi, M., & Amiri, A. (2013). Experimental analysis of thermal performance in a two-phase closed thermosiphon using graphene/water nanofluid. *Industrial & Engineering Chemistry Research, 52*(29), 10015-10021.

Baby, T. T., & Ramaprabhu, S. (2010). Investigation of thermal and electrical conductivity of graphene based nanofluids. *Journal of Applied Physics, 108*(12), 124308.

Bala, H., Fu, W., Zhao, J., Ding, X., Jiang, Y., Yu, K., & Wang, Z. (2005). Preparation of BaSO 4 nanoparticles with self-dispersing properties. *Colloids and Surfaces A: Physicochemical and Engineering Aspects, 252*(2), 129-134.

Baskaran, D., Mays, J. W., & Bratcher, M. S. (2004). Polymer-grafted multiwalled carbon nanotubes through surface-initiated polymerization. *Angewandte Chemie International Edition, 43*(16), 2138-2142.

Behzadmehr, A., Saffar-Avval, M., & Galanis, N. (2007). Prediction of turbulent forced convection of a nanofluid in a tube with uniform heat flux using a two phase approach. *International journal of heat and fluid flow, 28*(2), 211-219.

Berber, S., Kwon, Y.-K., & Tomanek, D. (2000). Unusually high thermal conductivity of carbon nanotubes. *Physical Review Letters, 84*(20), 4613-4616.

Bianco, V., Chiacchio, F., Manca, O., & Nardini, S. (2009). Numerical investigation of nanofluids forced convection in circular tubes. *Applied Thermal Engineering, 29*(17), 3632-3642.

Bianco, V., Manca, O., & Nardini, S. (2011). Numerical investigation on nanofluids turbulent convection heat transfer inside a circular tube. *International Journal of thermal sciences, 50*(3), 341-349.

Buongiorno, J. (2006). Convective transport in nanofluids. *Journal of heat transfer, 128*(3), 240-250.

Byl, O., Liu, J., & Yates, J. T. (2005). Etching of carbon nanotubes by ozone a surface area study. *Langmuir, 21*(9), 4200-4204.

Cao, B., Cai, W., & Zeng, H. (2006). Temperature-dependent shifts of three emission bands for< equation>< font face='verdana'> ZnO</equation> nanoneedle arrays. *Applied Physics Letters, 88*(16), 161101-161101-161103.

Chen, L., & Xie, H. (2010). Properties of carbon nanotube nanofluids stabilized by cationic gemini surfactant. *Thermochimica Acta, 506*(1), 62-66.

Chen, W.-Y., & Chen, Y.-C. (2010). Functional Fe3O4@ ZnO magnetic nanoparticle-assisted enrichment and enzymatic digestion of phosphoproteins from saliva. *Analytical and bioanalytical chemistry, 398*(5), 2049-2057.

Choi, S., Zhang, Z., & Keblinski, P. (2004). Nanofluids, Encyclopedia of Nanoscience and Nanotechnology (HS Nalwa, Editor), Vol. 5. p.(757-773): American Scientific Publisher.

Choi, S., Zhang, Z., Yu, W., Lockwood, F., & Grulke, E. (2001). Anomalous thermal conductivity enhancement in nanotube suspensions. *Applied Physics Letters, 79*(14), 2252-2254.

Choi, S. U. (2009). Nanofluids: from vision to reality through research. *Journal of heat transfer, 131*(3).

Choi, S. U., & Eastman, J. (1995). Enhancing thermal conductivity of fluids with nanoparticles: Argonne National Lab., IL (United States).

Choi, S. U., & Eastman, J. A. (2001). Enhanced heat transfer using nanofluids: Google Patents.

Chol, S. (1995). Enhancing thermal conductivity of fluids with nanoparticles. *ASME-Publications-Fed, 231*, 99-106.

Chopkar, M., Das, P. K., & Manna, I. (2006). Synthesis and characterization of nanofluid for advanced heat transfer applications. *Scripta Materialia, 55*(6), 549-552.

Chou, J.-C., & Liao, L. P. (2005). Study on pH at the point of zero charge of TiO 2 pH ion-sensitive field effect transistor made by the sputtering method. *Thin Solid Films, 476*(1), 157-161.

Chung, T. (2010). *Computational fluid dynamics*: Cambridge university press.

Das, R., Hamid, S. B. A., Ali, M., Annuar, M., Samsudin, E. M. B., & Bagheri, S. (2015). Covalent Functionalization Schemes for Tailoring Solubility of Multi-Walled Carbon Nanotubes in Water and Acetone Solvents. *Science of Advanced Materials, 7*(12), 2726-2737.

Das, S. K., Putra, N., Thiesen, P., & Roetzel, W. (2003). Temperature dependence of thermal conductivity enhancement for nanofluids. *Journal of heat transfer, 125*(4), 567-574.

Ding, Y., Alias, H., Wen, D., & Williams, R. A. (2006). Heat transfer of aqueous suspensions of carbon nanotubes (CNT nanofluids). *International journal of heat and mass transfer, 49*(1), 240-250.

Ding, Y., Chen, H., He, Y., Lapkin, A., Yeganeh, M., Šiller, L., & Butenko, Y. V. (2007). Forced convective heat transfer of nanofluids. *Advanced Powder Technology, 18*(6), 813-824.

Duangthongsuk, W., & Wongwises, S. (2009). Heat transfer enhancement and pressure drop characteristics of TiO 2–water nanofluid in a double-tube counter flow heat exchanger. *International Journal of Heat and Mass Transfer, 52*(7), 2059-2067.

Eastman, J., Choi, S., Li, S., Yu, W., & Thompson, L. (2001). Anomalously increased effective thermal conductivities of ethylene glycol-based nanofluids containing copper nanoparticles. *Applied Physics Letters, 78*(6), 718-720.

Eastman, J., Choi, U., Li, S., Thompson, L., & Lee, S. (1997). *Enhanced thermal conductivity through the development of nanofluids.* Paper presented at the Materials Research Society Symposium Proceedings.

El Bécaye Maïga, S., Tam Nguyen, C., Galanis, N., Roy, G., Maré, T., & Coqueux, M. (2006). Heat transfer enhancement in turbulent tube flow using Al2O3 nanoparticle suspension. *International Journal of Numerical Methods for Heat & Fluid Flow, 16*(3), 275-292.

Esfe, M. H., Saedodin, S., Mahian, O., & Wongwises, S. (2014). Heat transfer characteristics and pressure drop of COOH-functionalized DWCNTs/water nanofluid in turbulent flow at low concentrations. *International Journal of Heat and Mass Transfer*, *73*, 186-194.

Evans, W., Prasher, R., Fish, J., Meakin, P., Phelan, P., & Keblinski, P. (2008). Effect of aggregation and interfacial thermal resistance on thermal conductivity of nanocomposites and colloidal nanofluids. *International Journal of Heat and Mass Transfer, 51*(5), 1431-1438.

Fan, W., Zhang, L., & Liu, T. (2016). Graphene-Carbon Nanotube Hybrids for Energy and Environmental Applications. *SpringerBriefs in molecular science, Green chemistry for sustainability*

Fernandez-Seara, J., Uhía, F. J., Sieres, J., & Campo, A. (2007). A general review of the Wilson plot method and its modifications to determine convection coefficients in heat exchange devices. *Applied Thermal Engineering, 27*(17), 2745-2757.

Gan, Y., & Qiao, L. (2012). Optical properties and radiation-enhanced evaporation of nanofluid fuels containing carbon-based nanostructures. *Energy & Fuels, 26*(7), 4224-4230.

Garg, P., Alvarado, J. L., Marsh, C., Carlson, T. A., Kessler, D. A., & Annamalai, K. (2009). An experimental study on the effect of ultrasonication on viscosity and heat transfer performance of multi-wall carbon nanotube-based aqueous nanofluids. *International Journal of Heat and Mass Transfer*, *52*(21), 5090-5101.

Ghadimi, A., Saidur, R., & Metselaar, H. (2011). A review of nanofluid stability properties and characterization in stationary conditions. *International Journal of Heat and Mass Transfer*, *54*(17), 4051-4068.

Gharagozloo, P. E., & Goodson, K. E. (2010). Aggregate fractal dimensions and thermal conduction in nanofluids. *Journal of Applied Physics, 108*(7), 074309.

Gnielinski, V. (2015). Turbulent Heat Transfer in Annular Spaces—A New Comprehensive Correlation. *Heat Transfer Engineering, 36*(9), 787-789.

Hadjov, K. B. (2009). Modified self-consisted scheme to predict the thermal conductivity of nanofluids. *International Journal of thermal sciences, 48*(12), 2249-2254.

Harris, P. Carbon Nanotubes and Related Structures: New Materials for the Twenty-first Century. 1999: Cambridge University Press, Cambridge.

Heris, S. Z., Etemad, S. G., & Esfahany, M. N. (2006). Experimental investigation of oxide nanofluids laminar flow convective heat transfer. *International Communications in Heat and Mass Transfer, 33*(4), 529-535.

Hetsroni, G., & Rozenblit, R. (1994). Heat transfer to a liquid—solid mixture in a flume. *International Journal of Multiphase Flow, 20*(4), 671-689.

Hiemenz, P. C. (1986). *Principles of colloid and surface chemistry* (Vol. 188): M. Dekker New York.

Hong, K., Hong, T.-K., & Yang, H.-S. (2006). Thermal conductivity of Fe nanofluids depending on the cluster size of nanoparticles. *Applied physics letters, 88*(3), 031901.

Hong, T.-K., Yang, H.-S., & Choi, C. (2005). Study of the enhanced thermal conductivity of Fe nanofluids. *Journal of Applied Physics, 97*(6), 064311.

Huang, J., Wang, X., Long, Q., Wen, X., Zhou, Y., & Li, L. (2009). *Influence of pH on the stability characteristics of nanofluids.* Paper presented at the 2009 Symposium on Photonics and Optoelectronics.

Hwang, Y., Lee, J.-K., Lee, J.-K., Jeong, Y.-M., Cheong, S.-i., Ahn, Y.-C., & Kim, S. H. (2008). Production and dispersion stability of nanoparticles in nanofluids. *Powder Technology, 186*(2), 145-153.

Hwang, Y., Lee, J., Lee, C., Jung, Y., Cheong, S., Lee, C., . . . Jang, S. (2007). Stability and thermal conductivity characteristics of nanofluids. *Thermochimica Acta, 455*(1), 70-74.

Hwang, Y., Park, H., Lee, J., & Jung, W. (2006). Thermal conductivity and lubrication characteristics of nanofluids. *Current Applied Physics, 6*, e67-e71.

Iijima, S. (1991). Helical microtubules of graphitic carbon. *Nature, 354*(6348), 56-58.

Iijima, S., & Ichihashi, T. (1993). Single-shell carbon nanotubes of 1-nm diameter.

Indhuja, A., KS, S., Manikandan, S., & KS, R. (2013). Viscosity and thermal conductivity of dispersions of gum arabic capped MWCNT in water: Influence of MWCNT

concentration and temperature. *Journal of the Taiwan Institute of Chemical Engineers*.

Izadi, M., Behzadmehr, A., & Jalali-Vahida, D. (2009). Numerical study of developing laminar forced convection of a nanofluid in an annulus. *International Journal of Thermal Sciences, 48*(11), 2119-2129.

Jang, S. P., & Choi, S. U. (2004). Role of Brownian motion in the enhanced thermal conductivity of nanofluids. *Applied physics letters, 84*(21), 4316-4318.

Jung, J.-Y., Oh, H.-S., & Kwak, H.-Y. (2009). Forced convective heat transfer of nanofluids in microchannels. *International Journal of Heat and Mass Transfer, 52*(1), 466-472.

Kakac, S., & Pramuanjaroenkij, A. (2009). Review of convective heat transfer enhancement with nanofluids. *International Journal of Heat and Mass Transfer, 52*(13), 3187-3196.

Keblinski, P., Phillpot, S., Choi, S., & Eastman, J. (2002). Mechanisms of heat flow in suspensions of nano-sized particles (nanofluids). *International Journal of Heat and Mass Transfer, 45*(4), 855-863.

Kim, D., Kwon, Y., Cho, Y., Li, C., Cheong, S., Hwang, Y., . . . Moon, S. (2009). Convective heat transfer characteristics of nanofluids under laminar and turbulent flow conditions. *Current Applied Physics, 9*(2), e119-e123.

Kim, P., Shi, L., Majumdar, A., & McEuen, P. (2001). Thermal transport measurements of individual multiwalled nanotubes. *Physical Review Letters, 87*(21), 215502.

Kitagawa, M., & Tokiwa, Y. (2006). Polymerization of vinyl sugar ester using ascorbic acid and hydrogen peroxide as a redox reagent. *Carbohydrate polymers, 64*(2), 218-223.

Ko, G. H., Heo, K., Lee, K., Kim, D. S., Kim, C., Sohn, Y., & Choi, M. (2007). An experimental study on the pressure drop of nanofluids containing carbon nanotubes in a horizontal tube. *International Journal of Heat and Mass Transfer, 50*(23), 4749-4753.

Komarneni, S., Parker, J., & Wollenberger, H. (1997). Nanophase and Nanocomposite Materials IH.

kumar Saini, D., & Agarwal, G. D. Thermo-Physical Properties of Nano Fluids-A.

Launder, B. E., & Spalding, D. B. (1972). *Lectures in mathematical models of turbulence*. London ;: Academic Press.

Lee, D.-L., & Irvine, T. F. (1997). Shear rate dependent thermal conductivity measurements of non-Newtonian fluids. *Experimental Thermal and Fluid Science, 15*(1), 16-24.

Lee, J. H. (2009). *Convection performance of nanofluids for electronics cooling*: ProQuest.

Lee, K., Hwang, Y., Cheong, S., Kwon, L., Kim, S., & Lee, J. (2009). Performance evaluation of nano-lubricants of fullerene nanoparticles in refrigeration mineral oil. *Current Applied Physics, 9*(2), e128-e131.

Lee, S., Choi, S. U., Li, S., and, & Eastman, J. (1999). Measuring thermal conductivity of fluids containing oxide nanoparticles. *Journal of heat transfer, 121*(2).

Li, X., Zhu, D., Wang, X., Wang, N., Gao, J., & Li, H. (2008). Thermal conductivity enhancement dependent pH and chemical surfactant for Cu-H 2 O nanofluids. *Thermochimica Acta, 469*(1), 98-103.

Liu, M. S., Lin, M. C., Huang, I. T., & Wang, C. C. (2006). Enhancement of thermal conductivity with CuO for nanofluids. *Chemical engineering & technology, 29*(1), 72-77.

Loh, K. P., Bao, Q., Ang, P. K., & Yang, J. (2010). The chemistry of graphene. *Journal of Materials Chemistry, 20*(12), 2277-2289.

Madni, I., Hwang, C.-Y., Park, S.-D., Choa, Y.-H., & Kim, H.-T. (2010). Mixed surfactant system for stable suspension of multiwalled carbon nanotubes. *Colloids and Surfaces A: Physicochemical and Engineering Aspects, 358*(1), 101-107.

Maïga, S. E. B., Nguyen, C. T., Galanis, N., & Roy, G. (2004). Heat transfer behaviours of nanofluids in a uniformly heated tube. *Superlattices and Microstructures, 35*(3), 543-557.

Maiga, S. E. B., Palm, S. J., Nguyen, C. T., Roy, G., & Galanis, N. (2005). Heat transfer enhancement by using nanofluids in forced convection flows. *International Journal of heat and fluid flow, 26*(4), 530-546.

Mansour, R. B., Galanis, N., & Nguyen, C. T. (2007). Effect of uncertainties in physical properties on forced convection heat transfer with nanofluids. *Applied Thermal Engineering*, *27*(1), 240-249.

Marquis, F., & Chibante, L. (2005). Improving the heat transfer of nanofluids and nanolubricants with carbon nanotubes. *Jom*, *57*(12), 32-43.

Martel, R., Derycke, V., Lavoie, C., Appenzeller, J., Chan, K., Tersoff, J., & Avouris, P. (2001). Ambipolar electrical transport in semiconducting single-wall carbon nanotubes. *Physical Review Letters*, *87*(25), 256805.

Masuda, H., Ebata, A., Teramae, K., & Hishinuma, N. (1993). Alteration of thermal conductivity and viscosity of liquid by dispersing ultra-fine particles. *Netsu Bussei*, *7*(2), 227-233.

Mayer, C. R., Neveu, S., Secheresse, F., & Cabuil, V. (2004). Supramolecular assemblies of gold nanoparticles induced by hydrogen bond interactions. *Journal of colloid and interface science*, *273*(2), 350-355.

McAdams, W. H. (1954). Heat Transmission. 3rd. *New York*.

Mehrali, M., Sadeghinezhad, E., Tahan Latibari, S., Mehrali, M., Togun, H., Zubir, M. N. M., . . . Metselaar, H. (2014). Preparation, characterization, viscosity, and thermal conductivity of nitrogen-doped graphene aqueous nanofluids. *Journal of materials science*, *49*(20), 7156-7171. doi: http://dx.doi.org/10.1007/s10853-014-8424-8

Mintsa, H. A., Roy, G., Nguyen, C. T., & Doucet, D. (2009). New temperature dependent thermal conductivity data for water-based nanofluids. *International Journal of Thermal Sciences*, *48*(2), 363-371.

Mirmasoumi, S., & Behzadmehr, A. (2008a). Effect of nanoparticles mean diameter on mixed convection heat transfer of a nanofluid in a horizontal tube. *International Journal of heat and fluid flow*, *29*(2), 557-566.

Mirmasoumi, S., & Behzadmehr, A. (2008b). Numerical study of laminar mixed convection of a nanofluid in a horizontal tube using two-phase mixture model. *Applied Thermal Engineering*, *28*(7), 717-727.

Mohammed, K. A. K., Abdulkadhim, H. M., & Noori, S. I. (2016). Chemical Composition and Anti-bacterial Effects of Clove (Syzygium aromaticum) Flowers. *Int. J. Curr. Microbiol. App. Sci*, *5*(2), 483-489.

Mohamoud, M. J., Singh, T., Mahmoud, S. E., Koc, M., Samara, A., Isaifan, R. J., . . . 2, M. A. Critical Review on Nanofluids: Preparation, Characterization and Applications.

Murshed, S., Leong, K., & Yang, C. (2005). Enhanced thermal conductivity of TiO< sub> 2</sub>—water based nanofluids. *International Journal of Thermal Sciences, 44*(4), 367-373.

Murshed, S., Leong, K., & Yang, C. (2008). Investigations of thermal conductivity and viscosity of nanofluids. *International Journal of Thermal Sciences, 47*(5), 560-568.

Namburu, P. K., Das, D. K., Tanguturi, K. M., & Vajjha, R. S. (2009). Numerical study of turbulent flow and heat transfer characteristics of nanofluids considering variable properties. *International Journal of Thermal Sciences, 48*(2), 290-302.

Otsubo, Y., Fujiwara, M., Kouno, M., & Edamura, K. (2007). Shear-thickening flow of suspensions of carbon nanofibers in aqueous PVA solutions. *Rheologica acta, 46*(7), 905-912.

Özerinç, S., Kakaç, S., & Yazıcıoğlu, A. G. (2010). Enhanced thermal conductivity of nanofluids: a state-of-the-art review. *Microfluidics and Nanofluidics, 8*(2), 145-170.

Pak, B. C., & Cho, Y. I. (1998). Hydrodynamic and heat transfer study of dispersed fluids with submicron metallic oxide particles. *Experimental Heat Transfer an International Journal, 11*(2), 151-170.

Palm, S. J., Roy, G., & Nguyen, C. T. (2006). Heat transfer enhancement with the use of nanofluids in radial flow cooling systems considering temperature-dependent properties. *Applied Thermal Engineering, 26*(17), 2209-2218.

Pantzali, M., Mouza, A., & Paras, S. (2009). Investigating the efficacy of nanofluids as coolants in plate heat exchangers (PHE). *Chemical engineering science, 64*(14), 3290-3300.

Parthasarathy, V. A., Chempakam, B., & Zachariah, T. J. (2008). *Chemistry of spices*: CABI.

Peng, X., & Wong, S. S. (2009). Functional covalent chemistry of carbon nanotube surfaces. *Advanced Materials, 21*(6), 625-642.

Peterson, G., & Li, C. (2006). Heat and mass transfer in fluids with nanoparticle suspensions. *Advances in Heat Transfer, 39*, 257-376.

Petukhov, B. (1970). Heat transfer and friction in turbulent pipe flow with variable physical properties. *Advances in heat transfer, 6*, 503-564.

Philip, J., Shima, P., & Raj, B. (2007). Enhancement of thermal conductivity in magnetite based nanofluid due to chainlike structures. *Applied Physics Letters, 91*(20), 203108.

Phuoc, T. X., Massoudi, M., & Chen, R.-H. (2011). Viscosity and thermal conductivity of nanofluids containing multi-walled carbon nanotubes stabilized by chitosan. *International Journal of thermal sciences, 50*(1), 12-18.

Pramanik, N. B., & Singha, N. K. (2015). Direct functionalization of multi-walled carbon nanotubes (MWCNTs) via grafting of poly (furfuryl methacrylate) using Diels–Alder "click chemistry" and its thermoreversibility. *RSC Advances, 5*(114), 94321-94327.

Putra, N., Thiesen, P., & Roetzel, W. (2003). Temperature dependence of thermal conductivity enhancement for nanofluids. *Journal of heat transfer, 125*, 567-574.

Ramires, M. L., de Castro, C. A. N., Nagasaka, Y., Nagashima, A., Assael, M. J., & Wakeham, W. A. (1995). Standard reference data for the thermal conductivity of water. *Journal of Physical and Chemical Reference Data, 24*(3), 1377-1381.

Ruan, B., & Jacobi, A. M. (2012). Ultrasonication effects on thermal and rheological properties of carbon nanotube suspensions. *Nanoscale research letters, 7*(1), 1-14.

Sadri, R., Ahmadi, G., Togun, H., Dahari, M., Kazi, S. N., Sadeghinezhad, E., & Zubir, N. (2014a). An experimental study on thermal conductivity and viscosity of nanofluids containing carbon nanotubes. *Nanoscale research letters, 9*(1), 151.

Sadri, R., Ahmadi, G., Togun, H., Dahari, M., Kazi, S. N., Sadeghinezhad, E., & Zubir, N. (2014b). An experimental study on thermal conductivity and viscosity of nanofluids containing carbon nanotubes. *Nanoscale research letters, 9*(1), 1-16.

Sadri, R., Hosseini, M., Kazi, S., Bagheri, S., Ahmed, S., Ahmadi, G., . . . Dahari, M. (2017). Study of environmentally friendly and facile functionalization of graphene nanoplatelet and its application in convective heat transfer. *Energy Conversion and Management, 150*, 26-36.

Sadri, R., Hosseini, M., Kazi, S., Bagheri, S., Zubir, N., Ahmadi, G., . . . Zaharinie, T. (2017). A novel, eco-friendly technique for covalent functionalization of graphene nanoplatelets and the potential of their nanofluids for heat transfer applications. *Chemical Physics Letters, 675*, 92-97.

Sadri, R., Zangeneh Kamali, K., Hosseini, M., Zubir, N., Kazi, S., Ahmadi, G., . . . Moradi, A. (2016). Experimental Study on Thermo-Physical and Rheological Properties of Highly Stable and Green Reduced Graphene Oxide Nanofluids: Hydrothermal Assisted Technique. *Journal of dispersion science and technology*(just-accepted).

Saidur, R., Leong, K., & Mohammad, H. (2011). A review on applications and challenges of nanofluids. *Renewable and Sustainable Energy Reviews, 15*(3), 1646-1668.

Sarsam, W. S., Amiri, A., Shanbedi, M., Kazi, S., Badarudin, A., Yarmand, H., . . . Zaharinie, T. (2017). Synthesis, stability, and thermophysical properties of aqueous colloidal dispersions of multi-walled carbon nanotubes treated with beta-alanine. *International Communications in Heat and Mass Transfer, 89*, 7-17.

Sato, M., Abe, Y., Urita, Y., Di Paola, R., Cecere, A., & Savino, R. (2011). Thermal Performance of Self-rewetting Fluid Heat Pipe Containing Dilute solutions of Polymer-capped Silver Nanoparticles Synthesized by Microwave-Polyol Process. *International Journal of Transport Phenomena, 12*.

Serrano, E., Rus, G., & Garcia-Martinez, J. (2009). Nanotechnology for sustainable energy. *Renewable and Sustainable Energy Reviews, 13*(9), 2373-2384.

Sharma, K., Sundar, L. S., & Sarma, P. (2009). Estimation of heat transfer coefficient and friction factor in the transition flow with low volume concentration of Al< sub> 2</sub> O< sub> 3</sub> nanofluid flowing in a circular tube and with twisted tape insert. *International Communications in Heat and Mass Transfer, 36*(5), 503-507.

Shin, S., & Lee, S.-H. (2000). Thermal conductivity of suspensions in shear flow fields. *International Journal of Heat and Mass Transfer, 43*(23), 4275-4284.

Singh, V., & Gupta, M. (2016). Heat transfer augmentation in a tube using nanofluids under constant heat flux boundary condition: A review. *Energy Conversion and Management, 123*, 290-307.

Sohn, C., & Chen, M. (1981). Microconvective thermal conductivity in disperse two-phase mixtures as observed in a low velocity Couette flow experiment. *J. Heat Transfer;(United States), 103*(1).

Sommers, A. D., & Yerkes, K. L. (2010). Experimental investigation into the convective heat transfer and system-level effects of Al2O3-propanol nanofluid. *Journal of Nanoparticle Research, 12*(3), 1003-1014.

Sun, Y.-P., Fu, K., Lin, Y., & Huang, W. (2002). Functionalized carbon nanotubes: properties and applications. *Accounts of Chemical Research, 35*(12), 1096-1104.

Sundar, L. S., Singh, M. K., & Sousa, A. C. (2013). Investigation of thermal conductivity and viscosity of Fe 3 O 4 nanofluid for heat transfer applications. *International Communications in Heat and Mass Transfer, 44*, 7-14.

Sundar, L. S., Singh, M. K., & Sousa, A. C. (2014). Enhanced heat transfer and friction factor of MWCNT–Fe 3 O 4/water hybrid nanofluids. *International Communications in Heat and Mass Transfer, 52*, 73-83.

Suresh, S., Chandrasekar, M., Selvakumar, P., & Page, T. (2012). Experimental studies on heat transfer and friction factor characteristics of Al2O3/water nanofluid under laminar flow with spiralled rod inserts. *International Journal of Nanoparticles, 5*(1), 37-55.

Suzuki, T. O., D. (2000). Intermolecular energy transfer at a solid-liquid interface. *Microscale Thermophysical Engineering, 4*(3), 189-196.

Tasis, D., Tagmatarchis, N., Bianco, A., & Prato, M. (2006). Chemistry of carbon nanotubes. *Chemical reviews, 106*(3), 1105-1136.

Tavman, I., & Turgut, A. (2010). An investigation on thermal conductivity and viscosity of water based nanofluids *Microfluidics Based Microsystems* (pp. 139-162): Springer.

Thompson, W. (1998). An introduction to error analysis: The study of uncertainties in physical measurements, by John R. Taylor. *Physics Today, 51*, 57-58.

Timofeeva, E. V., Gavrilov, A. N., McCloskey, J. M., Tolmachev, Y. V., Sprunt, S., Lopatina, L. M., & Selinger, J. V. (2007). Thermal conductivity and particle agglomeration in alumina nanofluids: experiment and theory. *Physical Review E, 76*(6), 061203.

Trisaksri, V., & Wongwises, S. (2007). Critical review of heat transfer characteristics of nanofluids. *Renewable and Sustainable Energy Reviews, 11*(3), 512-523.

Vajjha, R., Das, D., & Mahagaonkar, B. (2009). Density measurement of different nanofluids and their comparison with theory. *Petroleum Science and Technology, 27*(6), 612-624.

Vilkhu, K., Mawson, R., Simons, L., & Bates, D. (2008). Applications and opportunities for ultrasound assisted extraction in the food industry—A review. *Innovative Food Science & Emerging Technologies, 9*(2), 161-169.

Wang, L., & Wei, X. (2009). Heat conduction in nanofluids. *Chaos, Solitons & Fractals, 39*(5), 2211-2215.

Wang, X.-j., & Zhu, D.-s. (2009). Investigation of pH and SDBS on enhancement of thermal conductivity in nanofluids. *Chemical Physics Letters, 470*(1), 107-111.

Wang, X.-Q., & Mujumdar, A. S. (2008). A review on nanofluids-part II: experiments and applications. *Brazilian Journal of Chemical Engineering, 25*(4), 631-648.

Wang, X., Xu, X., & S. Choi, S. U. (1999). Thermal conductivity of nanoparticle-fluid mixture. *Journal of thermophysics and heat transfer, 13*(4), 474-480.

Web of Science. (2017).

Wen, D., & Ding, Y. (2004). Effective thermal conductivity of aqueous suspensions of carbon nanotubes (carbon nanotube nanofluids). *Journal of Thermophysics and Heat Transfer, 18*(4), 481-485.

Wen, D., Lin, G., Vafaei, S., & Zhang, K. (2009). Review of nanofluids for heat transfer applications. *Particuology, 7*(2), 141-150.

Weydemeyer, E. J., Sawdon, A. J., & Peng, C.-A. (2015). Controlled cutting and hydroxyl functionalization of carbon nanotubes through autoclaving and sonication in hydrogen peroxide. *Chemical Communications, 51*(27), 5939-5942.

Williams, W., Buongiorno, J., & Hu, L.-W. (2008). Experimental investigation of turbulent convective heat transfer and pressure loss of alumina/water and zirconia/water nanoparticle colloids (nanofluids) in horizontal tubes. *Journal of heat transfer, 130*(4), 042412.

Worsley, M. A., Pauzauskie, P. J., Olson, T. Y., Biener, J., Satcher Jr, J. H., & Baumann, T. F. (2010). Synthesis of graphene aerogel with high electrical conductivity. *Journal of the American Chemical Society, 132*(40), 14067-14069.

Wu, D., Zhu, H., Wang, L., & Liu, L. (2009). Critical issues in nanofluids preparation, characterization and thermal conductivity. *Current Nanoscience, 5*(1), 103-112.

Xie, H., Lee, H., Youn, W., & Choi, M. (2003). Nanofluids containing multiwalled carbon nanotubes and their enhanced thermal conductivities. *Journal of Applied Physics, 94*(8), 4967-4971.

Xuan, Y., & Li, Q. (2000). Heat transfer enhancement of nanofluids. *International Journal of heat and fluid flow, 21*(1), 58-64.

Xuan, Y., & Li, Q. (2003). Investigation on convective heat transfer and flow features of nanofluids. *Journal of heat transfer, 125*(1), 151-155.

Yang, Y., Grulke, E. A., Zhang, Z. G., & Wu, G. (2006). Thermal and rheological properties of carbon nanotube-in-oil dispersions. *Journal of Applied Physics, 99*(11), 114307-114307-114308.

Yang, Y., Qiu, S., He, C., He, W., Yu, L., & Xie, X. (2010). Green chemical functionalization of multiwalled carbon nanotubes with poly (ε-caprolactone) in ionic liquids. *Applied Surface Science, 257*(3), 1010-1014.

Yang, Y., Qiu, S., Xie, X., Wang, X., & Li, R. K. Y. (2010). A facile, green, and tunable method to functionalize carbon nanotubes with water-soluble azo initiators by one-step free radical addition. *Applied Surface Science, 256*(10), 3286-3292.

Yang, Y., Zhang, Z. G., Grulke, E. A., Anderson, W. B., & Wu, G. (2005). Heat transfer properties of nanoparticle-in-fluid dispersions (nanofluids) in laminar flow. *International Journal of Heat and Mass Transfer, 48*(6), 1107-1116.

Yu, M.-F., Files, B. S., Arepalli, S., & Ruoff, R. S. (2000). Tensile loading of ropes of single wall carbon nanotubes and their mechanical properties. *Physical review letters, 84*(24), 5552.

Yu, Q., Kim, Y. J., & Ma, H. (2008). Nanofluids with plasma treated diamond nanoparticles. *Applied Physics Letters, 92*(10), 103111-103111-103113.

Yu, W., & Choi, S. (2003). The role of interfacial layers in the enhanced thermal conductivity of nanofluids: a renovated Maxwell model. *Journal of Nanoparticle Research, 5*(1-2), 167-171.

Yu, W., France, D. M., Routbort, J. L., & Choi, S. U. (2008). Review and comparison of nanofluid thermal conductivity and heat transfer enhancements. *Heat Transfer Engineering, 29*(5), 432-460.

Yu, W., Xie, H., Chen, L., & Li, Y. (2009). Investigation of thermal conductivity and viscosity of ethylene glycol based ZnO nanofluid. *Thermochimica Acta, 491*(1), 92-96.

Yu, W., Xie, H., Wang, X., & Wang, X. (2011). Significant thermal conductivity enhancement for nanofluids containing graphene nanosheets. *Physics Letters A, 375*(10), 1323-1328.

Zeinali Heris, S., Nasr Esfahany, M., & Etemad, S. G. (2007). Experimental investigation of convective heat transfer of Al< sub> 2</sub> O< sub> 3</sub>/water nanofluid in circular tube. *International journal of heat and fluid flow, 28*(2), 203-210.

Zhou, S., & Ni, R. (2008). Measurement of the specific heat capacity of water-based Al~ 2O~ 3 nanofluid. *Applied physics letters, 92*(9), 093123.

Zhu, H.-t., Lin, Y.-s., & Yin, Y.-s. (2004). A novel one-step chemical method for preparation of copper nanofluids. *Journal of colloid and interface science, 277*(1), 100-103.

Zhu, H., Zhang, C., Tang, Y., Wang, J., Ren, B., & Yin, Y. (2007). Preparation and thermal conductivity of suspensions of graphite nanoparticles. *Carbon, 45*(1), 226-228.

Zubir, M. N. M., Badarudin, A., Kazi, S., Huang, N. M., Misran, M., Sadeghinezhad, E., . . . Gharehkhani, S. (2015). Experimental investigation on the use of reduced graphene oxide and its hybrid complexes in improving closed conduit turbulent forced convective heat transfer. *Experimental Thermal and Fluid Science, 66*, 290-303.

Zubir, M. N. M., Badarudin, A., Kazi, S. N., Misran, M., Ibrahim, R., Amiri, A., & Sadri, R. (2016). Exploration of the environmentally benign and highly effective approach for improving carbon nanotube homogeneity in aqueous system. *Journal of Thermal Analysis and Calorimetry, 124*(2), 815-825.

LIST OF PUBLICATIONS AND AWARDS

1. Experimental study on heat transfer and thermo-physical properties of covalently functionalized carbon nanotubes nanofluids in an annular heat exchanger: A green and novel synthesis. Maryam Hosseini, Rad Sadri, Salim Newaz Kazi, Samira Bagheri, Chew Bee Teng. Energy & Fuels 2017,ACS.(10.1021/acs. energyfuels.6b02928).
2. A novel, eco-friendly technique for covalent functionalization of graphene nanoplatelets and the potential of their nanofluids for heat transfer applications. Rad Sadri, Maryam Hosseini,Goodarz Ahmadi, S.N. Kazi, Samira Bagheri, Nashrul Zubir , B.T. Chew .Chemical Physics Letters, 675 (2017) 92-97.
3. Experimental Study on Thermo-Physical and Rheological Properties of Highly Stable and Green Reduced Graphene Oxide Nanofluids: Hydrothermal Assisted Technique." Rad Sadri, K. Zangeneh Kamali, M. Hosseini, Nashrul Zubir, S.N. Kazi, Goodarz Ahmadi,Mahidzal Dahari, NM Huang, Amir Moradi. Journal of Dispersion Science and Technology , Teylor & Francis, 38(9) (2017) 1302-1310.
4. A bio-based, cost-effective, facile approach for preparation of covalently functionalized carbon nanotubes aqueous suspensions and their potential as heat transfer fluids. Rad Sadri, Maryam Hosseini, SN Kazi, Samira Bagheri, Nashrul Zubir, KH Solangi, Tuan Zaharinie, A Badarudin. Journal of Colloid and Interface Science. Volume 504, 15 October 2017, Pages 115-123.
5. Study of environmentally friendly and facile functionalization of graphene nanoplatelets and its application in convective heat transfer. Rad Sadri, M. Hosseini, S.N. Kazi, Nashrul Zubir ,S. Bagheri, Mahidzal Dahari, B.T. Chew, A. Badarudin. Energy Conversion and Management, Elsevier,150 (2017) 26-36.